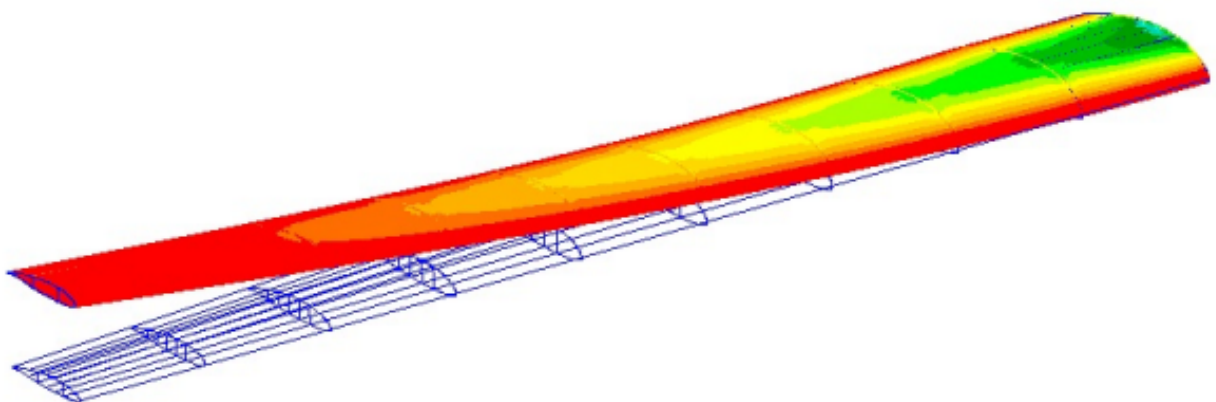


AE 508 Final Project



Kyron Saunders, Hunter Seamons, Tiger Sievers, Mayah Haug, and Zane Hermann

Instructor: Dr. Richard Hale



Department of Aerospace Engineering
May 30, 2025

Executive Summary

This stress report documents the preliminary structural design and analysis of the outboard wing section for a sailplane aircraft competing in the Electric Training Sailplane request for proposal, as part of the AIAA student design competition. The wing is required to be size appropriately to support a maximum take-off gross weight of 1,800 lbf and a load factor of 7.0, with a factor of safety of 1.5. A finite element model of the wing was created in MSC NASTRAN/Patran [1] to assist in the analysis. Aluminum 2024-T3 sheets were selected to construct the wing skin, spar webs, and aft spar caps. Aluminum 5052 H32 sheets were selected to construct the rib webs and rib caps. The stringers and forward spar caps were constructed with 2024-T3 unequal angle stock extrusions. Two spars and three upper and lower skin stringers were selected to support the provided wing geometry. The forward and aft spars were placed at 25 and 67.5 percent cord, respectively. The upper and lower skin stringers were each placed at 37.5, 50, and 75 percent cord. The stringers used T cross-sections while the spar and rib caps used L cross-sections. Several assumptions were made to simplify the structural analysis for the preliminary design portion of the wing.

- No buckling or crippling at yield
- An additional factor of safety of 1.5 for ultimate stress
- All elements are displacement constrained at the root

A uniformly distributed pressure load resulting in a 2250 lbf total load was applied across the total surface area of the skin. A fixed boundary condition was defined at the root section of the wing to constrain translational displacements about each of the three axes. Due to the nature of Patran [1] overestimating the loads as elements approach translation fixed boundary condition, the inner wing section was ignored. Wing sections one and two were deemed to be the most critical because these sections are the most stiff sections of the remaining wing.

The resulting total weight of the wing and maximum wing deflection can be seen in Table 0.0.1 . The resulting configuration of the wing fails in all analyzed wing failure modes except in all spar and rib web margins of safety and all crippling margins of safety, with the exception of spar web shear buckling. The margin of safety values for all analyzed failure modes for wing sections one and two can be seen in Table 0.0.2 through Table 0.0.4 , which display tension and compression, buckling, and crippling failure margins of safety, respectively. For this report, this is acceptable because this report's scope is focused on the first iteration of the preliminary design of this wing. However, the goal for the next immediate iteration is to adjust the structure so that all structural components in both wing sections have positive margins of safety. Future iterations beyond this could focus on making the structure more efficient by optimizing the skin and substructure material and geometry selection to redistribute the stresses derived from the lifting loads.

Table 0.0.1 Total Wing Weight and Max Deflection

Resulting Wing Properties	Value
Wing Weight	68.80 (lbf)
Max Wing Deflection	16.50 (in)



Table 0.0.2 M.S. Values for Tensile and Compressive Stresses

Structure	Tension	Compression
Wing Section 1		
Upper Skin Stress	0.938	-0.464
Lower Skin Stress	-0.309	3.920
Spar Web Shear Stress	0.332	1.713
Rib Web Shear Stress	3.656	1.934
Upper Skin Stringer Stress	3.645	-0.259
Lower Skin Stringer Stress	-0.158	3.505
Upper Spar Cap Stress	-	-0.319
Lower Spar Cap Stress	-0.069	-
Wing Section 2		
Upper Skin Stress	1.067	-0.270
Lower Skin Stress	-0.185	5.014
Spar Web Shear Stress	0.609	2.238
Rib Web Shear Stress	4.458	2.084
Upper Skin Stringer Stress	7.359	-0.216
Lower Skin Stringer Stress	0.003	4.474
Upper Spar Cap Stress	-	-0.249
Lower Spar Cap Stress	-0.105	-



Table 0.0.3 M.S. Values for Buckling Mode

Structure	M.S.
Wing Section 1	
Upper Skin Buckling	-0.952
Spar Web Shear Buckling	-0.621
Rib Web Shear Buckling	0.350
Upper Skin Stringer Buckling	-0.980
Upper Spar Cap Buckling	-0.980
Wing Section 2	
Upper Skin Buckling	-0.934
Spar Web Shear Buckling	-0.439
Rib Web Shear Buckling	0.703
Upper Skin Stringer Buckling	-0.977
Upper Spar Cap Buckling	-0.978

Table 0.0.4 M.S. Values for Crippling Mode

Structure	M.S.
Wing Section 1	
Upper Skin Stringer Crippling	1.157
Upper Spar Cap Crippling	3.463
Wing Section 2	
Upper Skin Stringer Crippling	1.489
Upper Spar Cap Crippling	3.932



Contents

Executive Summary	i
List of Figures	ix
List of Tables	x
1 Nomenclature	xi
1.1 Variables	xi
1.2 Subscripts	xi
1.2.1 Abbreviations	xi
2 Introduction	1
3 Design Summary	3
3.1 Geometry	3
3.2 Materials	6
3.3 External Loads	7
3.4 Boundary Conditions	7
4 Finite Element Model	8
4.1 Geometry, Meshing, and Element Properties	8
4.1.1 Shell Elements	14
4.1.2 Bar Elements	14
4.2 Component Properties	14
4.3 Applied Loads	17
4.4 Applied Boundary Conditions	18
5 Model Verification	20
6 Results and Analysis	29
6.1 Wing Section 1	29
6.1.1 Upper Skin	29
6.1.2 Lower Skin	35
6.1.3 Spar Web	40
6.1.4 Rib Web	44
6.1.5 Upper Skin Stringer	48
6.1.6 Lower Skin Stringer	57
6.1.7 Upper Spar Cap	61
6.1.8 Lower Spar Cap	67
6.2 Wing Section 2	70
6.2.1 Upper Skin	70
6.2.2 Lower Skin	75
6.2.3 Spar Web	80
6.2.4 Rib Web	83



6.2.5	Upper Skin Stringer	87
6.2.6	Lower Skin Stringer	90
6.2.7	Upper Spar Cap	95
6.2.8	Lower Spar Cap	99
6.3	Wing Weight	101
6.4	Wing Stress Distribution and Deflection	102
7	Summary	104
Appendix A		A1



List of Figures

2.0.0.1	Given Baseline Full Wing Geometry	1
2.0.0.2	Glider Wing Moldline	2
3.1.0.1	Sections of the Wing	3
3.1.0.2	Rib Numbering and Spacing	3
3.1.0.3	Placement of Longitudinal Members	4
3.1.0.4	Stringer Cross-Section Geometry	4
3.1.0.5	Spar Cap Cross-Section Geometry	5
4.1.0.1	Top View of Wing FEM with Bay Labeling	8
4.1.0.2	Bays 1 and 2 FEM	9
4.1.0.3	Inboard and Outboard Ribs FEM	10
4.1.0.4	FWD and AFT Spars FEM	10
4.1.0.5	Upper and Lower Stringers FEM	11
4.1.0.6	Upper and Lower Skin FEM	11
4.1.0.7	Patran [1] Section Display of Stringer Cross Section	12
4.1.0.8	Patran [1] Section Display of Spar Cap Cross Section	13
4.3.0.1	Patran Model Pressure Loads	18
4.4.0.1	Patran Model Displacement Constraints	19
5.0.0.1	Upper Skin Stress (Tension) vs DOFs	20
5.0.0.2	Lower Skin Stress (Compression) vs DOFs	21
5.0.0.3	Spar Web Stress (Tension) vs DOFs	22
5.0.0.4	Rib Web Stress (Compression) vs DOFs	23
5.0.0.5	Rib Web Stress (Tension) vs DOFs	24
5.0.0.6	O-Load Values from .f06 File	24
5.0.0.7	Epsilon Value from .f06 File	25
5.0.0.8	Zoomed Region of Interest for Inboard Rib Web WS 1 with Element Local Coordinate Systems . .	25
5.0.0.9	Zoomed Region of Interest for FWD Spar Web WS 1 with Element Local Coordinate Systems . .	26
5.0.0.10	Zoomed Region of Interest for Inboard Rib Web WS 2 with Element Local Coordinate Systems . .	27
5.0.0.11	Zoomed Region of Interest for FWD Spar Web WS 2 with Element Local Coordinate Systems . .	28
6.1.1.1	Fringe: SC1:DEFAULT, A1: Static Subcase, Stress Tensor, Max Principal, Maximum, 2 of 2 layers of Upper Skin for WS 1	29
6.1.1.2	Zoomed Fringe and Elements of Interest for Upper Skin Max Stress in WS1	29
6.1.1.3	Upper Skin Max Stress Element of Interest in WS1	30
6.1.1.4	.f06 NASTRAN Results for Upper Skin Max Stress in WS1	30
6.1.1.5	Fringe: SC1:DEFAULT, A1: Static Subcase, Stress Tensor, Min Principal, Minimum, 2 of 2 layers of Upper Skin for WS 1	31
6.1.1.6	Zoomed Fringe and Elements of Interest for Upper Skin Min Stress in WS1	31
6.1.1.7	Upper Skin Min Stress Element of Interest in WS1	32
6.1.1.8	.f06 NASTRAN Results for Upper Skin Min Stress in WS1	32
6.1.1.9	Compression Buckling Coefficient Graph From Curtis [2] Text	34
6.1.2.1	Fringe: SC1:DEFAULT, A2: Static Subcase, Stress Tensor, Max Principal, 2 of 2 layers (Maximum) of Lower Skin for WS 1	35
6.1.2.2	Zoomed Fringe and Elements of Interest for Lower Skin on WS1	35



6.1.2.3	.f06 NASTRAN Results for Lower Skin in WS1	36
6.1.2.4	Fringe: SC1:DEFAULT, A2: Static Subcase, Stress Tensor, Min Principal, 2 of 2 layers (Minimum) of Lower Skin for WS 1	37
6.1.2.5	Zoomed Fringe and Elements of Interest for Lower Skin on WS1	38
6.1.2.6	.f06 NASTRAN Results for Lower Skin in WS1	39
6.1.3.1	Fringe: SC1:DEFAULT, A1: Static Subcase, Stress Tensor, XY Component, Maximum, 2 of 2 layers of Forward Spar Web for WS 1	40
6.1.3.2	Zoomed Fringe and Elements of Interest for Forward Spar Web for WS 1	41
6.1.3.3	Element of Interest for Forward Spar Web for WS 1	41
6.1.3.4	.f06 NASTRAN Results for Forward Spar Web Shear Stress for WS 1	42
6.1.3.5	Shear-Buckling-Stress Coefficient as a Function of $\frac{a}{b}$ via Ewing [3]	43
6.1.4.1	Fringe: SC1:DEFAULT, A1: Static Subcase, Stress Tensor, XY Component, Maximum, 2 of 2 layers of Inboard Rib Web for WS 1	44
6.1.4.2	Zoomed Fringe and Elements of Interest for Inboard Rib Web for WS 1	45
6.1.4.3	Element of Interest for Inboard Rib Web for WS 1	45
6.1.4.4	.f06 NASTRAN Results for Inboard Rib Web Shear Stress for WS 1	46
6.1.5.1	Geometry of Upper Skin and Stringer	48
6.1.5.2	Fringe: SC1:DEFAULT, A1: Static Subcase, Bar Stresses, Maximum Combined, At Center of Upper Stringers for WS 1	48
6.1.5.3	Upper Stringer Max Stress Element of Interest and Surrounding Skin	49
6.1.5.4	.f06 NASTRAN Results for Upper Stringer Max Stress	49
6.1.5.5	Fringe: SC1:DEFAULT, A1: Static Subcase, Bar Stresses, Minimum Combined, At Center of Upper Stringers for WS 1	50
6.1.5.6	Upper Stringer Min Stress Element of Interest and Surrounding Skin	51
6.1.5.7	.f06 NASTRAN Results for Upper Stringer Min Stress	51
6.1.5.8	Crippling Stresses for 2024-T4 ALCLAD Sheet Graphical Method on Page C6 of Crippling Methods Handout	52
6.1.5.9	Effective Width of Stiffened Sheet Graphical Determination Page on C6 of Crippling Methods Handout	53
6.1.6.1	Geometry of Lower Skin and Stringers	58
6.1.6.2	Fringe: SC1:DEFAULT, A1: Static Subcase, Bar Stresses, Maximum Combined, At Center of Lower Stringers for WS 1	58
6.1.6.3	Lower Stringer Max Stress Element of Interest and Surrounding Skin	59
6.1.6.4	.f06 NASTRAN Results for Lower Stringer Max Stress	59
6.1.6.5	Fringe: SC1:DEFAULT, A1: Static Subcase, Bar Stresses, Minimum Combined, At Center of Lower Stringers for WS 1	60
6.1.6.6	Lower Stringer Min Stress Element of Interest and Surrounding Skin	60
6.1.6.7	.f06 NASTRAN Results for Lower Stringer Min Stress	61
6.1.7.1	WS1 Geometry of Upper Skin and Upper Spar Cap	62
6.1.7.2	Fringe: SC1:DEFAULT, A1: Static Subcase, Bar Stresses, Minimum Combined, At Center of Upper Spar Cap for WS 1	63
6.1.7.3	WS1 Upper Spar Cap Element of Interest and Surrounding Skin	63
6.1.7.4	.f06 NASTRAN Results for WS1 Upper Spar Cap Min Stress	64



6.1.8.1	WS1 Geometry of Lower Skin and Lower Spar Cap	67
6.1.8.2	Fringe: SC1:DEFAULT, A1: Static Subcase, Bar Stresses, Maximum Combined, At Center of Lower Spar Cap for WS 1	68
6.1.8.3	WS1 Lower Spar Cap Element of Interest and Surrounding Skin	68
6.1.8.4	.f06 NASTRAN Results for WS1 Lower Spar Cap Max Stress	69
6.1.8.5	Fringe: SC1:DEFAULT, A2: Static Subcase, Bar Stresses, Minimum Combined, At Center of Lower Spar Cap for WS 1	70
6.2.1.1	Fringe: SC1:DEFAULT, A2: Static Subcase, Stress Tensor, Min Principal, 2 of 2 layers (Minimum) of Upper Skin for WS 2	70
6.2.1.2	Zoomed Fringe and Elements of Interest for Upper Skin on WS2	71
6.2.1.3	.f06 NASTRAN Results for Upper Skin in WS2	71
6.2.1.4	Fringe: SC1:DEFAULT, A2: Static Subcase, Stress Tensor, Max Principal, 2 of 2 layers (Maximum) of Upper Skin for WS 2	72
6.2.1.5	Zoomed Fringe and Elements of Interest for Upper Skin on WS2	72
6.2.1.6	.f06 NASTRAN Results for Upper Skin in WS2	73
6.2.2.1	Fringe: SC1:DEFAULT, A1: Static Subcase, Stress Tensor, Max Principal, Maximum, 2 of 2 layers of Lower Skin for WS 2	75
6.2.2.2	Zoomed Fringe and Elements of Interest for Lower Skin on WS2	75
6.2.2.3	WS2 Lower Skin Max Stress Element of Interest	76
6.2.2.4	.f06 NASTRAN Results for WS2 Lower Skin Max Stress	76
6.2.2.5	Fringe: SC1:DEFAULT, A1: Static Subcase, Stress Tensor, Min Principal, Minimum, 2 of 2 layers of Lower Skin for WS 2	77
6.2.2.6	Zoomed Fringe and Elements of Interest for Lower Skin on WS2	78
6.2.2.7	WS2 Lower Skin Min Stress Element of Interest	78
6.2.2.8	.f06 NASTRAN Results for WS2 Lower Skin Min Stress	79
6.2.3.1	Fringe: SC1:DEFAULT, A1: Static Subcase, Stress Tensor, XY Component, Maximum, 2 of 2 layers of Forward Spar Web for WS 2	80
6.2.3.2	Zoomed Fringe and Elements of Interest for Forward Spar Web for WS 2	81
6.2.3.3	Element of Interest for Forward Spar Web for WS 2	81
6.2.3.4	.f06 NASTRAN Results for Forward Spar Web Shear Stress for WS 2	82
6.2.4.1	Fringe: SC1:DEFAULT, A1: Static Subcase, Stress Tensor, XY Component, Maximum, 2 of 2 layers of Inboard Rib Web for WS 2	84
6.2.4.2	Zoomed Fringe and Elements of Interest for Inboard Rib Web for WS 2	84
6.2.4.3	Element of Interest for Inboard Rib Web for WS 2	85
6.2.4.4	.f06 NASTRAN Results for Inboard Rib Web Shear Stress for WS 2	85
6.2.5.1	Upper Skin Stringer Placement for WS 2	87
6.2.5.2	Fringe: SC1:DEFAULT, A1: Static Subcase, Bar Stresses, Minimum Combined, Aft Upper Stringer for WS 2	88
6.2.5.3	.f06 NASTRAN Results for Aft Upper Stringer in WS 2	88
6.2.5.4	Fringe: SC1:DEFAULT, A1: Static Subcase, Bar Stresses, Maximum Combined, Aft Upper Stringer for WS 2	89
6.2.5.5	.f06 NASTRAN Results for Aft Upper Stringer in WS 2	89
6.2.6.1	Geometry of Lower Skin and Stringer	91



6.2.6.2	Fringe: SC1:DEFAULT, A1: Static Subcase, Bar Stresses, Maximum Combined, At Center of Lower Stringers for WS 2	91
6.2.6.3	Lower Stringer Max Stress Element of Interest and Surrounding Skin	92
6.2.6.4	.f06 NASTRAN Results for Lower Stringer Max Stress	92
6.2.6.5	Fringe: SC1:DEFAULT, A1: Static Subcase, Bar Stresses, Minimum Combined, At Center of Lower Stringers for WS 2	93
6.2.6.6	Lower Stringer Min Stress Element of Interest and Surrounding Skin	94
6.2.6.7	.f06 NASTRAN Results for Lower Stringer Min Stress	95
6.2.7.1	WS2 Geometry of Upper Skin and Upper Spar Cap	96
6.2.7.2	Fringe: SC1:DEFAULT, A1: Static Subcase, Bar Stresses, Minimum Combined, At Center of Upper Spar Cap for WS 2	96
6.2.7.3	WS2 Upper Spar Cap Element of Interest and Surrounding Skin	97
6.2.7.4	.f06 NASTRAN Results for WS2 Upper Spar Cap Min Stress	97
6.2.8.1	Lower Spar Cap Placement WS2	99
6.2.8.2	Fringe: SC1:DEFAULT, A2: Static Subcase, Bar Stresses, Maximum Combined, At Center of Lower Spar Cap for WS 2	100
6.2.8.3	Lower Spar Cap NASTRAN .f06 Results	100
6.2.8.4	Fringe: SC1:DEFAULT, A2: Static Subcase, Bar Stresses, Minimum Combined, At Center of Lower Spar Cap for WS 2	101
6.3.0.1	Weight of Outboard Wing Section	102
6.4.0.1	Deform: SC1:DEFAULT, A1:Static subcase, Displacements, Translational, (NON-LAYERED) Deflection of Outboard Wing Section	102
6.4.0.2	NASTRAN .f06 Results for Maximum Displacements	102
6.4.0.3	Fringe: SC1:DEFAULT, A1:Static subcase, Stress Tensor, Min Principal, At Z1 Stress Distribution for Outboard Wing Section	103

List of Tables

0.0.1	Total Wing Weight and Max Deflection	i
0.0.2	M.S. Values for Tensile and Compressive Stresses	ii
0.0.3	M.S. Values for Buckling Mode	iii
0.0.4	M.S. Values for Crippling Mode	iii
3.1.1	Buckling Panel Properties in Upper Skin, Spar Web, and Rib Web	5
3.1.2	1D Beam Element Cross Section Properties	5
3.2.1	Stress Allows for Project Gauge Selection of 2024 T3 Sheet	6
3.2.2	Stress Allows for Project Gauge Selection of 2024 T3 Extrusions	6
3.2.3	Stress Allows for Project Gauge Selection of 5052 H32 Sheet	6
3.2.4	Elastic Moduli, Poisson Ratios, & Specific Weight of Selected Materials	6
4.1.1	Meshing Strategy and Element Specifications for Structure Components	14
4.2.1	Wing Skin Node ID and Element ID of Maximum and Minimum Principle Stresses	15
4.2.2	Spar Web Node ID and Element ID of Maximum and Minimum Shear-XY Stresses	15
4.2.3	Spar Web Node ID and Element ID of Maximum and Minimum Shear-XY Stresses	16
4.2.4	Wing Skin Stringer Element ID of Maximum and Minimum Combined Bar Stresses	16
4.2.5	Forward Spar Cap Element ID of Maximum and Minimum Combined Bar Stresses	17



5.0.1	Mesh Densities vs. Number of Degrees of Freedom	20
6.1.1	Skin Stringer Unbuckled Crippling Table	54
6.1.1	Spar Cap Unbuckled Crippling Table	66
1.0.1	Analysis Team Contributions	A1



1. Nomenclature

1.1 Variables

F	= Stress	(psi)
A	= Area	(in ²)
P	= Pressure	(psi)
O	= Total Load	(lbf)
$M.S.$	= Margin of Safety	(-)
σ	= Sigma	(psi)
FS	= Factor of Safety	(-)
C	= Compression	(-)
T	= Tension	(-)
τ	= Shear	(-)
K	= Shear-buckling-stress coefficient	(-)
ν	= Poisson's ratio	(-)
E	= Elastic Modulus	(psi)
t	= Thickness	(in)
w	= Width	(in)
λ	= lambda	(in)
L_{eff}	= Effective Length	(in)
π	= pi	(-)
ρ	= Radius of Gyration	(in)
I	= Moment of Inertia	(in ⁴)

1.2 Subscripts

cu	= Compression Ultimate
cy	= Compression Yield
tu	= Tensile Ultimate
ty	= Tensile Yield
su	= Shear Ultimate

1.2.1 Abbreviations

$BSMNC$	= Bar Stresses, Minimum Combined
$BSMNC1$	= Bar Stresses, Minimum Combined Wing Section 1
$BSMXC$	= Bar Stresses, Maximum Combined
DOF	= Degree(s) of Freedom
FEM	= Finite Element Model
FWD	= Forward
$H32S$	= Aluminum 5052 H32 Sheet
LL	= Lifting Load



<i>LSC1</i>	= Lower Stringer Compression Wing Section 1
<i>LST1</i>	= Lower Stringer Tension Wing Section 1
<i>MAX</i>	= Maximum
<i>Min</i>	= Minimum
<i>MNMNP</i>	= Minimum of Minimum Principle Stress
<i>MNXYS</i>	= Minimum of XY Shear
<i>RW</i>	= Rib Web
<i>RWS1</i>	= Rib Web Shear in Wing Section 1
<i>RWSB1</i>	= Rib Web Shear Buckling in Wing Section 1
<i>RWSB2</i>	= Rib Web Shear Buckling in Wing Section 2
<i>SS</i>	= Simply Supported
<i>SS1</i>	= Skin Section 1
<i>ST</i>	= Skin Total
<i>SW</i>	= Spar Web
<i>SWS1</i>	= Spar Web Shear in Wing Section 1
<i>SWSB1</i>	= Spar Web Shear Buckling in Wing Section 1
<i>SXY</i>	= Shear stress in xy direction
<i>T3S</i>	= T3 Sheet
<i>TD</i>	= Total Distribution
<i>US1</i>	= Upper Skin Wing Section 1
<i>USB1</i>	= Upper Skin Compression Buckling in Wing Section 1
<i>USC1</i>	= Upper Skin Compression in Wing Section 1
<i>USCB1</i>	= Upper Spar Cap Buckling Wing Section 1
<i>USCB2</i>	= Upper Spar Cap Buckling Wing Section 2
<i>USCC2</i>	= Upper Spar Cap Compression Wing Section 2
<i>USPC1</i>	= Upper Spar Cap Wing Section 1
<i>USS1</i>	= Upper Skin Stringer Wing Section 1
<i>USS2</i>	= Upper Skin Stringer Wing Section 2
<i>USSB1</i>	= Upper Skin Stringer Buckling in Wing Section 1
<i>USSB2</i>	= Upper Skin Stringer Buckling in Wing Section 2
<i>USSC1</i>	= Upper Skin Stringer Crippling Wing Section 1
<i>UST1</i>	= Upper Skin Tension in Wing Section 1
<i>WS</i>	= Wing Section



2. Introduction

This report documents the preliminary design and structural analysis of the outboard wing section of a glider to compete in the Electric Training Sailplane design competition as part of the AIAA student design competition. The wing is required to support a maximum takeoff gross weight of 1,800 lbf and a load factor of 7.0, with a Factor of Safety (S.F.) of 1.5. A parasolid geometry with multiple substructure configurations was provided, seen in below in Figure 2.0.0.1 , for flexibility in the first iteration of preliminary design and structural analysis.

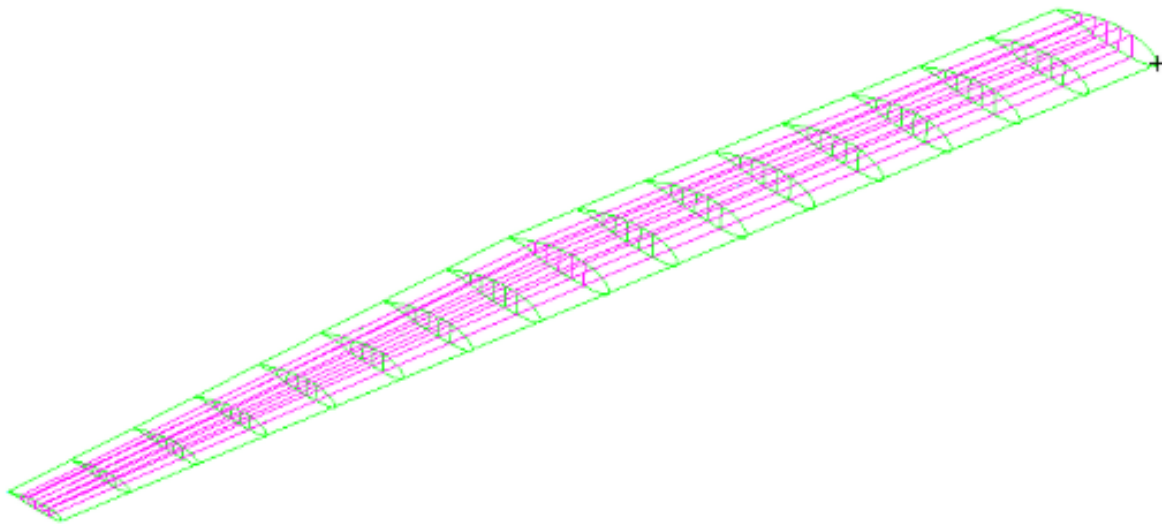


Fig. 2.0.0.1 Given Baseline Full Wing Geometry

Before any analysis of the wing and its substructure is conducted, a convergence study was performed with multiple models of varying mesh densities. Afterwards, the appropriate model will be used to analyze two wing sections margin of safety calculations performed for:

- Upper skin stress
- Upper skin buckling
- Lower skin stress
- Spar web shear stress
- Spar web shear buckling
- Rib web shear stress
- Rib web shear buckling
- Upper skin stinger stress
- Upper skin stringer crippling/buckling
- Lower skin stringer stress



- Upper spar cap stress
- Upper spar cap crippling/buckling
- Lower spar cap stress

In addition to the margin of safety calculations, an expected weight will be calculated for the given outboard wing section. Finally, comments will be made in regards to the stress distribution and wing deflection, and how this influences the wing's expected in-flight performance. Figure 2.0.0.2 shows the given outboard wing section that will be the basis of all analysis. Note that the upper skin has been removed to display the possible rib, spar, and stringer locations.

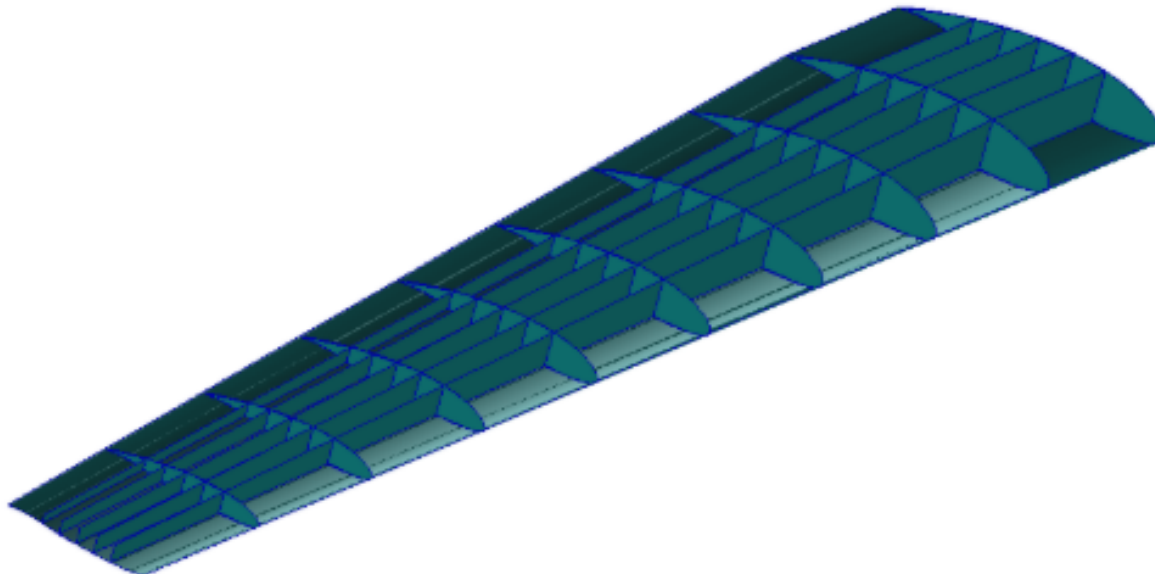


Fig. 2.0.0.2 Glider Wing Moldline

The inboard-most edge of this wing section is where the displacement constraint is placed, which creates a singularity and a region of unrealistically high stress. For this reason the section between Ribs 1 and 2 is ignored from the analysis. Since this section is ignored, the next two outboard sections are chosen as the wing sections of interest. It was evaluated that due to proximity to boundary constraints and high moments, these two sections would be the most critical in stress analysis.

3. Design Summary

3.1 Geometry

The wing is divided into eight distinct sections, as shown in Figure 3.1.0.1 . Bay 0 represents the most inboard section of the wing, while Bay 8 is located at the most outboard position.

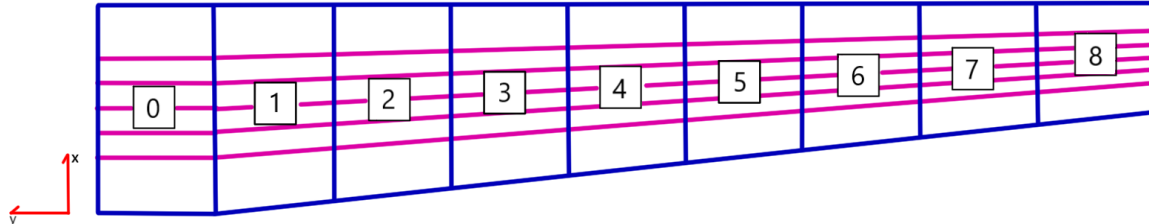


Fig. 3.1.0.1 Sections of the Wing

Figure 3.1.0.2 displays the placements of the ribs throughout the span of the wing section. Ribs are spaced 24.62 inches apart.

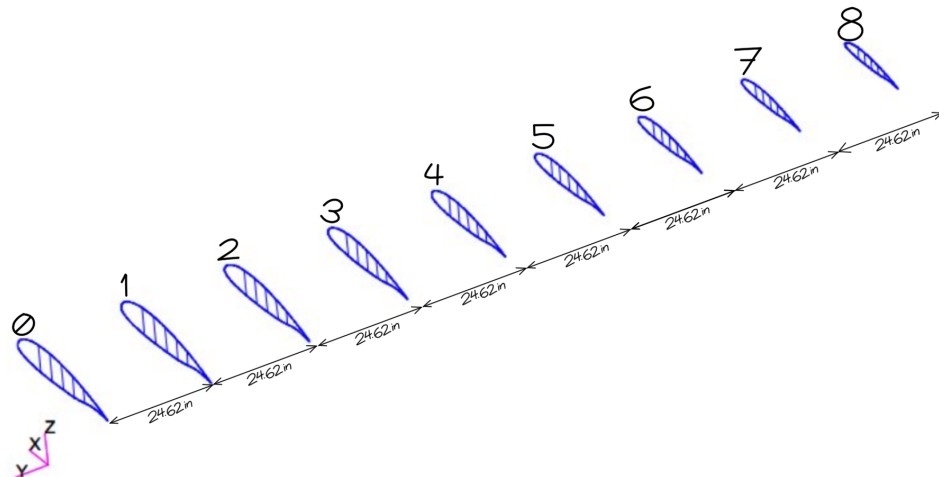


Fig. 3.1.0.2 Rib Numbering and Spacing

Figure 3.1.0.3 illustrates the placement of the longitudinal members, which include three upper and lower stringers attached to the skin. Spar caps are connected to the forward and aft spars, providing additional structural support.



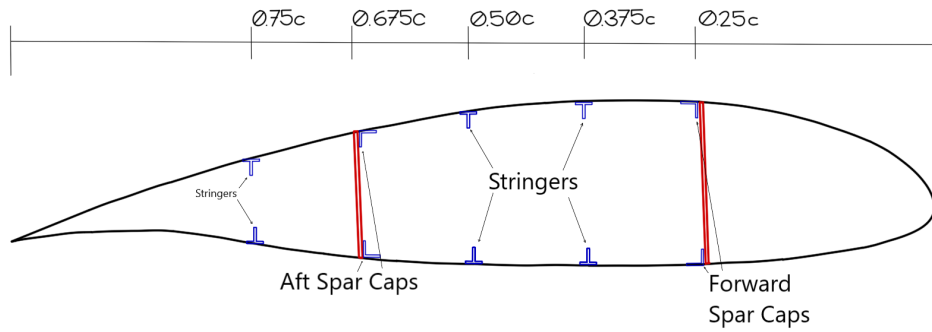


Fig. 3.1.0.3 Placement of Longitudinal Members

The stringers are designed using a T-shaped cross-section, with the flat side—labeled as Section 1—oriented towards the skin, as shown in Figure 3.1.0.3 . The major dimensions and thicknesses of these stringers are provided in Figure 3.1.0.4 . Sets of three stringers are located on both the upper and lower skins, with two placed between the spars and one behind of the aft spar. The dimensions of the stringers is detailed in Table 3.1.2 .

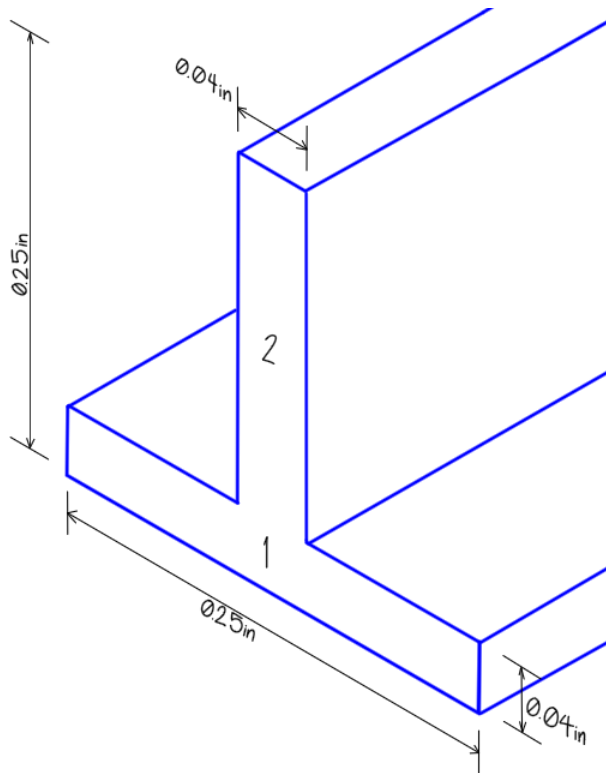


Fig. 3.1.0.4 Stringer Cross-Section Geometry

The spar caps feature an L-shaped cross-section, with the arms connected to both the skin and spars, as shown in Figure 3.1.0.3 . A sets of spar caps, top and bottom, are placed at the forward and aft spars. The dimensions and thicknesses of the spar caps are detailed in Figure 3.1.0.5 . The dimensions of the cap are detailed in Table 3.1.2 .



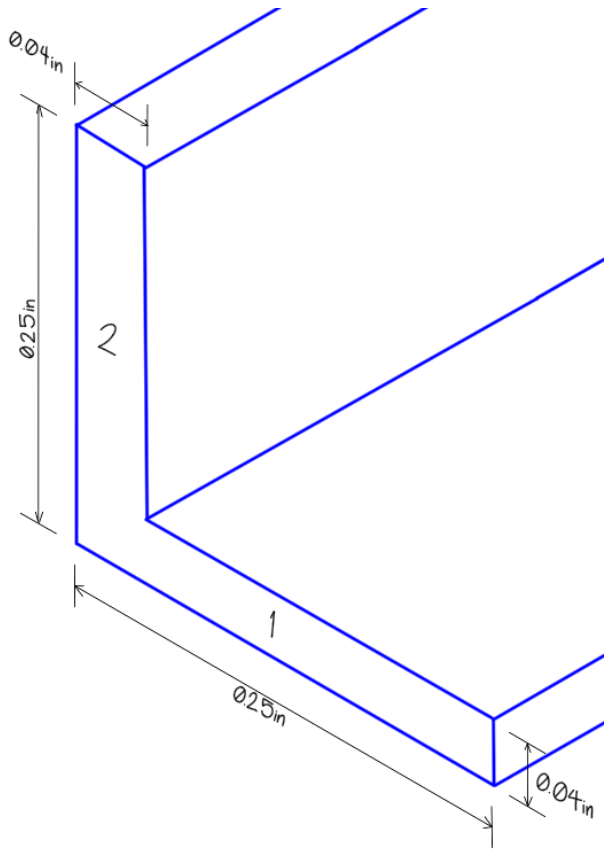


Fig. 3.1.0.5 Spar Cap Cross-Section Geometry

To provide further context on the structural design, Table 3.1.1 summarizes the buckling panel properties for key components of the wing structure, including the upper skin, spar web, and rib web. The table lists the panel dimensions, aspect ratio, and thickness, which are essential for analyzing buckling behavior under load. Table 3.1.2 displays the one-dimensional beam Element corss section properties of the skin stringers and the spar caps. Note that the rib caps also used the spar cap beam cross section.

Table 3.1.1 Buckling Panel Properties in Upper Skin, Spar Web, and Rib Web

Panel	<i>a</i> (in)	<i>b</i> (in)	Aspect Ratio (-)	<i>t</i> (in)
Upper Skin	24.62	4.43	5.55	0.035
Spar Web	24.62	5.54	4.45	0.060
Rib Web	13.54	6.20	2.19	0.060

Table 3.1.2 1D Beam Element Cross Section Properties

Beam Element	<i>I_x</i> (in ⁴)	A (in ²)	b ₁ (in)	t ₁ (in)	b ₂ (in)	t ₂ (in)
Skin Stringers	1.06×10^{-4}	1.84×10^{-2}	0.25	0.04	0.21	0.04
Spar Cap	1.06×10^{-4}	1.84×10^{-2}	0.25	0.04	0.21	0.04



3.2 Materials

Table 3.2.1 through Table 3.2.4 details material properties of the materials used in the structures, as found in Military Handbook 5H [4].

Table 3.2.1 Stress Allows for Project Gauge Selection of 2024 T3 Sheet

2024 T3 Sheet	Skin	Spar Webs
	0.0625" (psi)	0.125" (psi)
F_{tuT3S}	6.10E+04	6.10E+04
F_{tyT3S}	4.00E+04	4.00E+04
F_{cyT3S}	3.70E+04	3.70E+04
F_{suT3S}	3.80E+04	3.80E+04

Table 3.2.2 Stress Allows for Project Gauge Selection of 2024 T3 Extrusions

2024 T3 Extrusion	FWD Spar Caps & Stringers
	<0.25" (psi)
F_{tuT3E}	5.40E+04
F_{tyT3E}	3.70E+04
F_{cyT3E}	3.40E+04
F_{suT3E}	2.90E+04

Table 3.2.3 Stress Allows for Project Gauge Selection of 5052 H32 Sheet

5052 H32 Sheet	Ribs & Rib Caps
	0.017-2.0" (psi)
F_{tuH32}	3.10E+04
F_{tyH32}	2.20E+04
F_{cyH32}	2.30E+04
F_{suH32}	1.90E+04

Table 3.2.4 Elastic Moduli, Poisson Ratios, & Specific Weight of Selected Materials

Material	E (psi)	ν (-)	ω ($\frac{lb}{in^3}$)
2024 T3 Sheet	1.05E+07	0.33	0.1
2024 T3 Extrusions	1.08E+07	0.33	0.1
5052 H32 Extrusions	1.01E+07	0.33	0.097



3.3 External Loads

The glider wings are required to support a maximum takeoff weight of 1800 lbf with a load factor of 7 and a Factor of Safety of 1.5 per Design Project [5]. The wing is also assumed to have an elliptical lift distribution that is uniform across all skin surface area. The total half-span limit lifting load is 6300 lbf per Design Project [5]. The approximate external pressure load of the outboard section results in a 2250 lbf total load on the wing.

3.4 Boundary Conditions

The applied boundary condition in wing bay zero serves as a fixed constraint for the outboard wing section. The purpose of applying this boundary condition is to analyze stress in wing bay one and two in the absence of stress singularities. This constrains the root of wing bay zero to have no translation in the x, y, or z axes.



4. Finite Element Model

The following section outlines the creation of the finite element model (FEM) used to complete the structural analysis of the wing structure using the MSC NASTRAN/Patran [1] structural analysis software.

4.1 Geometry, Meshing, and Element Properties

A parasolid geometry was provided to begin the FEM abstraction of the outboard portion of the wing. This parasolid geometry included several groups which divided the wing into discrete sections. These groups were further divided into more specific groups to allow for better model handling during analysis. These groups are as follows

- Upper Skin
- Lower Skin
- Inboard Ribs
- Outboard Ribs
- FWD Spar 25c
- AFT Spar 67.5c
- FWD Upper Spar Caps
- FWD Lower Spar Caps
- AFT Upper Spar Caps
- AFT Lower Spar Caps
- Upper Skin Stringers
- Lower Skin Stringers
- Rib Caps
- Default Group

A top view of the FEM of the wing can be seen in Figure 4.1.0.1

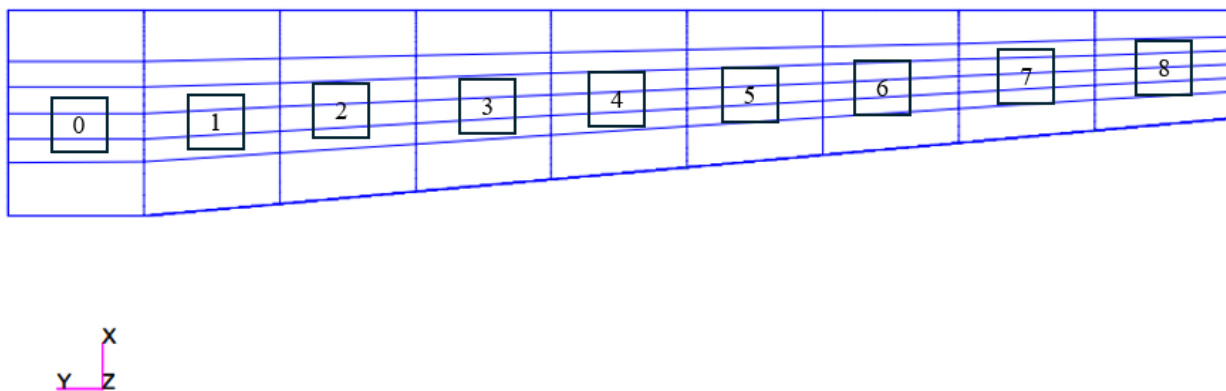


Fig. 4.1.0.1 Top View of Wing FEM with Bay Labeling



Stress analysis will be conducted on bays one and two, as labeled in 4.1.0.1 . A closer view of these two bays can be seen in Figure 4.1.0.2 below.

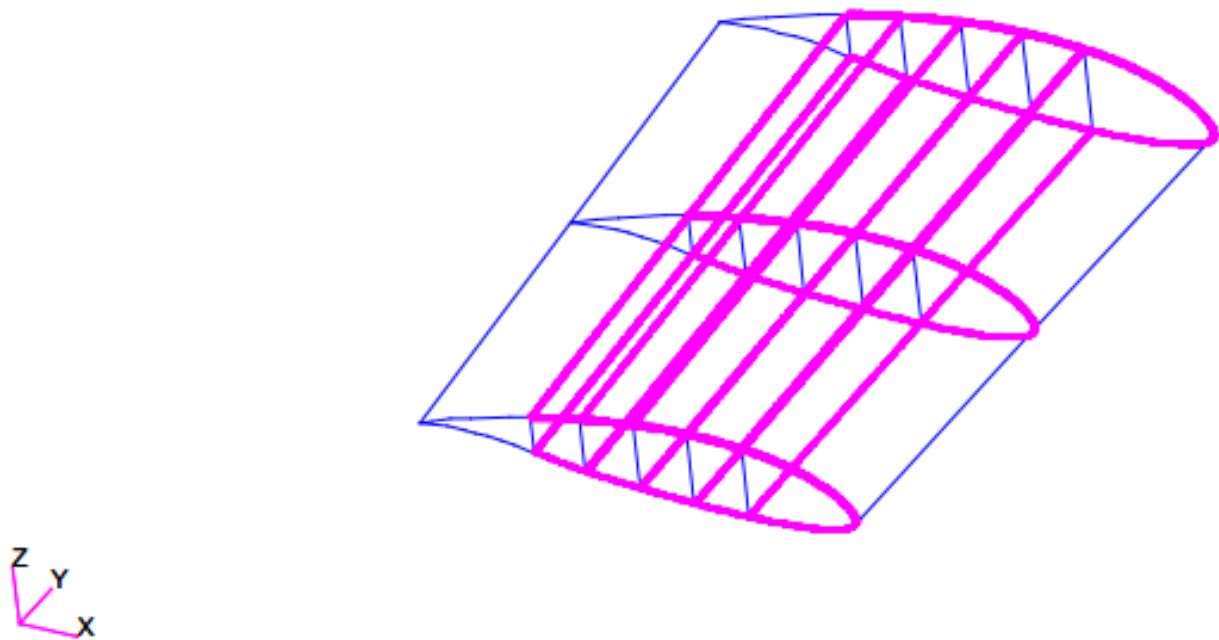


Fig. 4.1.0.2 Bays 1 and 2 FEM

Figure 4.1.0.2 depicts a closer view of the two bays used for stress analysis in this report. The outlines of the the rib caps, spar caps, and stringers are shown in pink while the outline of the skin is shown in blue. Closer views of each component will be examined further, beginning with the rib webs and rib caps as shown in Figure 4.1.0.3 below.

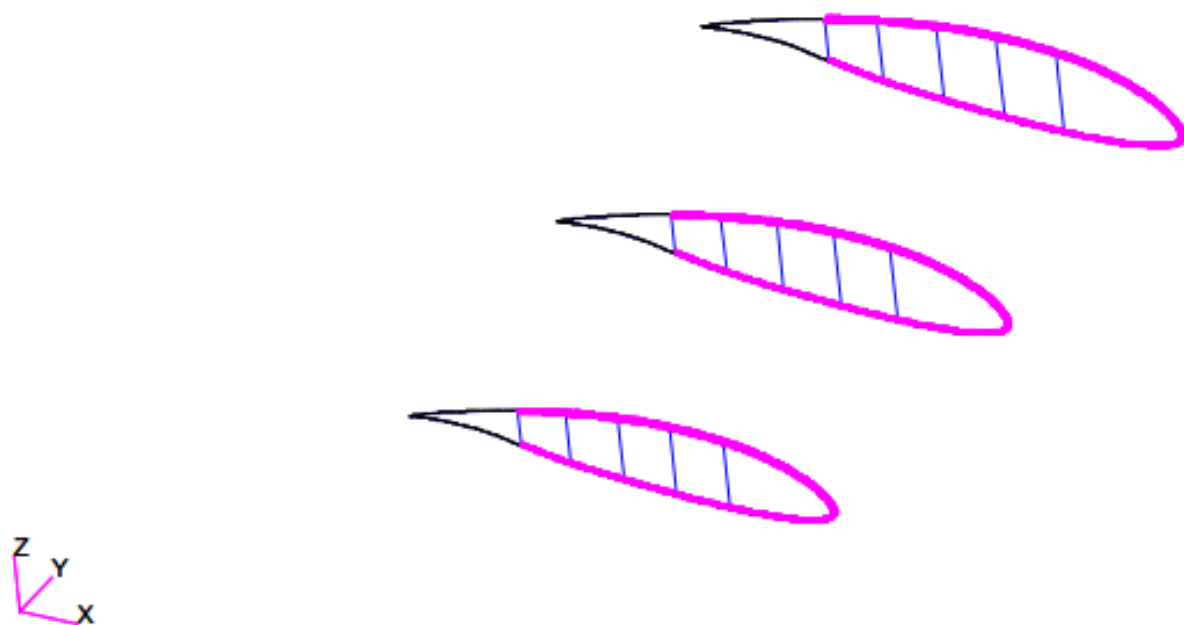


Fig. 4.1.0.3 Inboard and Outboard Ribs FEM

A closer look at the spar webs and spar caps is shown in Figure 4.1.0.4 below.

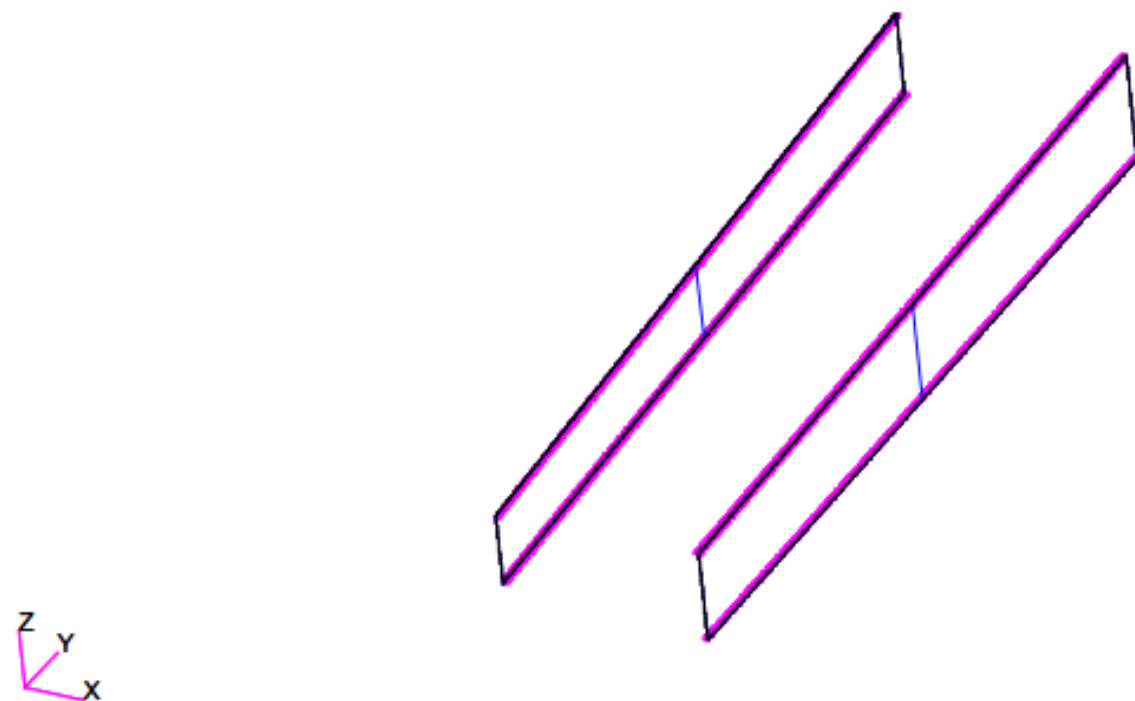


Fig. 4.1.0.4 FWD and AFT Spars FEM



For further clarity, an adjusted view of the upper and lower stringers can be seen in Figure 4.1.0.5 below.



Fig. 4.1.0.5 Upper and Lower Stringers FEM

Lastly, the upper and lower skin outline is shown in Figure 4.1.0.6 below.

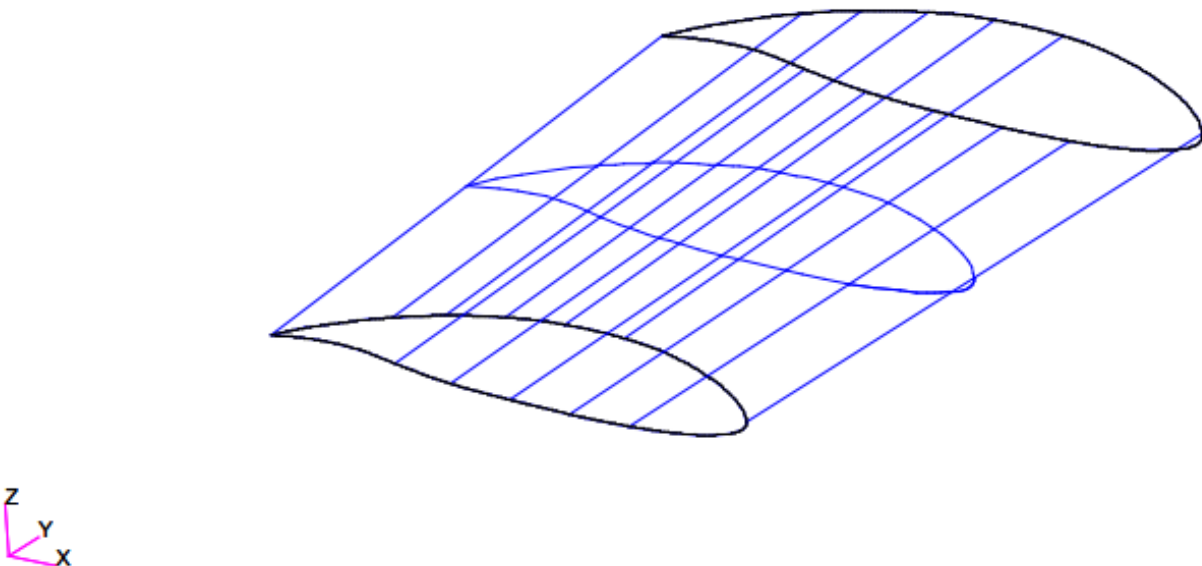


Fig. 4.1.0.6 Upper and Lower Skin FEM

Figure 4.1.0.7 and Figure 4.1.0.8 display the Patran [1] section display of the 1D beam element cross sections for



the stringers and spar caps, respectively. Note that all spar and rib caps used the same cross section geometry. Several properties are displayed in these section display windows, including section area, A, moments of inertia, I, and cross section dimensions. These reflect the selected cross section values as previously described in Table 3.1.2 .

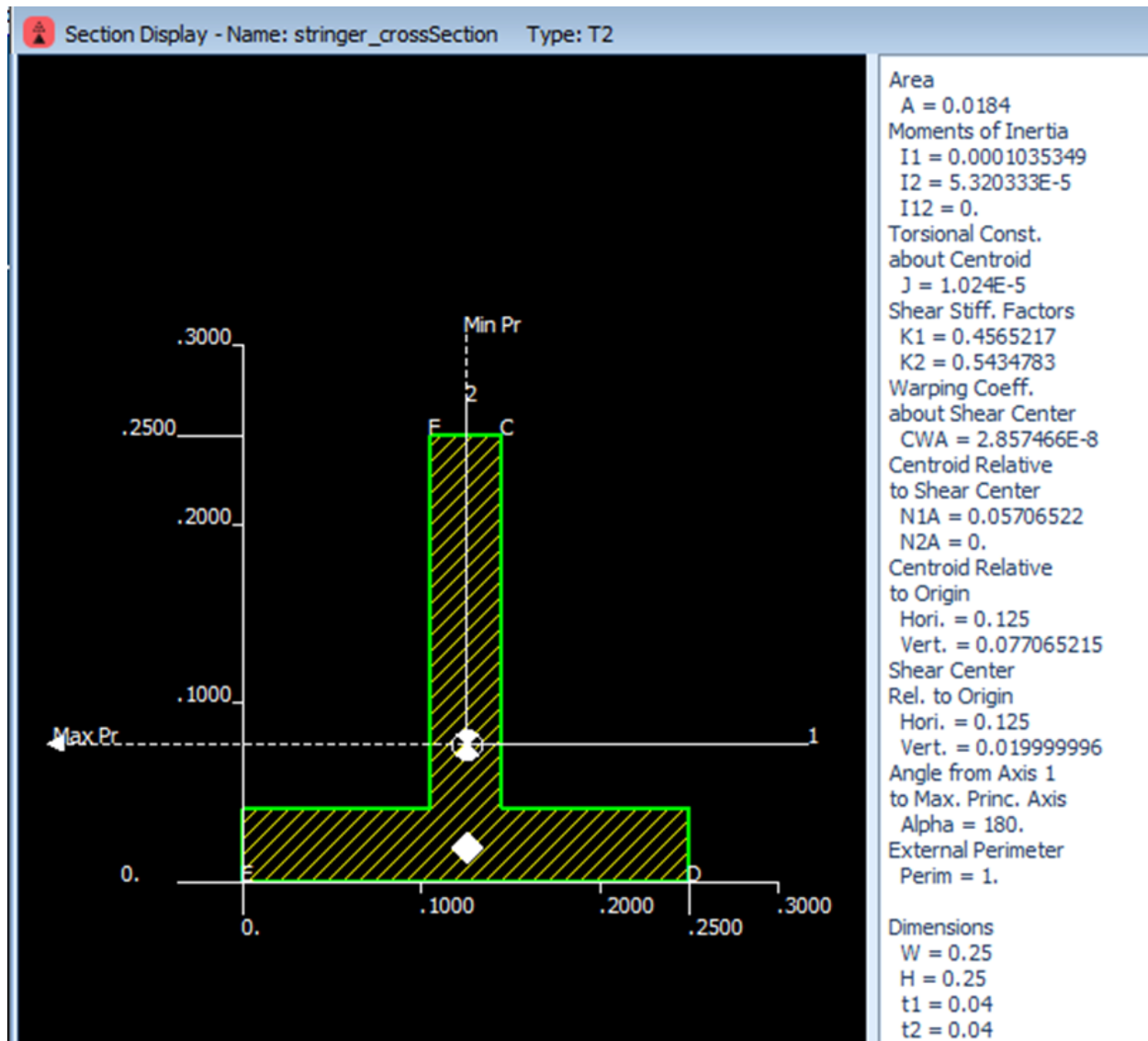


Fig. 4.1.0.7 Patran [1] Section Display of Stringer Cross Section



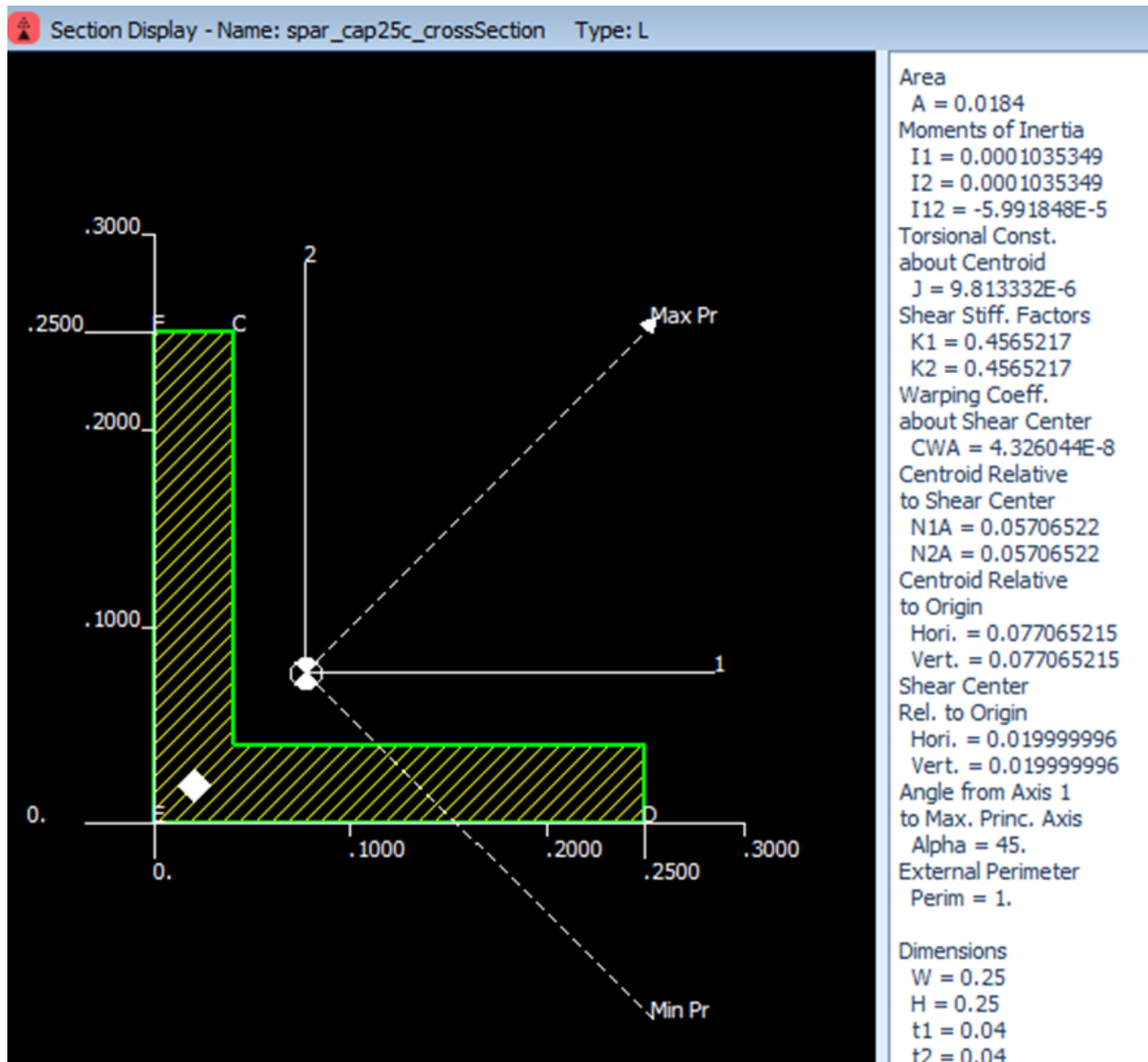


Fig. 4.1.0.8 Patran [1] Section Display of Spar Cap Cross Section

The process for meshing these structural components will be described by walking through the wing by major components, that is, the skin, spar webs, rib webs, stringers, spar caps, and rib caps. Because this is a preliminary design, element components will not vary from wing section to wing section. All mesh seeds used a element length of $\frac{1}{8}$ inch. This was selected over the number of element setting due to the curvature of the wing and to allow for a quicker creation of mostly unskewed, rectangular surfaces, when used to create 2D mesh elements. A table summarizing the meshing strategy and element specifications of the wing can be seen below in Table 4.1.1



Table 4.1.1 Meshing Strategy and Element Specifications for Structure Components

Component	Element Shape	Mesher	Topology	Element Object	Element Type
Skins	Quad	IsoMesh	Quad4	2D	Shell
Spar Webs	Quad	IsoMesh	Quad4	2D	Shell
Spar Caps	Bar	-	Bar2	1D	Beam
Rib Webs	Quad	IsoMesh	Quad4	2D	Shell
Rib Caps	Bar	-	Bar2	1D	Beam
Stringers	Bar	-	Bar2	1D	Beam

4.1.1 Shell Elements

Shell elements, used for thin shell structures, such as wing skins, rib webs, and spar webs, were created using the existing surface geometry. The initial surface geometry of the wing was constructed as a continuous, unmeshed surface geometry representing the skin of the wing, which was then discretized into smaller finite elements for further analysis. This discretization process involved the application of constant-length mesh seeds, ensuring a uniform distribution of nodes across the surface. The geometry was meshed into quadrilateral elements with automatic triangular elements created as nodes crossed over. This is not ideal, but these triangular shell elements were not located in critical areas within the skin and web elements.

In Patran [1], the meshing process began with the creation of a structured grid for relatively flat or planar surfaces. Quadrilateral elements were the primary shape used, but when needed, Patran [1] uses triangular elements to fix any mesh mismatches.

Once the geometry was discretized into mesh shell elements, the next step was to assign the appropriate material and sheet properties to each element. The shell elements in Patran [1] were defined for thin-walled structures. These shell elements were assigned a thickness value, representing the actual thickness of the respective part. The thickness could be applied uniformly across the mesh or adjusted in areas where local changes in thickness were necessary to match the design requirements. These sheet values can be seen in Table 3.1.1 .

4.1.2 Bar Elements

Bar elements, used for 1-D members such as stringers and caps, were created using the existing geometry along the wing skin, spar web, and rib webs. The discretization process involved adding the provided geometry and defining the appropriate bar elements along the length of the members. A similar method to that of the 2-D element meshing was used, discretizing the elements into constant element lengths. These elements were then assigned beam properties to accurately represent the structural behavior under both axial and transverse loads. By assigning material properties, such as Young's modulus as seen in Table 3.2.4 , and cross-sectional properties like shape and dimensions as seen in Table 3.1.2 , the bar elements were properly modeled to capture the effects of both axial forces and bending moments, ensuring the structure's response to loading conditions was correctly simulated.

4.2 Component Properties

Due to the nature of the wing meshing, nodes and elements can sometimes be nonsensically numbered and cannot be properly displayed in tabular format. Therefore, the following sub-subsections describe the locations of critical stresses in each structural component.



Skin The wing skins were analyzed with maximum and minimum principle stresses. Table 4.2.1 displays the nodes and element locations of these stresses.

Table 4.2.1 Wing Skin Node ID and Element ID of Maximum and Minimum Principle Stresses

	Stress Type	Node #	Element #
WS 1			
WS 2	Upper Skin MXMXP	846994	846994
	Upper Skin MNMNP	761618	739519
	Lower Skin MXMXP	15493	168103
	Lower MNMNP	320573	309494
WS 2	Upper Skin MXMXP	443959	868961
	Upper Skin MNMNP	769176	746842
	Lower Skin MXMXP	31103	152788
	Lower MNMNP	313416	302569

Spar Web The spar webs were analyzed with maximum and minimum shear-xy stresses. Table 4.2.2 displays the nodes and element locations of these stresses. The critical elements were located in the forward spar web.

Table 4.2.2 Spar Web Node ID and Element ID of Maximum and Minimum Shear-XY Stresses

	Stress Type	Node #	Element #
WS 1			
WS 2	MXXYS	27858	986749
	MNXYS	1016535	986647
WS 2	MXXYS	39773	997273
	MNXYS	1027313	997181

Rib Web The rib webs were analyzed with maximum and minimum shear-xy stresses. Table 4.2.3 displays the nodes and element locations of these stresses.



Table 4.2.3 Spar Web Node ID and Element ID of Maximum and Minimum Shear-XY Stresses

	Stress Type	Node #	Element #
WS 1			
	Rib 2 MXXYS	19771	19036
	Rib 2 MNXYS	15607	15013
WS 2			
	Rib 3 MXXYS	34828	33515
	Rib 3 MNXYS	31211	29993

Stringers The skin stringers were analyzed with maximum and minimum combined bar stresses. Table 4.2.4 displays the nodes and element locations of these stresses.

Table 4.2.4 Wing Skin Stringer Element ID of Maximum and Minimum Combined Bar Stresses

	Stress Type	Element #
WS 1		
	Upper Stringer BSMXC	1311526
	Upper Stringer BSMNC	1307980
	Lower Stringer BSMXC	1302857
	Lower Stringer BSMNC	1304434
WS 2		
	Upper Stringer BSMXC	1311919
	Upper Stringer BSMNC	1308177
	Lower Stringer BSMXC	1303054
	Lower Stringer BSMNC	1304631

Spar Caps The skin stringers were analyzed with maximum and minimum combined bar stresses. Table 4.2.5 displays the nodes and element locations of these stresses.



Table 4.2.5 Forward Spar Cap Element ID of Maximum and Minimum Combined Bar Stresses

	Stress Type	Element #
WS 1		
	Upper Spar Cap BSMXC	–
	Upper Spar Cap BSMNC	1288673
	Lower Spar Cap BSMXC	1290277
	Lower Spar Cap BSMNC	–
WS 2		
	Upper Spar Cap BSMXC	–
	Upper Spar Cap BSMNC	1288870
	Lower Spar Cap BSMXC	1290447
	Lower Spar Cap BSMNC	–

4.3 Applied Loads

The applied pressure distribution across the top and bottom skin were obtained by first estimating the total surface area of the outboard wing section. Using Patran's [1] Show Surface Attributes within the Geometry toolbar, the total surface area was obtained and is,

$$A_{ST} = 11613 \text{ in}^2. \quad (1)$$

This total surface area and lifting load of 2250 lbf were then used to calculate the total pressure distribution for the skin as seen below in Equation 2.

$$P_{TD} = \frac{F_{LL}}{A_{ST}}, \quad (2)$$

where P_{TD} is the total pressure distribution, F_{LL} is the lifting load, and A_{ST} is the total surface area.

Plugging in values,

$$P_{TD} = \frac{2250 \text{ lbf}}{11613 \text{ in}^2}, \quad (3)$$

$$P_{TD} = 0.1937 \text{ psi}. \quad (4)$$

This result was then applied as an element uniform pressure distribution to the top and bottom skin respectively. The model was executed and the NASTRAN results for O_{Load} in the z-direction was as follows,

$$O_{Load_z} = 2533.856 \text{ lbf}. \quad (5)$$

This result is larger than the lifting load value, the needed correction was obtained via a scaling process. The method for scaling to obtain the correct total pressure distribution is outlined in Equation 6 below.

$$P_{TD_{correct}} = \frac{F_{LL}}{O_{Load_z}} \times P_{TD}, \quad (6)$$



where $P_{TD_{correct}}$ is the corrected pressure distribution.

Plugging in values,

$$P_{TD_{correct}} = \frac{2250 \text{ lbf}}{2533.856 \text{ lbf}} \times 0.1937 \text{ psi}, \quad (7)$$

$$P_{TD_{correct}} = 0.1720 \text{ psi}. \quad (8)$$

This result was run and the NASTRAN outputs seen in Figure 5.0.0.6 were verified with the lifting load value. The pressure loads applied to the model can be seen in Figure 4.3.0.1 below.

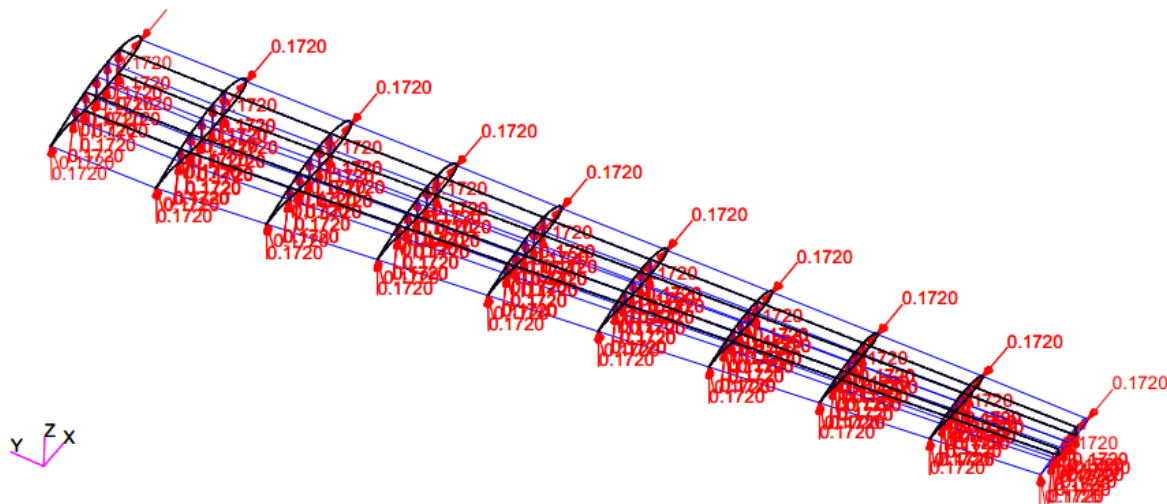


Fig. 4.3.0.1 Patran Model Pressure Loads

4.4 Applied Boundary Conditions

The applied boundary condition in wing bay zero as seen in 4.4.0.1 serves as a fix constraint for the outboard wing section. The purpose of applying this boundary condition is to analyze stress in wing bay one and two without having unrealistic values due to stress singularities that occur at fixed boundary constraints. This constrains wing bay zero to have no translation in the x, y, or z axes.



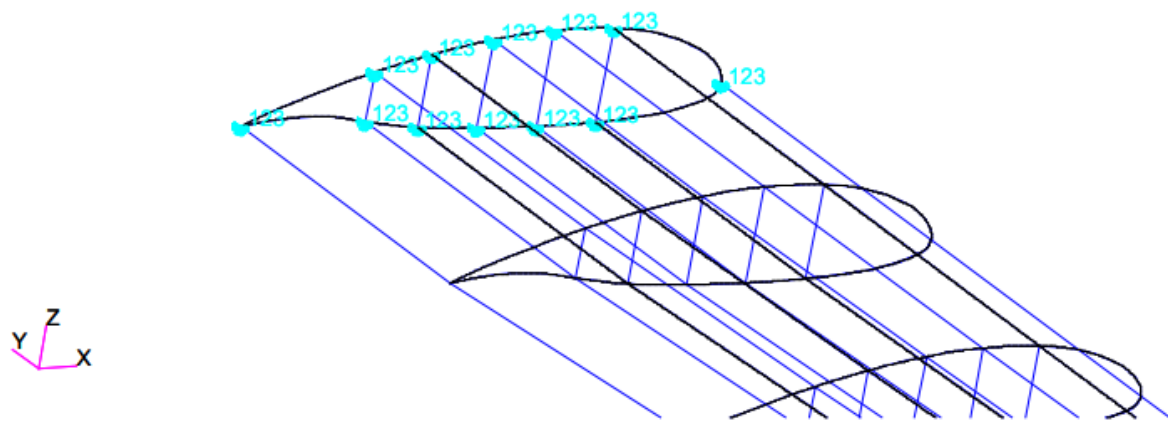


Fig. 4.4.0.1 Patran Model Displacement Constraints

5. Model Verification

Model verification was achieved by running multiple models each with increasing element mesh densities and degrees of freedom. First, a convergence study was conducted to identify the chosen model in comparison to the other models. This convergence study consists of five stress plots in comparison to the number of degrees of freedom for each model. Table 5.0.1 below shows the model's mesh densities and respective degrees of freedom.

Table 5.0.1 Mesh Densities vs. Number of Degrees of Freedom

Mesh Density (in)	Number of Degrees of Freedom
$\frac{1}{2}$	397230
$\frac{1}{4}$	1624479
$\frac{3}{16}$	2901207
$\frac{1}{8}$	6527892

Table 5.0.1 shows the four models and their respective mesh densities and number of degrees of freedom. The number of degrees of freedom for each model was obtained from the command window during the running process to analyze the results. The stress values from the other three models were obtained from each model's respective .f06 file. The five stress plots, fitted with logarithmic trendlines, to convey convergence are as follows. First, upper skin tensile stress for each model was obtained and compared as seen by Figure 5.0.0.1 , which shows the convergence plot for upper skin tensile stress.

Upper Skin Stress (Tension) vs DOFs

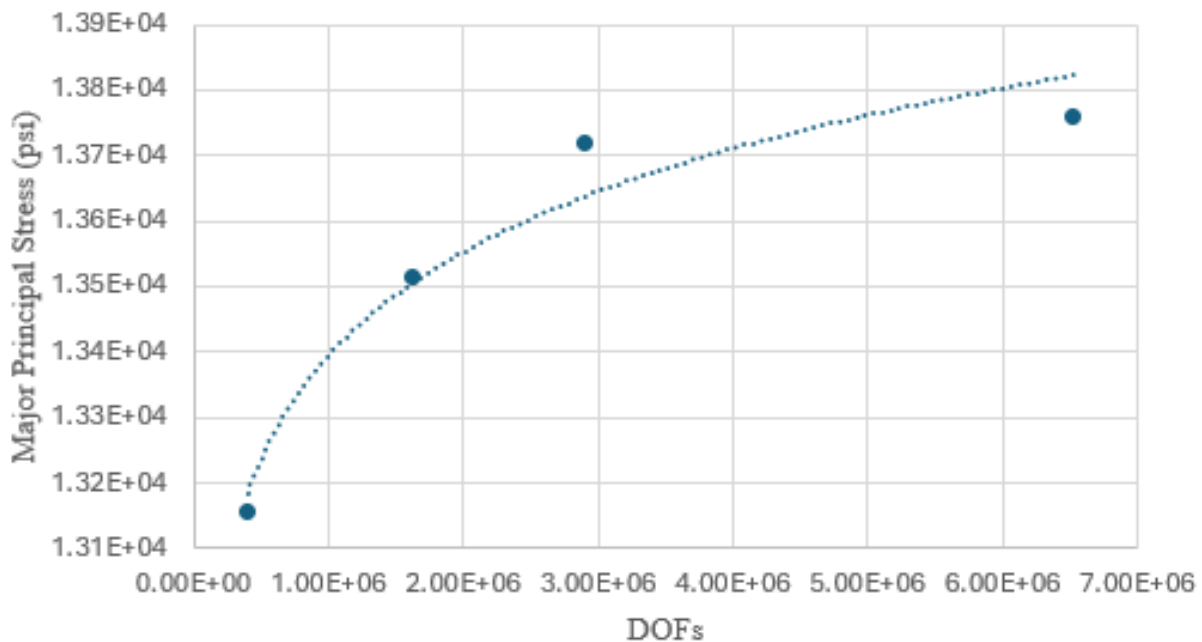


Fig. 5.0.0.1 Upper Skin Stress (Tension) vs DOFs

Secondly, lower skin compressive stress will be evaluated, shown in Figure 5.0.0.2 below.



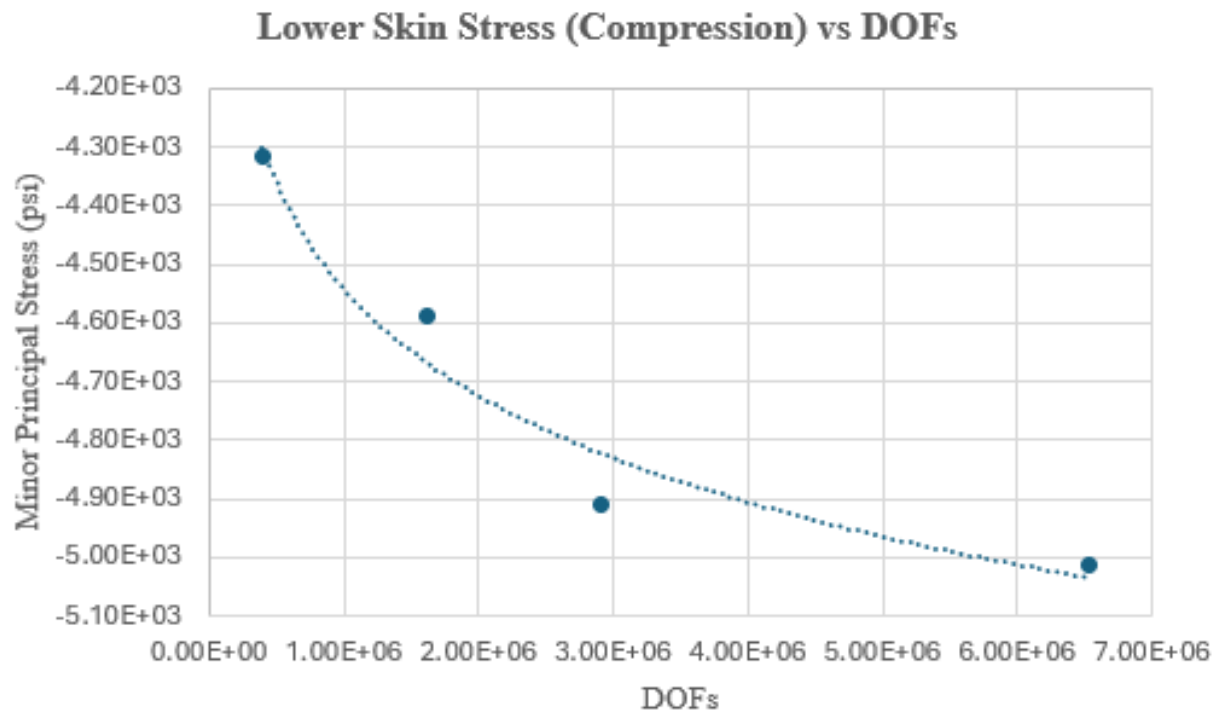


Fig. 5.0.0.2 Lower Skin Stress (Compression) vs DOFs

Figure 5.0.0.2 shows the convergence plot for lower skin compressive stress. Thirdly, spar web tensile stress will be evaluated in Figure 5.0.0.3 below.



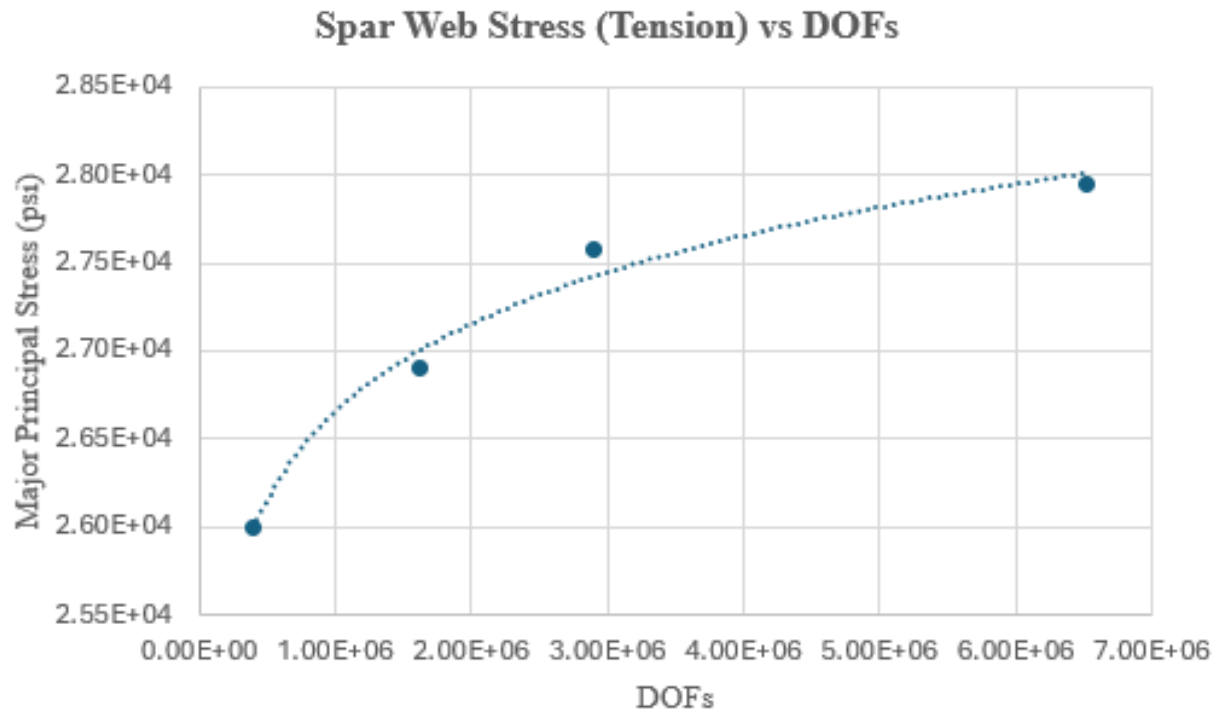


Fig. 5.0.0.3 Spar Web Stress (Tension) vs DOFs

Figure 5.0.0.3 shows the convergence plot for spar web tensile stress. Next, rib web compressive stress will be evaluated in Figure 5.0.0.4 below.



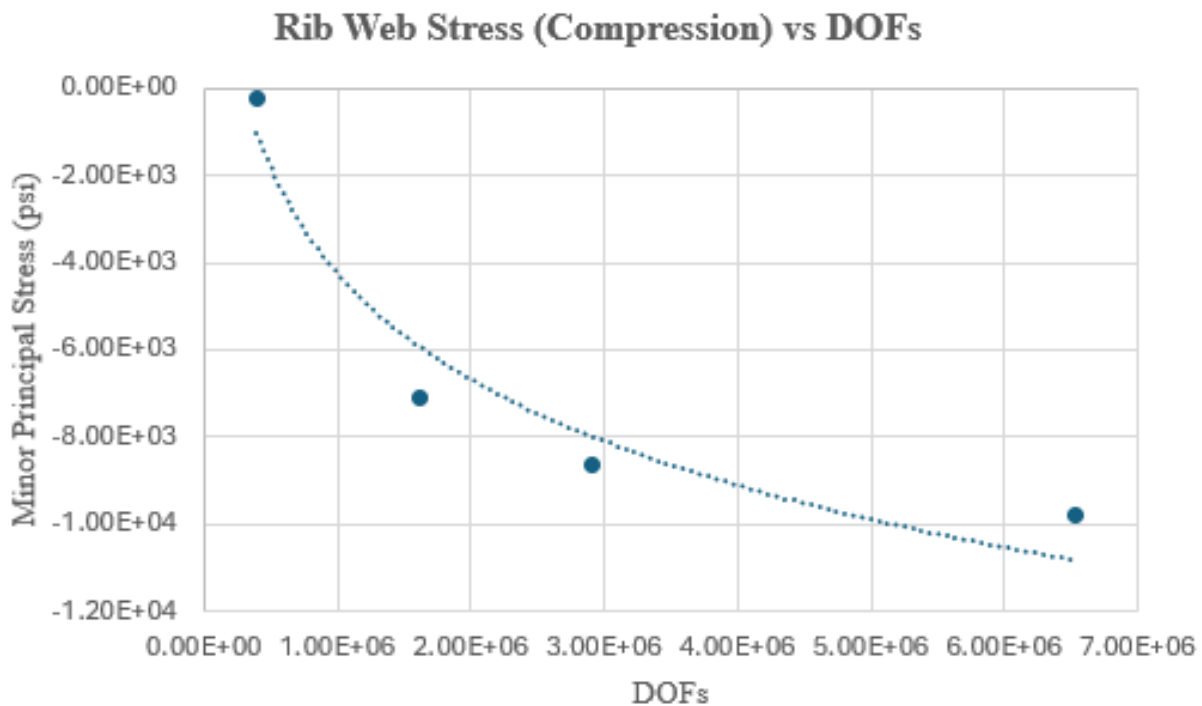


Fig. 5.0.0.4 Rib Web Stress (Compression) vs DOFs

Figure 5.0.0.4 shows the convergence plot for rib web compressive stress. Finally, rib web tensile stress will be evaluated in Figure 5.0.0.5 below.



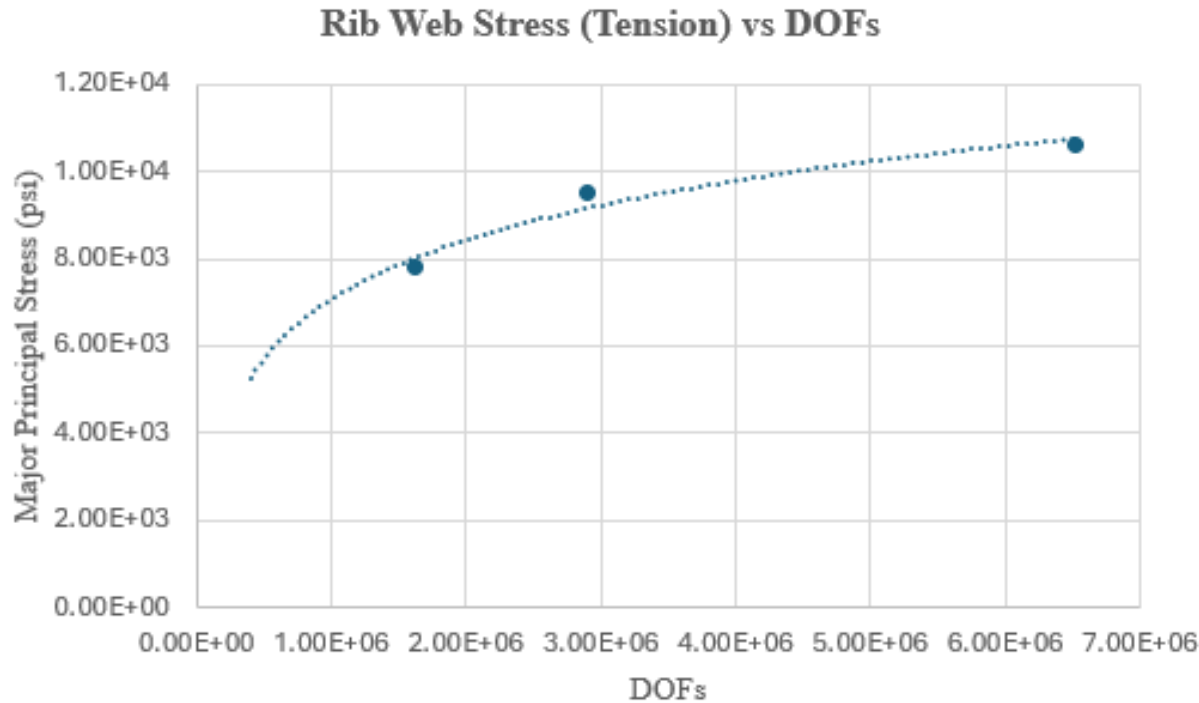


Fig. 5.0.0.5 Rib Web Stress (Tension) vs DOFs

Figure 5.0.0.5 shows the convergence plot for rib web tensile stress. Each of these five convergence plots indicates a level of convergence within the models. This suggests that a more refined mesh density is adequate for capturing the various stresses within the outboard section of the wing. Following these convergence plots, the selected model used for this report had an element mesh density of $\frac{1}{8}$ in, as outlined in Table 5.0.1 .

Verification of the approximate pressure distribution for the outboard section of the wing can be seen in Figure 5.0.0.6

SUBCASE/ DAREA ID	LOAD TYPE	OLOAD RESULTANT					
		T1	T2	T3	R1	R2	R3
1	FX	3.807993E-06	----	----	----	1.223570E-05	6.390951E-04
	FY	----	-1.189816E+01	----	4.558696E+01	----	2.435865E+02
	FZ	----	----	2.250000E+03	-6.096212E+05	3.439961E+04	----
	MX	----	----	----	0.000000E+00	----	----
	MY	----	----	----	----	0.000000E+00	----
	MZ	----	----	----	----	----	0.000000E+00
	TOTALS	3.807993E-06	-1.189816E+01	2.250000E+03	-6.095756E+05	3.439961E+04	2.435872E+02
MSC.NASTRAN JOB CREATED ON 30-APR-25 AT 09:58:55							
MAY 3, 2025 MSC Nastran 5/13/24 PAGE 10							

Fig. 5.0.0.6 O-Load Values from .f06 File

Figure 5.0.0.6 shows the O-Load Resultants for both translation and rotation in the x, y, and z axes. The pressure distribution load in the z-direction as seen in Figure 5.0.0.6 is 2250 lbf. This load meets the guideline specified in Design Project [5]. Further verification of the actual model itself is evident in Figure 5.0.0.7 as seen below.



LOAD SEQ. NO. 1 EPSILON **1.2874441E-07** EXTERNAL WORK 5.8136409E+03 EPSILONS LARGER THAN 0.001 ARE FLAGGED WITH ASTERisks
 MSC.NASTRAN JOB CREATED ON 30-APR-25 AT 09:58:55 MAY 3, 2025 MSC Nastran 5/13/24 PAGE 11

Fig. 5.0.0.7 Epsilon Value from .f06 File

Figure 5.0.0.7 shows the epsilon value for the chosen model. A relatively small epsilon value indicates that the degrees of freedom at each of the nodes within the model are compatible. This is further verification that the chosen model does not contain substantial errors in compatible elements and nodes.

Another check to verify the integrity of the model is the verify element boundaries function within the meshing section. By using this, the model can be checked for unexpected free edges. The model was checked and no free edges were found to exist in incorrect locations.

The last check of the model before running it through the NASTRAN solver was an equivalence check. This functionality will check for and correct duplicate nodes. The final version of the model passed the equivalence check, showing there are no duplicate nodes that could cause large issues in the model validity.

A verification of element coordinate system in the rib and spar webs was conducted to ensure reporting of the shear-xy stress from the .f06 was consistent with element orientation. Figure 5.0.0.8 and Figure 5.0.0.9 display the rib and spar web elements in WS 1 while Figure 5.0.0.10 and Figure 5.0.0.11 display the rib and spar web elements in WS 2, respectively.

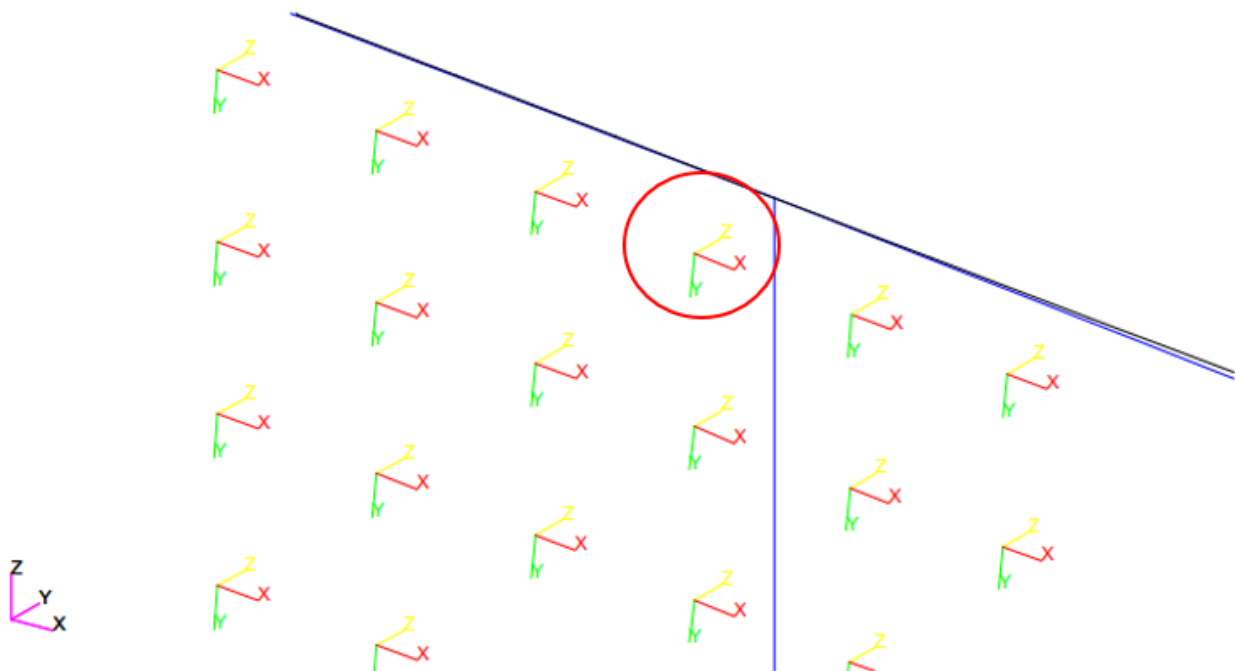


Fig. 5.0.0.8 Zoomed Region of Interest for Inboard Rib Web WS 1 with Element Local Coordinate Systems



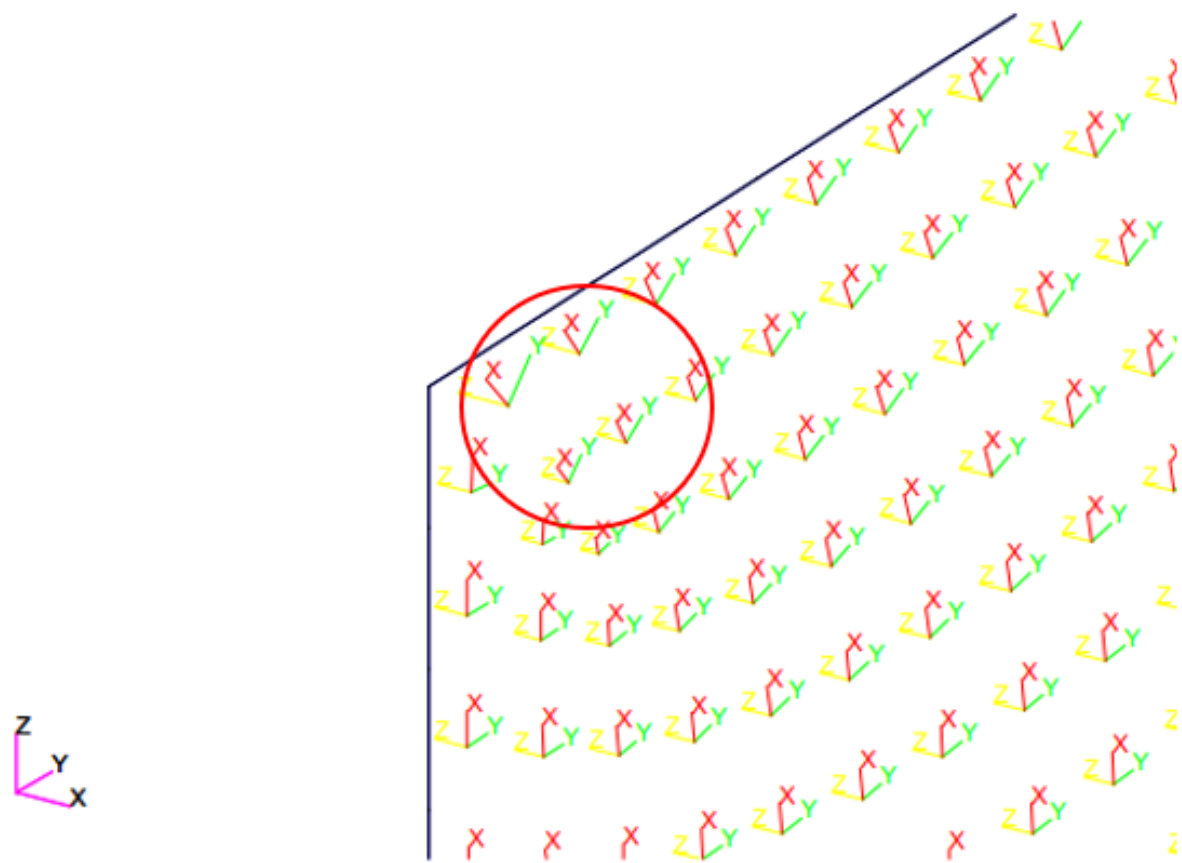


Fig. 5.0.0.9 Zoomed Region of Interest for FWD Spar Web WS 1 with Element Local Coordinate Systems

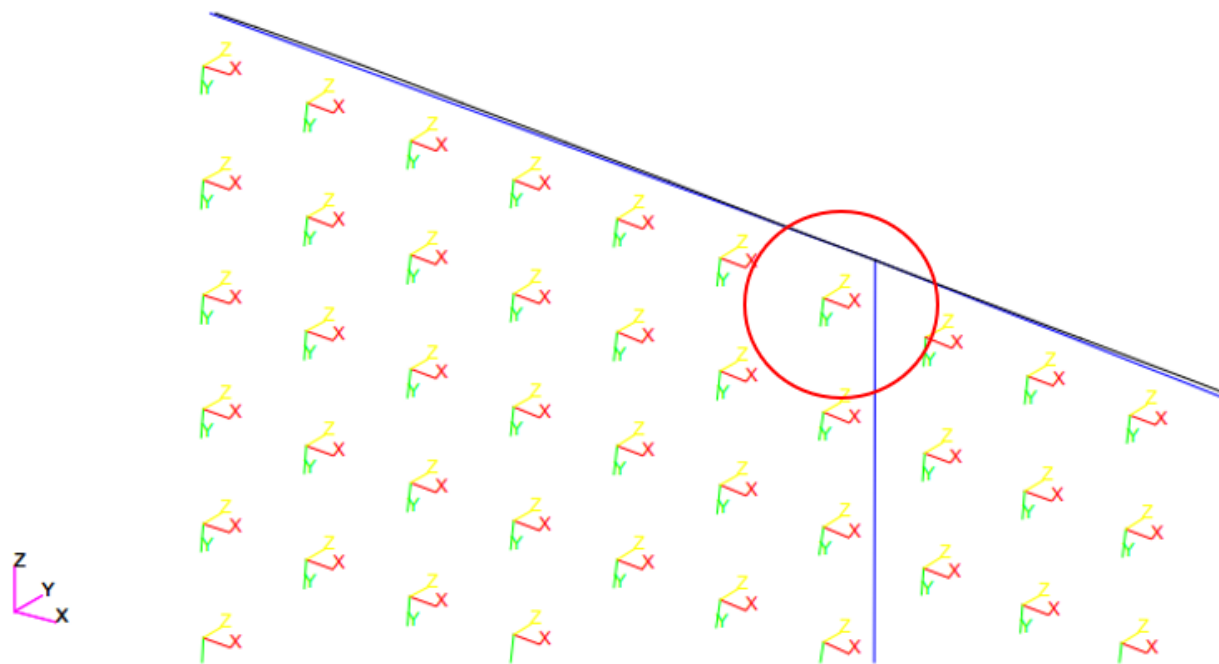


Fig. 5.0.0.10 Zoomed Region of Interest for Inboard Rib Web WS 2 with Element Local Coordinate Systems

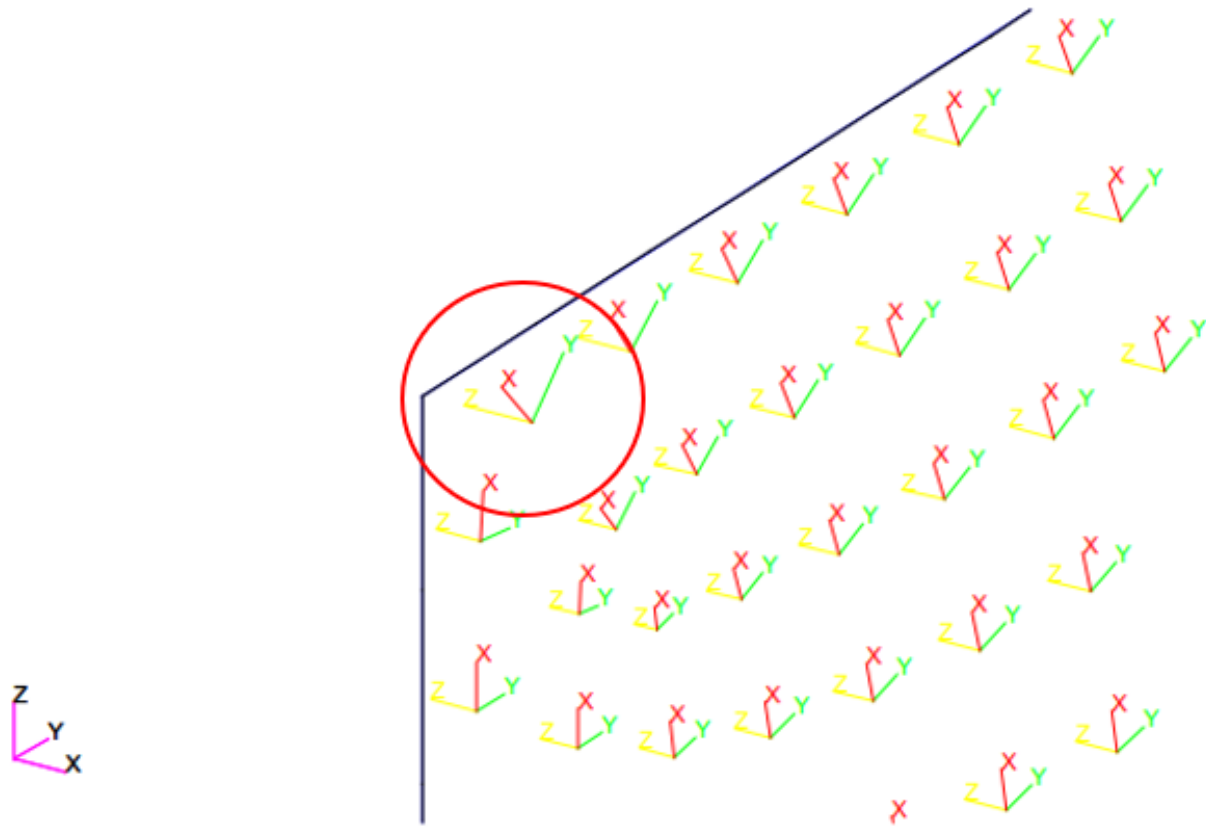


Fig. 5.0.0.11 Zoomed Region of Interest for FWD Spar Web WS 2 with Element Local Coordinate Systems

6. Results and Analysis

6.1 Wing Section 1

6.1.1 Upper Skin

Tension The first analysis of the wing upper skin is the absolute maximum tensile and compressive stress analysis. In this, the respective material allowable stresses are compared with the stresses output from the Patran [1] model in order to see if the skin will fail purely in tension or compression. The first failure mode that is analyzed is the maximum (tensile) stress. Figure 6.1.1.1 below shows the fringe plot results for maximum principal stress within the top skin of the first wing section.

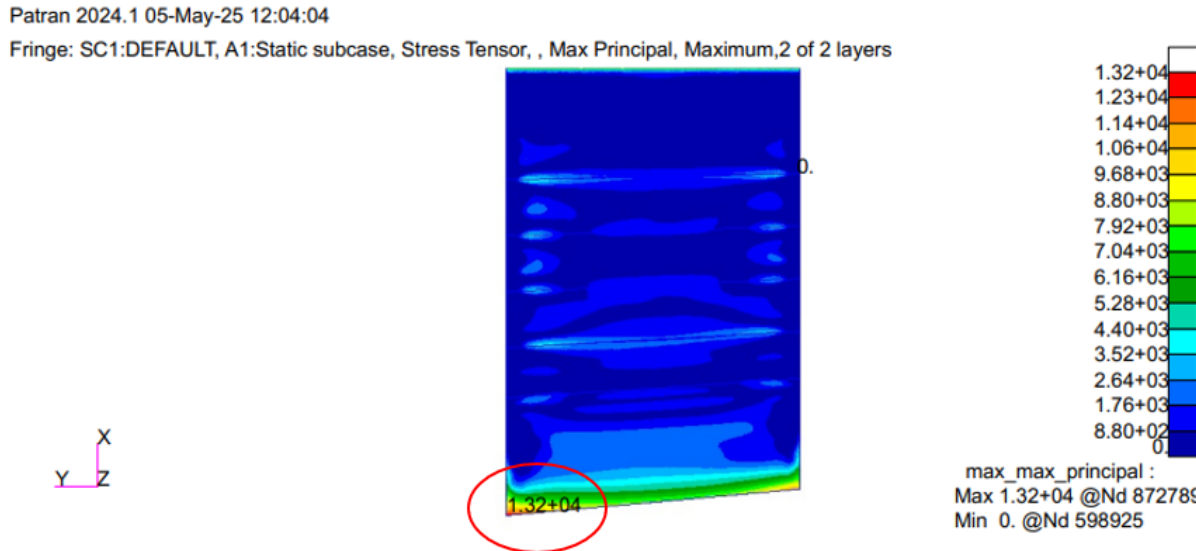


Fig. 6.1.1.1 Fringe: SC1:DEFAULT, A1: Static Subcase, Stress Tensor, Max Principal, Maximum, 2 of 2 layers of Upper Skin for WS 1

Taking a closer look at the high-stress region located in the aft-inboard area, Figure 6.1.1.2 a shows a zoomed view of the fringe results in the region of interest and the meshing of the Elements in the surrounding area.

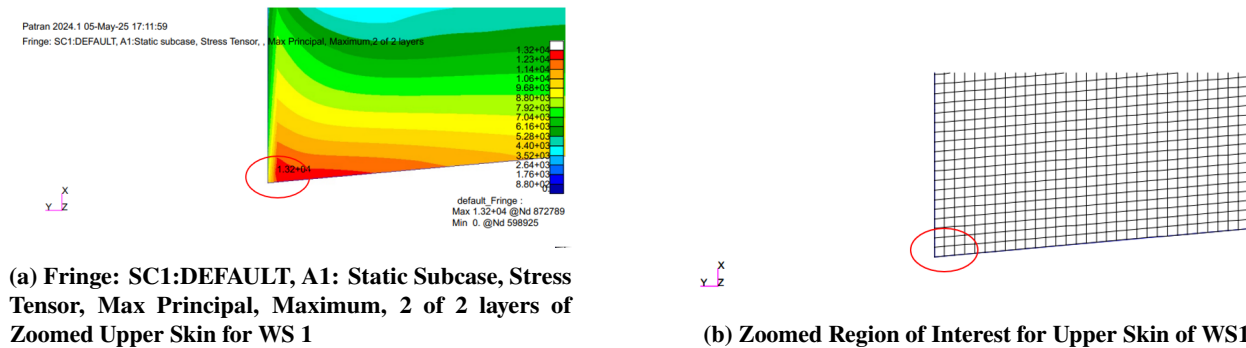


Fig. 6.1.1.2 Zoomed Fringe and Elements of Interest for Upper Skin Max Stress in WS1

Further zooming into the region of interest, a specific element of interest can be identified. In this case, the element of interest is Element 846994 which is surrounded by Nodes 25706, 466430, 872789, and 23637. Element 846994 and



the surrounding nodes are identified in Figure 6.1.1.3 below.

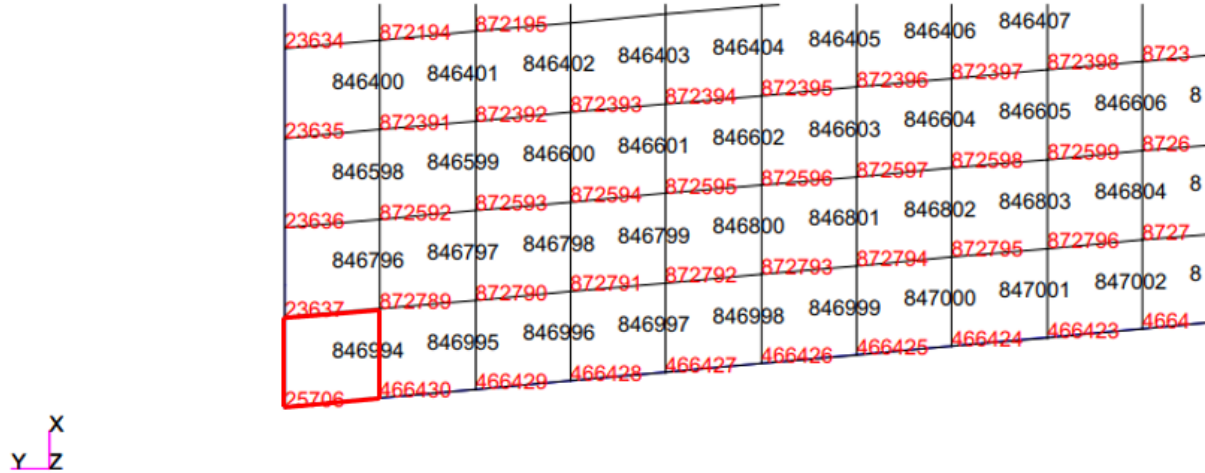


Fig. 6.1.1.3 Upper Skin Max Stress Element of Interest in WS1

The .f06 file generated by the NASTRAN run can be searched for Element 846994, where a maximum major stress of 1.38×10^4 is found. Figure 6.1.1.4 shows the location of this stress value within the .f06 file.

STRESSES IN QUADRILATERAL ELEMENTS (QUAD 4)								OPTION = BILIN	
ELEMENT ID	FIBER GRID-ID	DISTANCE	STRESSES IN ELEMENT COORD SYSTEM			PRINCIPAL STRESSES (ZERO SHEAR)			VON MISES
			NORMAL-X	NORMAL-Y	SHEAR-XY	ANGLE	MAJOR	MINOR	
0 846994	CEN/4	-1.75000E-02	1.052891E+04	-2.004020E+02	-1.339979E+03	-7.0122	1.069373E+04	-3.652196E+02	1.088094E+04
		1.75000E-02	1.359327E+04	7.129605E+02	-7.800601E+02	-3.4531	1.364034E+04	6.658903E+02	1.331988E+04
23637	-1.75000E-02	1.031878E+04	-3.421692E+02	-1.325418E+03	-6.9817	1.048109E+04	-5.044801E+02	1.074222E+04	
	1.75000E-02	1.347704E+04	5.278455E+02	-7.676271E+02	-3.3807	1.352239E+04	4.824994E+02	1.328771E+04	
872789	-1.75000E-02	1.031920E+04	-5.935140E+01	-1.337043E+03	-7.2241	1.048868E+04	-2.288316E+02	1.060495E+04	
	1.75000E-02	1.347764E+04	8.976895E+02	-7.828306E+02	-3.5472	1.352617E+04	8.491623E+02	1.312221E+04	
466430	-1.75000E-02	1.073912E+04	-5.858661E+01	-1.354546E+03	-7.0423	1.090645E+04	-2.259180E+02	1.102115E+04	
	1.75000E-02	1.370953E+04	8.981385E+02	-7.924974E+02	-3.5263	1.375836E+04	8.493017E+02	1.335398E+04	
25706	-1.75000E-02	1.073859E+04	-3.414753E+02	-1.342914E+03	-6.8129	1.089903E+04	-5.019145E+02	1.115845E+04	
	1.75000E-02	1.370887E+04	5.282020E+02	-7.772875E+02	-3.3633	1.375455E+04	4.825223E+02	1.351975E+04	

Fig. 6.1.1.4 .f06 NASTRAN Results for Upper Skin Max Stress in WS1

First, the upper skin's tensile stress margin of safety is calculated to check if the panel fails at tensile yield stress. This is done using Equation 9,

$$M.S.UST1 = \frac{F_{ty}^{2024-T3S}}{FS \times F_{MXMXP}_{846994}} - 1, \quad (9)$$

where $F_{ty}^{2024-T3S}$ is the tensile yield stress as previously outlined in Table 3.2.1 , FS is the factor of safety, and F_{MXMXP}_{846994} is the major principle stress value circled in Figure 6.1.1.4 for Element 846994. Plugging in the values,

$$M.S.UST1 = \frac{4 \times 10^4 \text{ psi}}{1.5 \times (1.38 \times 10^4 \text{ psi})} - 1, \quad (10)$$



$$\underline{\underline{M.S.}_{UST1}} = 0.938. \quad (11)$$

This result yields a positive margin of safety at limit load and the value is less than one which is considered ideal in the optimization of the structure.

Compression The next type of upper skin analysis is compression. In order to show possible compressive stress concentrations, a minimum principal stress fringe plot is used, which can be seen in Figure 6.1.1.5 .

Patran 2024.1 05-May-25 12:09:19

Fringe: SC1:DEFAULT, A1:Static subcase, Stress Tensor, , Min Principal, Minimum,2 of 2 layers

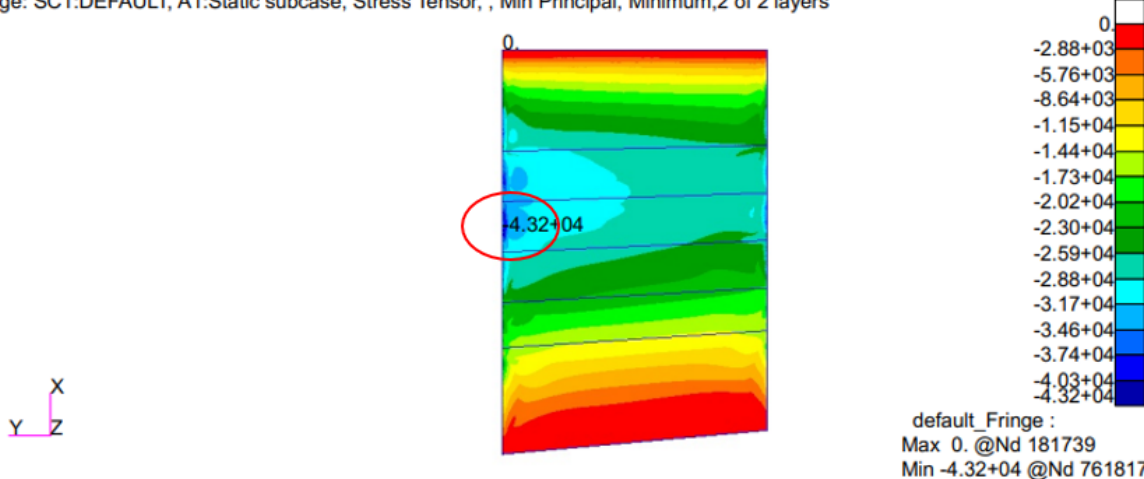


Fig. 6.1.1.5 Fringe: SC1:DEFAULT, A1: Static Subcase, Stress Tensor, Min Principal, Minimum, 2 of 2 layers of Upper Skin for WS 1

A zoomed view into the fringe plot around the region of concentrated minimum stress is shown in Figure 6.1.1.6 a along side 6.1.1.6 b which shows the meshing of this region of interest.

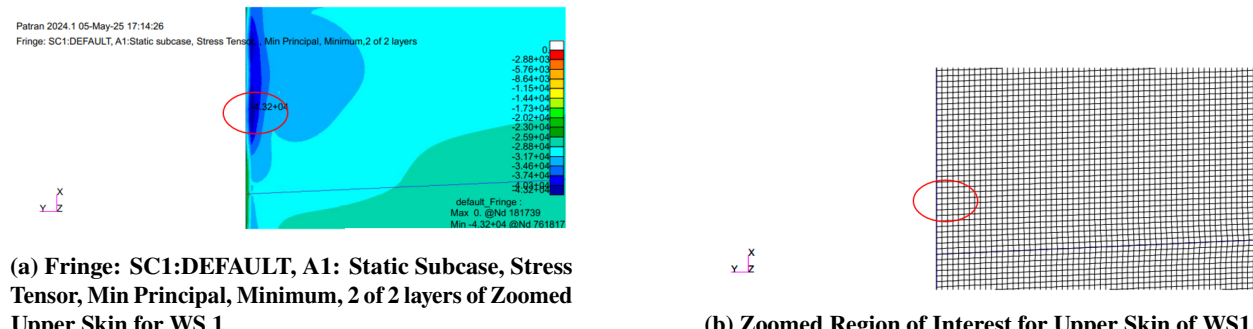


Fig. 6.1.1.6 Zoomed Fringe and Elements of Interest for Upper Skin Min Stress in WS1

Zooming in further to the region of interest, Element 739519 can be identified as the specific element of interest, which is surrounded by Nodes 761618, 17636, 17637, and 761817. The highlighted element of interest and surrounding nodes is show in Figure 6.1.1.7 .



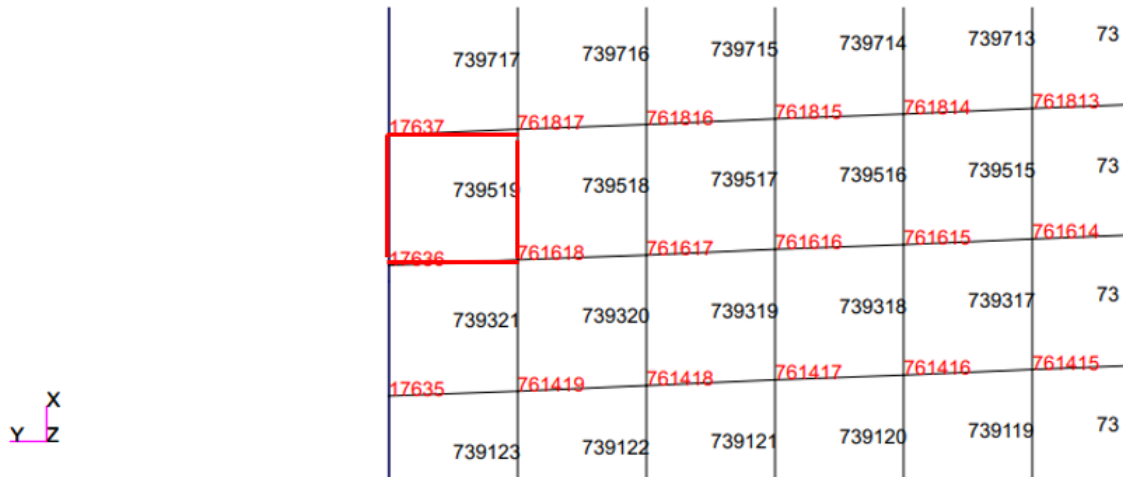


Fig. 6.1.1.7 Upper Skin Min Stress Element of Interest in WS1

The .f06 file output by the NASTRAN run can be searched for Element 739519, where a maximum major stress of -4.6×10^4 is found. Figure 6.1.1.8 shows the location of this stress value within the .f06 file.

STRESSES IN QUADRILATERAL ELEMENTS (QUAD4)							OPTION = BILIN		
ELEMENT ID	GRID-ID	FIBER DISTANCE	STRESSES IN ELEMENT COORD SYSTEM			PRINCIPAL STRESSES (ZERO SHEAR)			
			NORMAL-X	NORMAL-Y	SHEAR-XY	ANGLE	MAJOR	MINOR	
739519	CEN/4	-1.750000E-02	-4.591532E+04	-1.016551E+04	-7.580470E+02	-88.7858	-1.014944E+04	-4.593139E+04	4.179146E+04
		1.750000E-02	-1.974740E+04	-2.376812E+03	3.089252E+01	89.8981	-2.376757E+03	-1.974745E+04	1.867287E+04
761618		-1.750000E-02	-4.600317E+04	-9.939979E+03	-7.606264E+02	-88.7923	-9.923943E+03	-4.601920E+04	4.194711E+04
		1.750000E-02	-1.964906E+04	-2.545599E+03	3.217559E+01	89.8922	-2.545539E+03	-1.964912E+04	1.850811E+04
17636		-1.750000E-02	-4.600328E+04	-1.039106E+04	-7.519759E+02	-88.7909	-1.037519E+04	-4.601915E+04	4.180848E+04
		1.750000E-02	-1.964900E+04	-2.207984E+03	2.570152E+01	89.9156	-2.207946E+03	-1.964904E+04	1.864338E+04
17637		-1.750000E-02	-4.582754E+04	-1.039099E+04	-7.554676E+02	-88.7793	-1.037489E+04	-4.584364E+04	4.163718E+04
		1.750000E-02	-1.984567E+04	-2.208065E+03	2.960892E+01	89.9038	-2.208015E+03	-1.984572E+04	1.883901E+04
761817		-1.750000E-02	-4.582731E+04	-9.939914E+03	-7.641201E+02	-88.7808	-9.923651E+03	-4.584358E+04	4.177531E+04
		1.750000E-02	-1.984586E+04	-2.545674E+03	3.608541E+01	89.8805	-2.545599E+03	-1.984593E+04	1.870351E+04

Fig. 6.1.1.8 .f06 NASTRAN Results for Upper Skin Min Stress in WS1

The compressive stress margin of safety for the upper skin is calculated to check if the panel fails at compressive yield stress. This is done using Equation 12,

$$M.S.USC1 = \frac{F_{cy}^{2024-T3S}}{FS \times |F_{MNMNP}_{739519}|} - 1, \quad (12)$$

where $F_{cy}^{2024-T3S}$ is the compressive yield stress as previously outlined in Table 3.2.1 and F_{MNMNP}_{739519} is the major principle stress value circled in Figure 6.1.1.8 for Element 739519. Plugging in the values,

$$M.S.USC1 = \frac{3.7 \times 10^4 \text{ psi}}{1.5 \times |-4.6 \times 10^4 \text{ psi}|} - 1, \quad (13)$$



$$\underline{\underline{M.S.USC1 = -0.464}} \quad (14)$$

This result yields a negative margin of safety at limit load, leading to the reasoning that this section of skin will fail in compression under the given load.

Buckling The final failure type to analyze for the upper skin is compression buckling. A conservative approach to compression buckling analysis is used in which the minimum principal stress is used, seeing how this would be the absolute maximum compressive stress any element would experience. This value is the same value from Figure 6.1.1.8 above, located in Element 739519. To perform the margin of safety analysis, Equation 15, as seen below, is used.

$$M.S.USB1 = \frac{\sigma_{cr\ 739519}}{FS \times |F_{MNMNP\ 739519}|} - 1, \quad (15)$$

where $\sigma_{cr\ 739519}$ is the skin buckling stress as defined by skin material properties and section geometry, as shown in Equation 16 below.

$$\sigma_{cr\ 739519} = C_{SS1} \frac{\pi^2 E_{2024-T3S}}{12(1 - \nu_{2024-T3S}^2)} \left(\frac{t_{skin}}{b_{SS1}} \right)^2 \quad (16)$$

The skin thickness and panel length can be found in Table 3.1.1 , and Young's modulus and Poisson's ratio can be found in Table 3.2.4 . The last variable needed is the compression buckling coefficient which is found from the graph given in the Curtis [2] text. The graph is used in combination with the aspect ratio as defined in Table 3.1.1 in order to get the compression buckling coefficient, C_{SS1} . The buckling coefficients curves are shown in Figure 6.1.1.9 below.



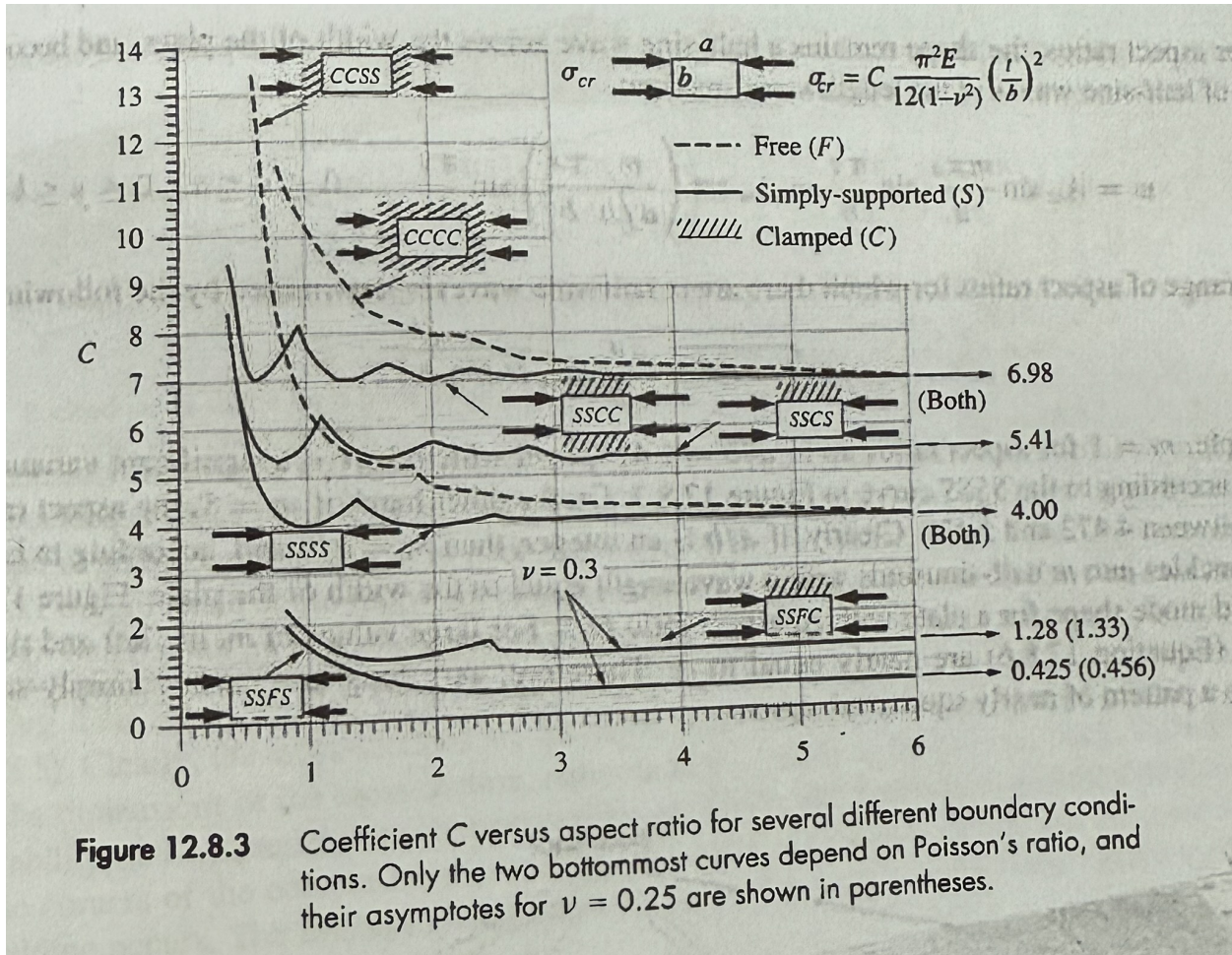


Fig. 6.1.1.9 Compression Buckling Coefficient Graph From Curtis [2] Text

An average of the clamped, $C_{clamped}$, and simply supported, C_{ss} , curves is taken at the aspect ratio of 5.55 to get a compression buckling coefficient, as shown in Equation 17.

$$C_{SS1} = \frac{C_{ss} + C_{clamped}}{2} \quad (17)$$

$$C_{SS1} = \frac{6.98 + 4.00}{2} \quad (18)$$

$$C_{SS1} = 5.49 \quad (19)$$

Substituting into Equation 16 to solve for σ_{cr} gives the following:

$$\sigma_{cr} = 5.49 \frac{\pi^2 \times 1.05 \times 10^7 \text{ psi}}{12(1 - 0.33^2)} \left(\frac{0.035 \text{ in}}{4.43 \text{ in}} \right)^2 \quad (20)$$

$$\sigma_{cr} = 3.32 \times 10^3 \text{ psi} \quad (21)$$

Finally, plugging this value into Equation 15 along with F_{MNMNP} from Figure 6.1.1.8 the margin of safety for



the skin section can be calculated.

$$M.S.USB1 = \frac{3.32 \times 10^3 \text{ psi}}{1.5 \times | - 4.6 \times 10^4 \text{ psi} |} - 1, \quad (22)$$

$$\underline{\underline{M.S.USB1 = -0.952}} \quad (23)$$

Though the previous section showed that the material fails in pure compression, the buckling analysis shows that the panel will also fail in buckling. The large negative value of the calculated margin of safety leads to the belief that this section of skin will fail in compression buckling long before it fails in pure compression.

6.1.2 Lower Skin

Tension Figure 6.1.2.1 illustrates the distribution of the maximum principle stress present on the lower skin of Section 1. This region exhibits the highest stress values, which are primarily located on the most inboard elements, closest to the rib. The location of the peak stress and its magnitude are shown in Figure 6.1.2.1. For a more detailed view, Figure 6.1.2.2 a highlights the critical elements where the maximum stress occurs, providing a clearer picture of the stress concentration in this area.

Patran 2024.1 06-May-25 17:25:10

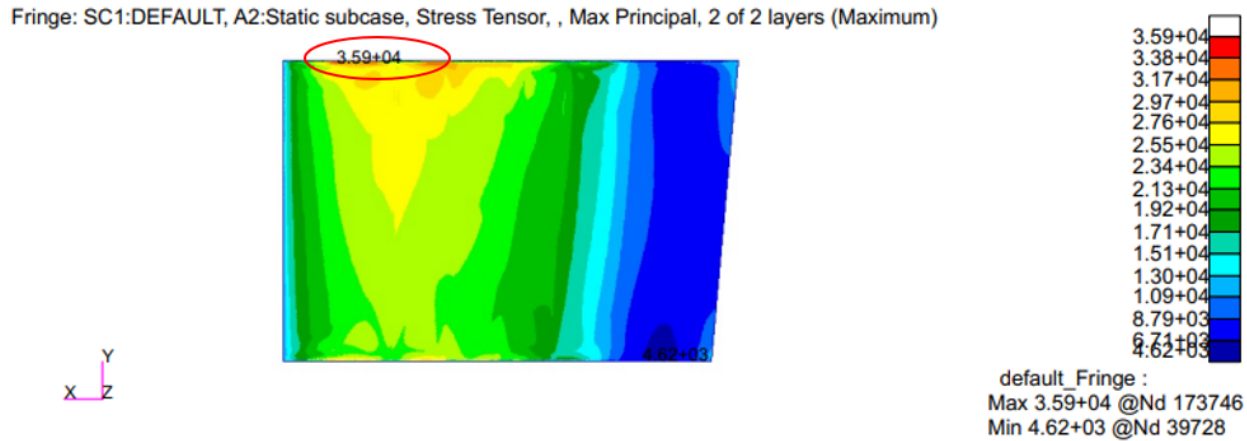
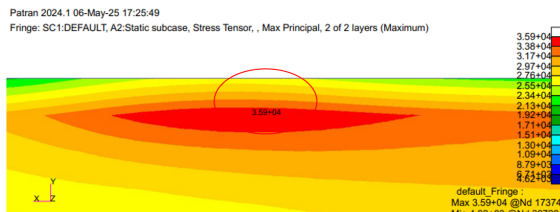
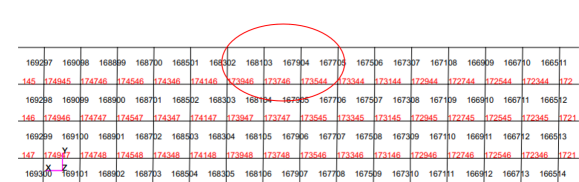


Fig. 6.1.2.1 Fringe: SC1:DEFAULT, A2: Static Subcase, Stress Tensor, Max Principal, 2 of 2 layers (Maximum) of Lower Skin for WS 1



(a) Fringe: SC1:DEFAULT, A2: Static Subcase, Stress Tensor, Max Principal, 2 of 2 layers (Maximum) of Zoomed Lower Skin for WS 1



(b) Zoomed Region of Lower Skin for WS1

Fig. 6.1.2.2 Zoomed Fringe and Elements of Interest for Lower Skin on WS1



manufacturing processes, and operating conditions. This accounts for uncertainties and potential variations in material properties, manufacturing processes, and operating conditions. F_{MXMXP}_{167904} is the maximum principle stress at Element 167904, located in the critical region of the wing. This stress value is obtained from the finite element analysis results, and in this case, it is 3.85×10^4 psi.

The margin of safety equation essentially compares the applied stress with the material strength, scaled by the safety factor, and then subtracts one to express the difference relative to the allowable strength. The result indicates whether the material can withstand the applied loads without failure.

Next, the known values are substituted into the equation:

$$M.S.LST1 = \frac{4.00 \times 10^4 \text{ psi}}{1.5 \times 3.85 \times 10^4 \text{ psi}} - 1, \quad (25)$$

After performing the calculation:

$$\underline{\underline{M.S.LST1 = -0.31}} \quad (26)$$

This result indicates that the margin of safety for the wing component is -0.31. A negative margin of safety suggests that the applied stresses exceed the material's allowable strength, even with the safety factor applied. In other words, the component is likely to fail under the given loading conditions.

Compression In contrast to the tension analysis, Figure 6.1.2.4 presents the distribution of the minimum principle stress over the lower skin of Section 1, with a closer view shown in Figures 6.1.2.5 a and 6.1.2.5 b. This stress distribution differs from the maximum principle stress distribution and is located more outboard within the section. The region of interest shifts slightly compared to the tension zone, highlighting areas where compressive stresses dominate.

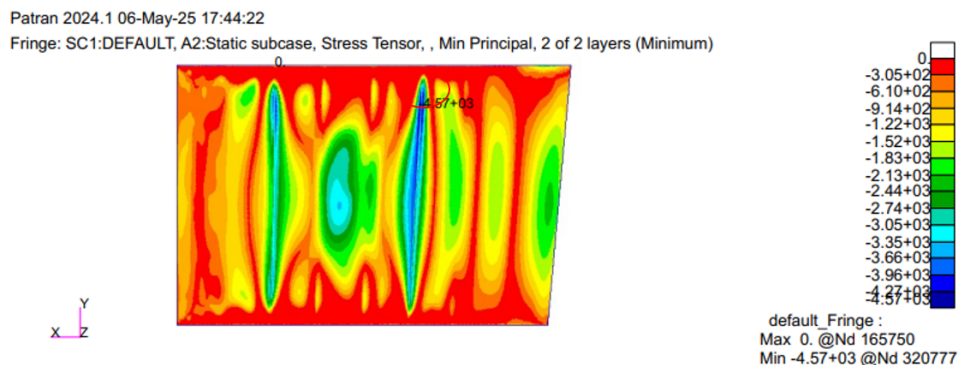
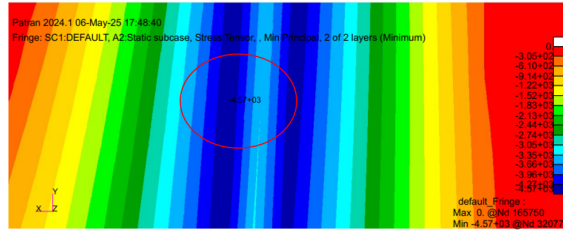


Fig. 6.1.2.4 Fringe: SC1:DEFAULT, A2: Static Subcase, Stress Tensor, Min Principal, 2 of 2 layers (Minimum) of Lower Skin for WS 1





(a) Fringe: SC1:DEFAULT, A2: Static Subcase, Stress Tensor, Min Principal, 2 of 2 layers (Minimum) of Zoomed Lower Skin for WS1

077	310879	310881	310483	310285	310887	309889	309891	309894	457235	457234	457233	457232	457231	457230	457229	457228	457227
078	310880	310882	310484	310286	310888	309890	309892	309895	457201	457200	457199	457198	457197	457196	457195	457194	457193
079	310881	310883	310485	310287	310889	309891	309893	309896	457197	457196	457195	457194	457193	457192	457191	457190	457189
80	310882	310884	310486	310288	310890	309892	309894	309897	457197	457196	457195	457194	457193	457192	457191	457190	457189
81	310883	310885	310487	310289	310891	309893	309895	309898	457199	457198	457197	457196	457195	457194	457193	457192	457191
82	310884	310886	310488	310290	310892	309894	309896	309899	457195	457194	457193	457192	457191	457190	457189	457188	457187
3310885	310887	310489	310291	310893	309895	309897	309899	457190	457191	457192	457193	457194	457195	457196	457197	457198	

(b) Zoomed Region of Lower Skin of WS1

Fig. 6.1.2.5 Zoomed Fringe and Elements of Interest for Lower Skin on WS1

In addition, Figure 6.1.2.6 presents the .f06 NASTRAN results for the lower skin in Section 1 under compressive loading conditions. The data reveals critical compressive stresses in elements located more outboard compared to the tension case.



$$M.S._{LSC1} = \frac{3.70 \times 10^4 \text{ psi}}{1.5 \times |-5.01 \times 10^3 \text{ psi}|} - 1, \quad (28)$$

After performing the calculation:

$$\underline{\underline{M.S._{LSC1} = 3.92}} \quad (29)$$

This result indicates that the margin of safety for the component under compressive loading is 3.92. A positive margin of safety suggests that the material can withstand compressive stress with a comfortable margin, indicating that the design is structurally sound under the given loading conditions.

6.1.3 Spar Web

The two stresses analyzed for the forward spar web are shear in the xy direction and shear buckling, respectively. Figure 6.1.3.1 indicates the shear stress gradients in the xy direction for the forward spar web.

Patran 2024.1 05-May-25 11:48:49

Fringe: SC1:DEFAULT, A1:Static subcase, Stress Tensor, XY Component, Maximum,2 of 2 layers

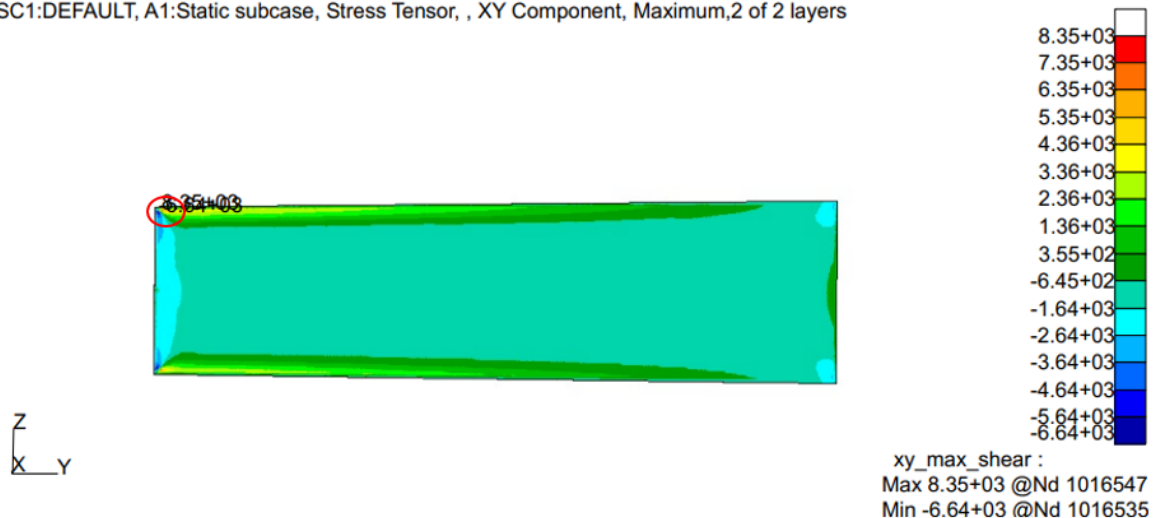


Fig. 6.1.3.1 Fringe: SC1:DEFAULT, A1: Static Subcase, Stress Tensor, XY Component, Maximum, 2 of 2 layers of Forward Spar Web for WS 1

Figure 6.1.3.1 shows the fringe plot of shear stress in the xy direction for the forward spar web. The area of interest in the web is outlined by the red circle as seen in the upper left region of the plot. Typically it is best practice to use a seventy percent shear gradient to capture the shear stress throughout the panel. For this preliminary analysis, the most conservative approach to capturing shear stress will be taken from the maximum xy shear stress values. For clarity, a closer look at the region of interest will be shown in Figures 6.1.3.2 a and 6.1.3.2 b below.



Patran 2024.1 05-May-25 12:25:01

Fringe: SC1:DEFAULT, A1:Static subcase, Stress Tensor, XY Component, Maximum, 2 of 2 layers

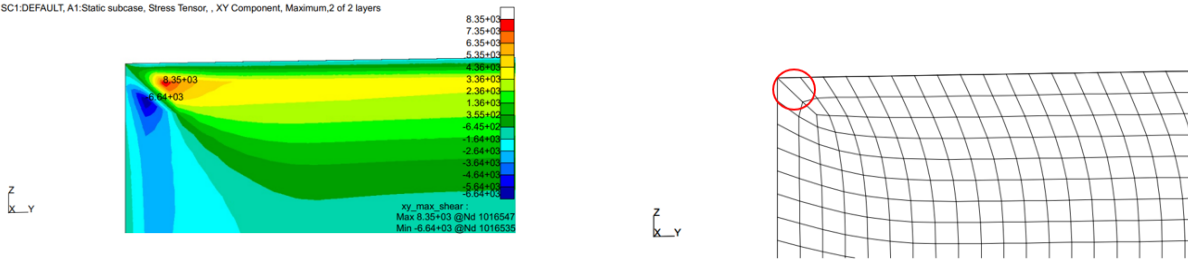


Fig. 6.1.3.2 Zoomed Fringe and Elements of Interest for Forward Spar Web for WS 1

Figure 6.1.3.2 a shows opposing shear stresses in close proximity to each other. Figure 6.1.3.2 b shows unequal angle elements near the upper left corner of the spar web. These unequal angle elements yield inaccurate shear stress results. An ideal discretization of the spar web would consist of perfectly rectangular elements with no skewed interior angles. A closer view of the element of interest is shown in Figure 6.1.3.3 .

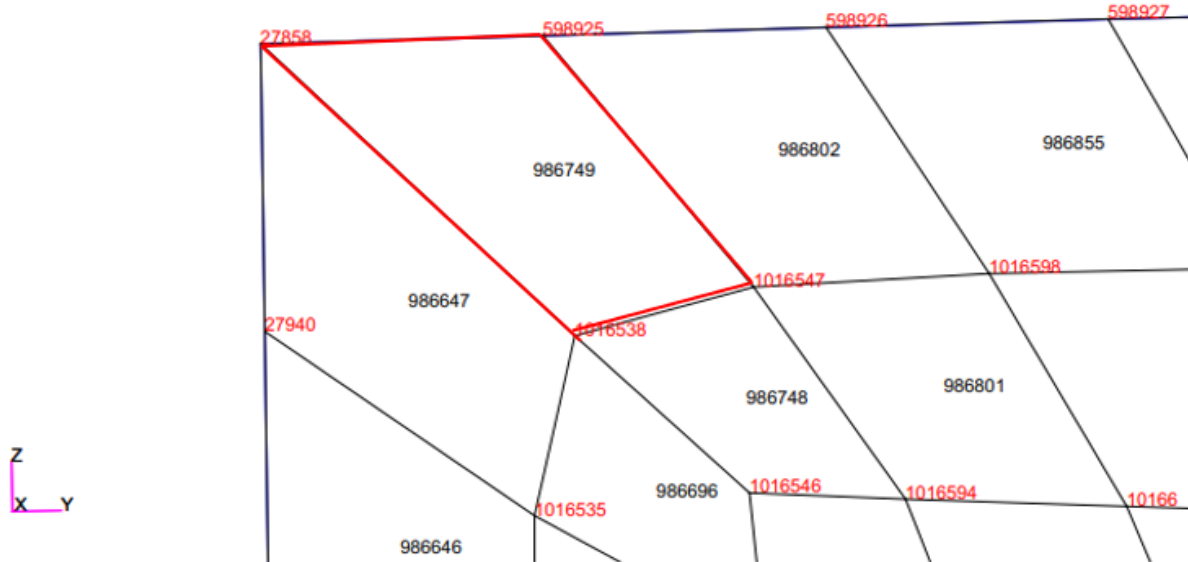


Fig. 6.1.3.3 Element of Interest for Forward Spar Web for WS 1

As seen in Figure 6.1.3.3 Element 986749 outlined in red is the element of interest that contains the absolute maximum shear value in the xy direction. Figure 6.1.3.4 is an excerpt of the.f06 file results from NASTRAN concerning maximum shear in the xy direction for the forward spar web.



STRESSES IN QUADRILATERAL ELEMENTS (QUAD 4)								OPTION = BILIN	
ELEMENT ID	FIBER GRID-ID	DISTANCE	STRESSES IN ELEMENT COORD SYSTEM			PRINCIPAL STRESSES (ZERO SHEAR)			VON MISES
			NORMAL-X	NORMAL-Y	SHEAR-XV	ANGLE	MAJOR	MINOR	
986748	CEN/4	-3.000000E-02	-7.101292E+03	-1.724615E+04	9.226198E+03	30.5993	-1.645081E+03	-2.270236E+04	2.192616E+04
		3.000000E-02	-7.855190E+03	-1.739442E+04	8.888734E+03	30.8912	-2.537247E+03	-2.271236E+04	2.155602E+04
1016546		-3.000000E-02	-7.414263E+03	-1.726305E+04	9.285329E+03	31.0306	-1.828328E+03	-2.284898E+04	2.199189E+04
		3.000000E-02	-8.090007E+03	-1.774222E+04	9.070565E+03	30.9921	-2.641561E+03	-2.319067E+04	2.198921E+04
1016538		-3.000000E-02	-7.315695E+03	-1.724708E+04	9.262339E+03	30.9018	-1.771914E+03	-2.279086E+04	2.195859E+04
		3.000000E-02	-7.911163E+03	-1.709227E+04	8.774129E+03	31.1909	-2.599265E+03	-2.240416E+04	2.122424E+04
1016547		-3.000000E-02	-6.905878E+03	-1.723521E+04	9.189115E+03	30.3311	-1.529498E+03	-2.261158E+04	2.188695E+04
		3.000000E-02	-7.704668E+03	-1.715714E+04	8.766297E+03	30.8346	-2.471723E+03	-2.239008E+04	2.126225E+04
1016594		-3.000000E-02	-6.811791E+03	-1.724209E+04	9.176245E+03	30.1945	-1.472260E+03	-2.258162E+04	2.188266E+04
		3.000000E-02	-7.751911E+03	-1.765969E+04	8.980320E+03	30.5586	-2.449722E+03	-2.296188E+04	2.184030E+04
986749	CEN/4	-3.000000E-02	-9.953760E+03	-1.886086E+04	1.139678E+04	34.3279	-2.171271E+03	-2.664335E+04	2.562679E+04
		3.000000E-02	-1.009400E+04	-1.911814E+04	1.033202E+04	33.2044	-3.331789E+03	-2.588035E+04	2.438577E+04
1016538		-3.000000E-02	-1.093392E+04	-1.667454E+04	1.047427E+04	37.3376	-2.943799E+03	-2.466466E+04	2.333246E+04
		3.000000E-02	-1.020518E+04	-1.715169E+04	9.387825E+03	34.8484	-3.668703E+03	-2.368817E+04	2.208356E+04
27858		-3.000000E-02	-1.176716E+04	-2.092716E+04	1.267569E+04	35.0671	-2.869418E+03	-2.982490E+04	2.849874E+04
		3.000000E-02	-1.112032E+04	-2.094261E+04	1.137586E+04	33.3247	-3.640763E+03	-2.842216E+04	2.678799E+04
598925		-3.000000E-02	-9.314285E+03	-2.127344E+04	1.248044E+04	32.2001	-1.454904E+03	-2.913282E+04	2.843330E+04
		3.000000E-02	-1.015389E+04	-2.128260E+04	1.139837E+04	31.9899	-3.034202E+03	-2.840229E+04	2.701330E+04
1016547		-3.000000E-02	-7.517612E+03	-1.617559E+04	9.722940E+03	32.9999	-1.203495E+03	-2.248971E+04	2.191276E+04
		3.000000E-02	-8.727415E+03	-1.674812E+04	8.971109E+03	32.9570	-2.911084E+03	-2.256445E+04	2.125893E+04

Fig. 6.1.3.4 .f06 NASTRAN Results for Forward Spar Web Shear Stress for WS 1

Figure 6.1.3.4 confirms the node of interest within Element 986749 and provides the respective xy shear stress value. First, the spar web's shear stress margin of safety equation is calculated to check if the panel fails at ultimate shear stress. This is done using the following equation, as seen in Equation 30,

$$M.S._{SWS1} = \frac{F_{su\ 2024-T3S}}{1.5 \times FS \times F_{SXY\ 986749}} - 1, \quad (30)$$

where $F_{su\ 2024-T3S}$ is as previously outlined in Table 3.2.1 and $F_{SXY\ 986749}$ is the xy-shear value circled in Figure 6.1.3.4 for Element 986749. Plugging in the values,

$$M.S._{SWS1} = \frac{3.80 \times 10^4 \text{ psi}}{1.5 \times 1.5 \times (12.6757 \times 10^3 \text{ psi})} - 1, \quad (31)$$

$$\underline{\underline{M.S._{SWS1} = 0.332}} \quad (32)$$

This result yields a positive margin of safety at ultimate load and the value is less than one which is considered ideal in the optimization of the structure.

Focusing on the shear buckling analysis, Equation 33 is used to calculate the shear buckling allowable for the spar web.

$$\tau_{cr\ SW1} = K_{s\ SW} \frac{\pi^2 E_{2024-T3}}{12(1 - v_{2024-T3}^2)} \left(\frac{t_{SW}}{b_{SW1}} \right)^2, \quad (33)$$

where $\tau_{cr\ SW1}$ is the allowable buckling stress of the spar web, $K_{s\ SW}$ is the spar shear-buckling-stress coefficient, $E_{2024-T3}$ is the elastic modulus for a 2024 – T3 aluminum sheet, $v_{2024-T3}$ is Poisson ratio, t_{SW} is the thickness of the



spar web and b_{SW1} is the height of the spar web.

To obtain $K_{s_{SW}}$ the graph seen in Figure 6.1.3.5 is used.

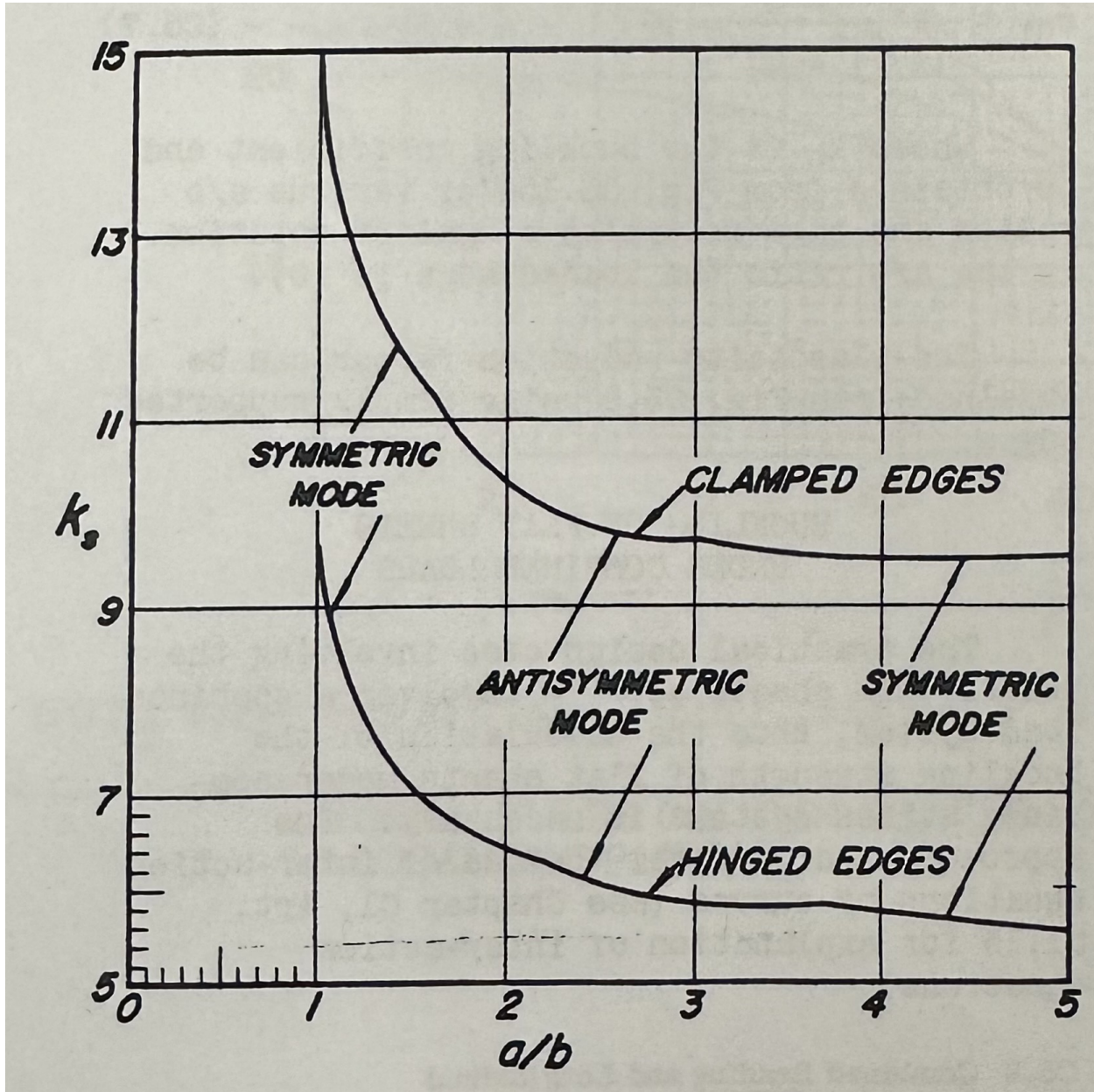


Fig. 6.1.3.5 Shear-Buckling-Stress Coefficient as a Function of $\frac{a}{b}$ via Ewing [3]

Figure 6.1.3.5 shows the shear-buckling-stress coefficient as a function of aspect ratio ($\frac{a}{b}$). Since the spar web is clamped between the upper and lower spar caps, the clamped curve will be used. Obtaining the aspect ratio for the spar web from Table 3.1.1, the value for $K_{s_{SW}}$ is thus:

$$K_{s_{SW}} = 9.5. \quad (34)$$



Using values from Table 3.1.1 and Table 3.2.4 , the buckling allowable from Equation 33 is thus:

$$\tau_{cr\ SW1} = 9.5 \times \frac{\pi^2 \times (1.05 \times 10^7 \text{ psi})}{12(1 - 0.33^2)} \left(\frac{0.06 \text{ in}}{5.54 \text{ in}} \right)^2, \quad (35)$$

$$\tau_{cr\ SW1} = 10817.3 \text{ psi} \quad (36)$$

To determine the shear buckling margin of safety, Equation 37 is used below.

$$M.S._{SWSB1} = \frac{\tau_{cr\ SW1}}{1.5 \times FS \times F_{SXY\ 986749}} - 1, \quad (37)$$

where $M.S._{SWSB1}$ is the margin of safety in the forward spar web that accounts for shear buckling, and τ_{cr} is the material allowable obtained from Table 3.2.1 , and $F_{SXY\ 986749}$ is xy direction shear stress in Element 986749 at Node 27858. Substituting and solving:

$$M.S._{SWSB1} = \frac{10817.3 \text{ psi}}{1.5 \times 1.5 \times 12675.69 \text{ psi}} - 1, \quad (38)$$

$$\underline{\underline{M.S._{SWSB1} = -0.621}} \quad (39)$$

The negative results indicates that the structure will fail at ultimate shear despite having a factor of safety. Essentially, the spar web should be redesigned/resized to account for shear buckling at ultimate shear stress.

6.1.4 Rib Web

The two methods of analysis used for the inboard rib web are shear stress in the xy direction and shear buckling, respectively. Figure 6.1.4.1 indicates the shear stress gradients in the xy direction for the inboard rib web.

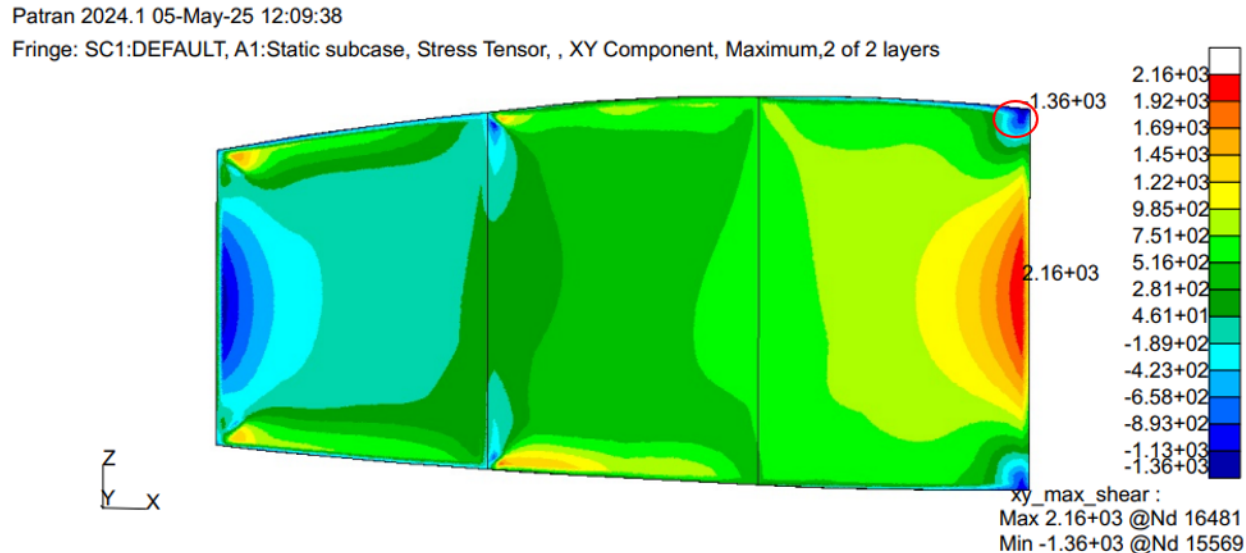


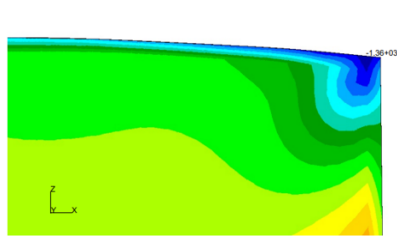
Fig. 6.1.4.1 Fringe: SC1:DEFAULT, A1: Static Subcase, Stress Tensor, XY Component, Maximum, 2 of 2 layers of Inboard Rib Web for WS 1

6.1.4.1 shows the fringe plot of shear stress in the xy direction for the inboard rib web. Typically it is best practice

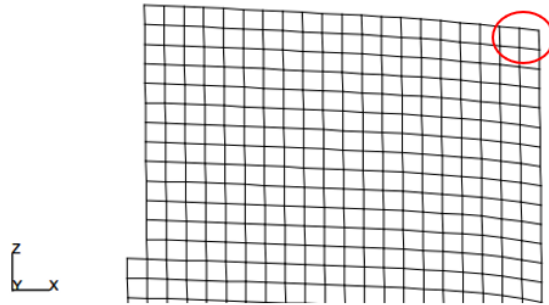


to use a seventy percent shear gradient to capture the shear stress throughout the panel. For the purposes of this preliminary analysis, the most conservative approach to capturing shear stress will be taken from the maximum xy shear stress values. The area of interest in the web is indicated by the red circle in the upper right region of the plot. A rectangular approximation of the rib sheet was made due to the complex curvature present in the wing's airfoil shape. This rectangular approximation is a conservative approximation because the resulting rectangular panel has a larger aspect ratio than compared to the exact shape of the wing's airfoil. For clarity, a closer look at the region of interest will be visible in Figures 6.1.4.2 a and 6.1.4.2 b below.

Patran 2024.1 05-May-25 14:08:06
Fringe: SC1:DEFAULT, A1:Static subcase, Stress Tensor, XY Component, Maximum,2 of 2 layers



(a) Fringe: SC1:DEFAULT, A1: Static Subcase, Stress Tensor, XY Component, Maximum, 2 of 2 layers of Zoomed Inboard Rib Web for WS 1



(b) Zoomed Region of Interest for Inboard Rib Web for WS 1

Fig. 6.1.4.2 Zoomed Fringe and Elements of Interest for Inboard Rib Web for WS 1

Figure 6.1.4.2 a shows a shear stress gradient that concentrates near the corner of the rib web. Figure 6.1.4.2 b shows the quad Elements the rib web is composed of and the region of interest indicated by the red circle. A closer view of Figure 6.1.4.2 b to identify the specific Element will be shown in Figure 6.1.4.3 .

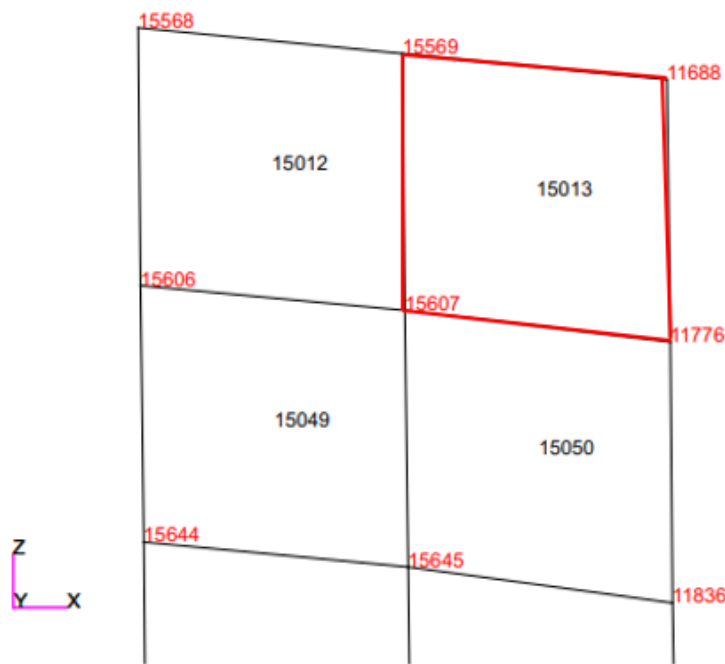


Fig. 6.1.4.3 Element of Interest for Inboard Rib Web for WS 1



$$M.S.RWS1 = \frac{1.90 \times 10^4 \text{ psi}}{1.5 \times 1.5 \times (2.88 \times 10^3 \text{ psi})} - 1, \quad (41)$$

$$\underline{\underline{M.S.RWS1 = 1.93}} \quad (42)$$

The result yields a positive margin of safety which indicates that the inboard rib web does not fail at shear ultimate. Due to the value being slightly over one, there could be additional material reduction or redesign to better optimize the structure for weight savings.

Next, focusing on the shear buckling analysis of the rib web, Equation 43 is used to calculate the shear buckling allowable.

$$\tau_{cr\ RW1} = K_{s\ 5052-H32S} \frac{\pi^2 E_{H32S}}{12(1 - \nu_{H32S}^2)} \left(\frac{t_{RW}}{b_{RW1}} \right)^2, \quad (43)$$

where $\tau_{cr\ RW1}$ is the shear stress in the rib web, $K_{s\ RW}$ is the rib shear-buckling-stress coefficient, $E_{5052-H32}$ and $\nu_{5052-H32}$ are the elastic modulus and Poisson's ratio for a 5052-H32 aluminum sheet used in the rib web, respectively, t_{RW} is the panel thickness of the rib web, and b_{RW1} is the height of the rib web. $K_{s\ RW}$ is obtained in the same way as in the spar web by using Figure 6.1.3.5. Since the rib web is clamped between the wings spar and the lower and upper skin, the clamped curve will be used. This is also a conservative estimate due to clamped elements having higher resulting stresses than a comparatively loaded hinged edge element. Using the $(\frac{a}{b})$ ratio as described in Table 3.1.1, the resulting value for $K_{s\ RW}$ is:

$$K_{s\ RW} = 10. \quad (44)$$

Now, using the remaining values from Table 3.1.1 and Table 3.2.3, Equation 43 becomes,

$$\tau_{cr\ RW1} = 10 \times \frac{\pi^2 \times (1.01 \times 10^7 \text{ psi})}{12(1 - 0.33^2)} \left(\frac{0.06 \text{ in}}{2.19 \text{ in}} \right)^2, \quad (45)$$

$$\tau_{cr\ RW1} = 8742.49 \text{ psi}. \quad (46)$$

The margin of safety for rib web shear buckling can be calculated using Equation 47,

$$M.S.RWSB1 = \frac{\tau_{cr\ RW1}}{1.5 \times FS \times F_{SXY15013}} - 1, \quad (47)$$

and plugging in the values becomes,

$$M.S.RWSB1 = \frac{8742.49 \text{ psi}}{1.5 \times 1.5 \times (2878.52 \text{ psi})} - 1, \quad (48)$$

$$\underline{\underline{M.S.RWSB1 = 0.350}} \quad (49)$$

The positive MS indicates that the rib web is sized appropriately to resist buckling in shear. While MS values less than one are considered adequate, the rib web can be made more efficient by reducing the panel thickness.



6.1.5 Upper Skin Stringer

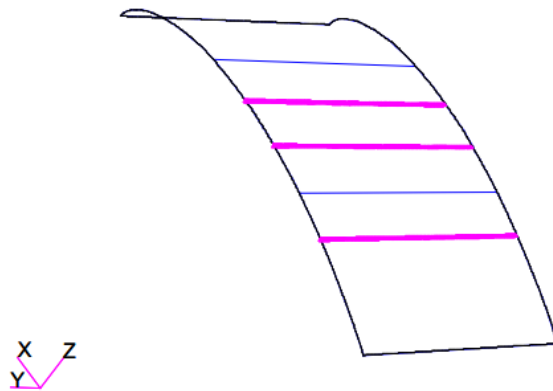


Fig. 6.1.5.1 Geometry of Upper Skin and Stringer

Tension Figure 6.1.5.2 presents the maximum combined stress observed on the aftmost upper stringer. It also highlights the region of interest.

Patran 2024.1 07-May-25 02:48:57

Fringe: SC1:DEFAULT, A1:Static subcase, Bar Stresses, Maximum Combined, , At Center



Fig. 6.1.5.2 Fringe: SC1:DEFAULT, A1: Static Subcase, Bar Stresses, Maximum Combined, At Center of Upper Stringers for WS 1

This region of interest, shown in Figure 6.1.5.3, contains the critical element that will be used to further analyze the tension stresses within the upper stringer.



$$M.S.USST1 = \frac{F_{ty} \text{ 2024-T3S}}{FS \times F_{MNMNP} \text{ 1311526}} - 1, \quad (50)$$

where $F_{ty} \text{ 2024-T3S}$ is the tensile yield stress as previously outlined in Table 3.2.1 , FS is the factor of safety, and $F_{MNMNP} \text{ 1311526}$ is the minor principle stress value circled in Figure 6.1.5.4 . for Element 1311526.

Plugging in the values,

$$M.S.USST1 = \frac{3.40 \times 10^4 \text{ psi}}{1.5 \times (4.88 \times 10^3 \text{ psi})} - 1, \quad (51)$$

$$\underline{M.S.USST1 = 3.64.} \quad (52)$$

A large positive margin of safety indicates that the element is oversized for the tension caused by this loading, meaning the element would not fail in tension.

Compression Figure 6.1.5.5 presents the minimum combined stress observed on the inboard upper stringer. It also highlights the region of interest.

Patran 2024.1 07-May-25 02:49:17

Fringe: SC1:DEFAULT, A1:Static subcase, Bar Stresses, Minimum Combined, , At Center

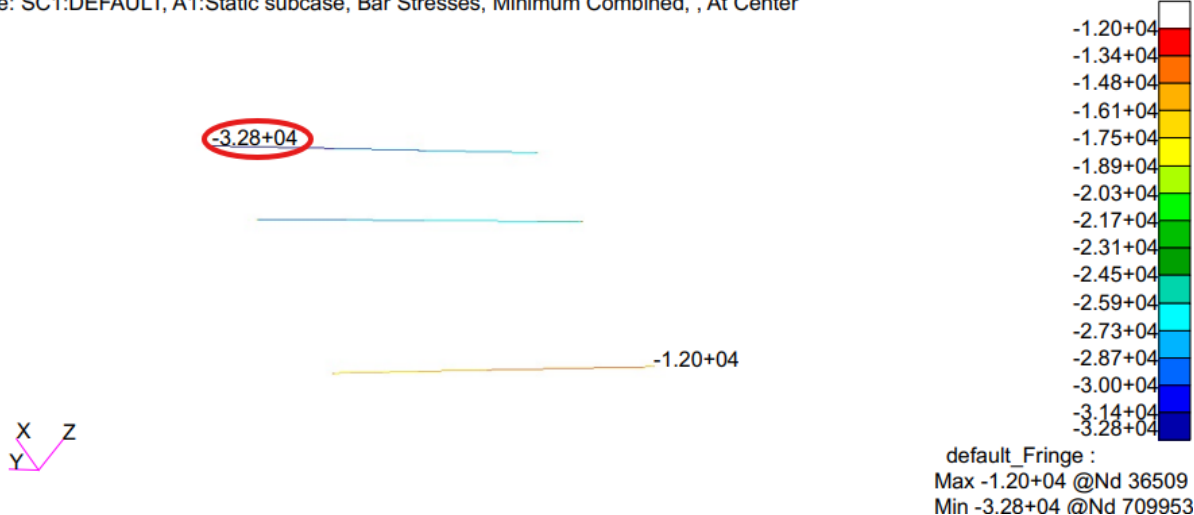


Fig. 6.1.5.5 Fringe: SC1:DEFAULT, A1: Static Subcase, Bar Stresses, Minimum Combined, At Center of Upper Stringers for WS 1

This region of interest, shown in Figure 6.1.5.6 , contains the element of interest that will be used to further analyze the compression stresses within the upper stringer.



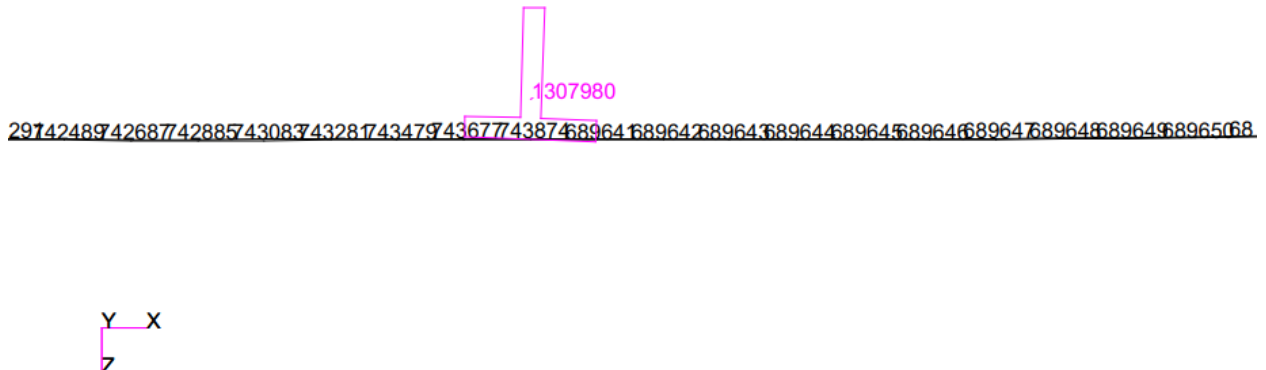


Fig. 6.1.5.6 Upper Stringer Min Stress Element of Interest and Surrounding Skin

The compressive stresses were taken from the resulting .f06, shown in Figure 6.1.5.7 .

ELEMENT ID.	S T R E S S E S I N B A R E L E M E N T S				(C B A R)		
	SA1 SB1	SA2 SB2	SA3 SB3	SA4 SB4	AXIAL STRESS	SA-MAX SB-MAX	SA-MIN SB-MIN
0 1307977	1.160964E+04 1.333688E+04	-4.829580E+03 -5.443785E+03	-5.471872E+03 -6.376395E+03	1.150688E+04 1.318767E+04	-2.653059E+04 -2.623821E+04	-1.492095E+04 -1.319371E+04	-3.200246E+04 -3.290698E+04
0 1307978	1.287570E+04 1.456506E+04	-5.239058E+03 -5.810032E+03	-6.170190E+03 -7.080672E+03	1.272672E+04 1.436176E+04	-2.623821E+04 -2.608021E+04	-1.336251E+04 -1.167315E+04	-3.240840E+04 -3.331888E+04
0 1307979	1.439725E+04 1.601195E+04	-5.735978E+03 -6.338602E+03	-7.005262E+03 -7.826192E+03	1.419417E+04 1.577393E+04	-2.608021E+04 -2.579685E+04	-1.168296E+04 -1.006826E+04	-3.308547E+04 -3.390640E+04
0 1307980	1.527714E+04 1.411426E+04	-5.943068E+03 -5.641117E+03	-7.557760E+03 -6.852063E+03	1.501879E+04 1.392051E+04	-2.579685E+04 -2.051971E+04	-1.051971E+04 -3.335461E+04	-3.264891E+04 -3.264891E+04
0 1307981	1.447600E+04 1.300711E+04	-5.822111E+03 -5.411146E+03	-6.996112E+03 -6.130336E+03	1.428816E+04 1.289204E+04	-2.601130E+04 -2.153530E+04	-1.153530E+04 -1.300419E+04	-3.300742E+04 -3.214164E+04

Fig. 6.1.5.7 .f06 NASTRAN Results for Upper Stringer Min Stress

$$M.S.USSC_1 = \frac{3.70 \times 10^4 \text{ psi}}{1.5 \times |(-3.33 \times 10^4 \text{ psi})|} - 1, \quad (53)$$

$$\underline{\underline{M.S.USSC_1 = -0.259}} \quad (54)$$

A negative margin of safety indicates that the element is over-sized for the compression caused by this loading, indicating the element would fail in compression.

Crippling and Buckling The MS for upper skin stringer crippling is as follows in Equation 55,

$$M.S.USSC_1 = \frac{P_{ccUSSC_1}}{1.5 \times FS \times P_{BSMNC1}_{1307980}} - 1, \quad (55)$$

where P_{ccUSSC_1} is the critical crippling load allowable for the upper skin stringer, and $P_{BSMNC1}_{1307980}$ is the load in the stringer due to the maximum compressive load. A unbuckled skin method will be used to calculate the properties



used in the stringer allowable value. First, F_{cc_n} needs to be found for each component of the stringer. Using the $(\frac{b}{t})$ ratio for the stringer flanges, using b and t values displayed in Table 3.1.2 , their respective F_{cc_n} values can be looked up using "Crippling Stresses for 2024-T4 Alcad Sheet" on page C6 of the Crippling Handout [6]. The graph and the respective lines can be seen in Figure 6.1.5.8 .

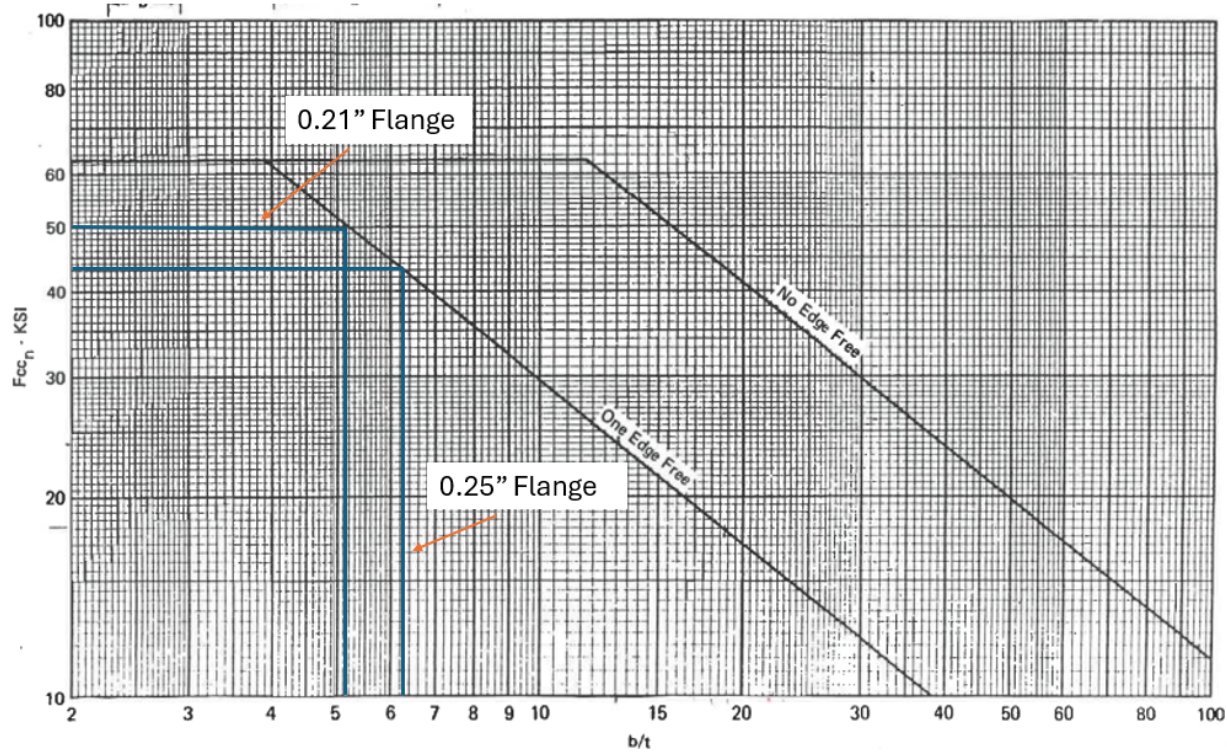


Fig. 6.1.5.8 Crippling Stresses for 2024-T4 ALCLAD Sheet Graphical Method on Page C6 of Crippling Methods Handout

The flange's crippling stress can then be summed together to get a total crippling stress, which can be seen in Equation 56

$$F_{cc_{totUSS1}} = \frac{\sum F_{cc_i} b_i t_i}{\sum b_i t_i}, \quad (56)$$

where $F_{cc_{totUSS1}}$ is the total crippling stress of the upper skin stringers, F_{cc_i} is the individual crippling stress of the flange elements, b_i and t_i are the individual width and thickness of the flange elements, respectively. For the upper skin stringer, this becomes,

$$F_{cc_{totUSS1}} = \frac{F_{cc1_{USS1}} b_{1USS1} t_{1USS1} + F_{cc2_{USS1}} b_{2USS1} t_{2USS1}}{b_{1USS1} t_{1USS1} + b_{2USS1} t_{2USS1}}, \quad (57)$$

$$F_{cc_{totUSS1}} = \frac{((4.40 \times 10^4 \text{ psi}) \times 0.25 \text{ in} \times 0.04 \text{ in}) + ((5.00 \times 10^4 \text{ psi}) \times 0.21 \text{ in} \times 0.04 \text{ in})}{0.25 \text{ in} \times 0.04 \text{ in} + 0.21 \text{ in} \times 0.04 \text{ in}}, \quad (58)$$

$$F_{cc_{totUSS1}} = 46739.13 \text{ psi}. \quad (59)$$

Now using page C4 of the Crippling Handout [6], the non-dimensional unbuckled skin width can be determined



with the stringer's crippling stiffness. This graphical method is demonstrated in Figure 6.1.5.9

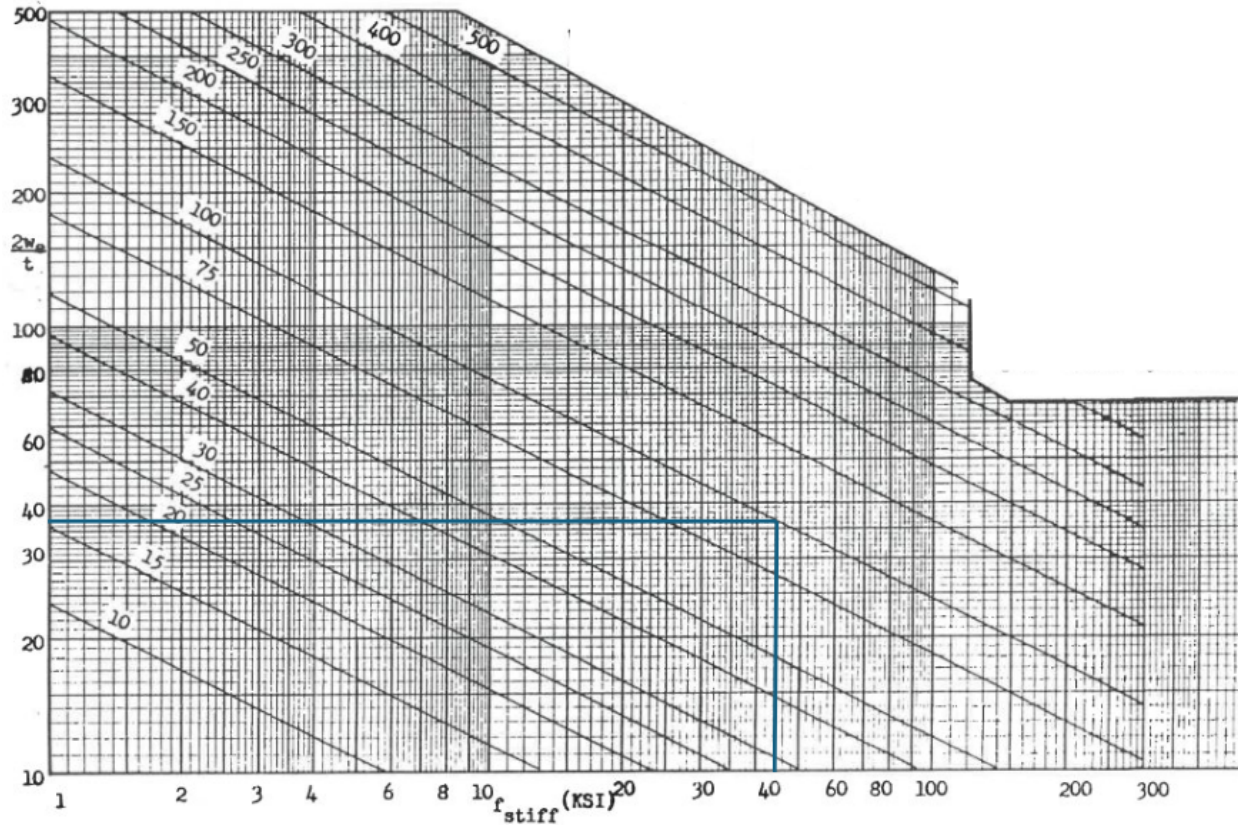


Fig. 6.1.5.9 Effective Width of Stiffened Sheet Graphical Determination Page on C6 of Crippling Methods Handout

After the non-dimensional effective skin width is determined, the dimension of the effective skin width can be found by multiplying this value with the sheet's thickness. For skins, this is shown in Equation 60.

$$w_{e\text{skin}} = \left(\frac{2w_e}{t} \right)_{\text{stringer}} \times \left(\frac{t_{USS1}}{2} \right), \quad (60)$$

where $\left(\frac{2w_e}{t} \right)_{\text{stringer}}$ is the stringer's non-dimensional effective sheet value and t_{USS1} is the sheet thickness of the wing skin.

$$w_{e\text{skin}} = 37 \times \left(\frac{0.035\text{in}}{2} \right), \quad (61)$$

$$w_{e\text{skin}} = 0.6475\text{in}. \quad (62)$$

The skin thickness and effective skin width can be multiplied together to get the area of the cross section. Then, the critical crippling load can be found for each element with Equation 63 below,

$$P_{cc\ USS_i} = F_{cc\ USS} \times A_{USS_i}, \quad (63)$$

where $P_{cc\ USS_i}$ is the upper skin stringer element critical load and A_{USS_i} is the upper skin stringer element area. The



following table, Table 6.1.1 , is a summary of this stringer crippling process. The final stringer-unbuckled skin critical load is highlighted in yellow. The elements critical load is found in the same way, by dividing the max compressive stress by the stringer area to get the critical load.

Table 6.1.1 Skin Stringer Unbuckled Crippling Table

Stringer Element	b (in)	t (in)	b/t (-)	$F_{cc_{tot}}$	$\frac{2w_e}{t}$	w_e (in)	Area (in^2)	P_{cc}
1	0.25	0.04	6.25	46739.1304	-	-	0.01	4.67E+02
2	0.21	0.04	5.25	46739.1304	-	-	0.0084	3.93E+02
3	-	0.035	N/A	46739.1304	37	0.6475	0.0227	1.06E+03
4	-	0.035	N/A	46739.1304	37	0.6475	0.0227	1.06E+03
Sum	-	-	-	-	-	-	0.0637	2978.4511

Now, the MS of the upper skin stringer can be calculated using the value displayed in Table 6.1.1 . The stress displayed in Figure 6.1.5.7 can be converted to a load using the same area used in converting the critical crippling stress to a critical load. Using Equation 55 from above, the process is as follows,

$$M.S.USSC_1 = \frac{2978.4511 \text{ lb}}{1.5 \times 1.5 \times (613.72 \text{ lb})} - 1, \quad (64)$$

$$\underline{\underline{M.S.USSC_1 = 1.16}} \quad (65)$$

The positive margin of safety indicates the structure is adequately sized according to the structural analysis applied to this structure. For future analysis, it would be more appropriate to take the margin of safety of the unbuckled skin stringer allowable against the summation of stringer and unbuckled skin loads. This would result in a lower margin of safety for this structural component.

The upper skin stringer also has the potential to fail in beam buckling. Instead of being located to local elements, beam buckling happens across the entire structural component. The following process follows the example calculation as outlined in Example 12.9.2 in Curtis [2]. First, flange element buckling stresses need to be found. This is outlined in Equation 66 below,

$$\sigma_{cc_{USSB1_1}} = \sigma_{cy_{T3E}} \times 0.546 \times \lambda_{USSB1_1}^{-0.8}, \quad (66)$$

where $\sigma_{cc_{USSB1_1}}$ is the flange element buckling stress, $\sigma_{cy_{T3E}}$ is the material property from Table 3.2.1 . λ_{USSB1_1} is as calculated below, in Equation 67,

$$\lambda_{USSB1_1} = \sqrt{\frac{\sigma_{cy_{T3E}}}{E_{T3E}}} \left(\frac{b_{USSB1_1}}{t_{USSB1_1}} \right), \quad (67)$$

where E_{T3E} comes from Table 3.2.4 , t_{USSB1_1} and b_{USSB1_1} are the thickness and width of the panel as used in the crippling analysis and shown in Table 6.1.1 , respectively. Now, plugging in these values into their respective formulas is as follows,

$$\lambda_{USSB1_1} = \sqrt{\frac{3.40 \times 10^4 \text{ psi}}{1.08 \times 10^7 \text{ psi}}} \left(\frac{0.25 \text{ in}}{0.04 \text{ in}} \right), \quad (68)$$



$$\lambda_{USSB1_1} = 3.51 \times 10^{-1}, \quad (69)$$

$$\sigma_{cc_{USSB1_1}} = (3.40 \times 10^4 \text{ psi}) \times 0.546 \times (3.51 \times 10^{-1})^{-0.8}, \quad (70)$$

$$\sigma_{cc_{USSB1_1}} = 4.29 \times 10^4 \text{ psi}. \quad (71)$$

The values for the second flange element use the same process, which is as follows,

$$\sigma_{cc_{USSB1_2}} = \sigma_{cy_{T3E}} \times 0.546 \times \lambda_{USSB1_2}^{-0.8}, \quad (72)$$

$$\lambda_{USSB1_2} = \sqrt{\frac{\sigma_{cy_{T3E}}}{E_{T3E}}} \left(\frac{b_{USS1_2}}{t_{USS1_2}} \right), \quad (73)$$

$$\lambda_{USSB1_1} = \sqrt{\frac{3.40 \times 10^4 \text{ psi}}{1.08 \times 10^7 \text{ psi}}} \left(\frac{0.21 \text{ in}}{0.04 \text{ in}} \right), \quad (74)$$

$$\lambda_{USSB1_1} = 2.95 \times 10^{-1}, \quad (75)$$

$$\sigma_{cc_{USSB1_1}} = (3.40 \times 10^4 \text{ psi}) \times 0.546 \times (2.95 \times 10^{-1})^{-0.8}, \quad (76)$$

$$\sigma_{cc_{USSB1_1}} = 4.94 \times 10^4 \text{ psi}. \quad (77)$$

Now, summing these element buckling stress allowables together to get a total buckling allowable as seen in Equation 78

$$\sigma_{cc_{tot_{USSB1}}} = \frac{\sum \sigma_{cc_i} b_i t_i}{\sum b_i t_i}, \quad (78)$$

which expanding and plugging in the values becomes,

$$\sigma_{cc_{tot_{USSB1}}} = \frac{((4.29 \times 10^4 \text{ psi}) \times 0.25 \text{ in} \times 0.04 \text{ in}) + ((4.94 \times 10^4 \text{ psi}) \times 0.21 \text{ in} \times 0.04 \text{ in})}{0.25 \text{ in} \times 0.04 \text{ in} + 0.21 \text{ in} \times 0.04 \text{ in}}, \quad (79)$$

$$\sigma_{cc_{tot_{USSB1}}} = 45861.85 \text{ psi}. \quad (80)$$

Now, the critical slenderness for this geometry and materials are checked using Equation 81

$$\left(\frac{L_e}{\rho} \right)_{crit_{USSB1}} = \pi \sqrt{\frac{2}{\sigma_{cc_{tot_{USSB1}}} / E_{T3E}}} \quad (81)$$

where $\left(\frac{L_e}{\rho} \right)_{crit_{USSB1}}$ is the critical slenderness ratio the beam. This value, when checked against the upper skin stringer's actual slenderness ratio, determines what type of beam buckling analysis to use. If the upper skin stringer's actual slenderness ratio is less than the critical value, then the Johnson's beam buckling method can be used, otherwise, Euler's beam buckling method would instead be used. The critical value comes out to,



$$\left(\frac{L_e}{\rho}\right)_{crit_{USSB1}} = \pi \sqrt{\frac{2}{(45861.85 \text{ psi})/(1.08 \times 10^7 \text{ psi})}}, \quad (82)$$

$$\left(\frac{L_e}{\rho}\right)_{crit_{USSB1}} = 68.18. \quad (83)$$

For the upper skin stringer, ρ_{USS1} can be calculated using Equation 84,

$$\rho_{USS1} = \sqrt{\frac{I_{x_{USS1}}}{A_{USS1}}} \quad (84)$$

where ρ_{USS1} is the radius of gyration of the upper skin stringer, $I_{x_{USS1}}$ is the moment of inertia about the stringer's x-axis, and A_{USS1} is the upper skin stringer's cross sectional area from Table 3.1.2 . Plugging in these values,

$$\rho_{USS1} = \sqrt{\frac{1.06 \times 10^{-4} \text{ in}^4}{1.84 \times 10^{-2}/\text{in}^2}}, \quad (85)$$

$$\rho_{USS1} = 0.08 \text{ in.} \quad (86)$$

Next, the effective length for the upper skin stringer using Equation 87, which is as follows,

$$L_{eff} = \frac{L_{USS1}}{\sqrt{C}}, \quad (87)$$

where L_{eff} is the effective length of the upper skin stringers, L_{USS1} is the actual length of the upper skin stringers, and C is the end fixity coefficient for longitudinal members, as outlined in the Design Project [5]. Plugging in this values,

$$L_{eff} = \frac{24.62}{\sqrt{1.5}}, \quad (88)$$

$$L_{eff} = 20.10 \text{ in.} \quad (89)$$

Now, the upper skin stringer's slenderness ratio can be calculated using Equation 90,

$$\left(\frac{L_{eff}}{\rho_{USS1}}\right) = 267.933. \quad (90)$$

Because the actual slenderness ratio of the upper skin stringer is larger than the critical slenderness ratio of the cross section, the Euler buckling method will be used to determine the critical buckling stress allowable load for the upper skin stringer margin of safety. The Euler equation is shown below in Equation 91,

$$\sigma_{crEuler_{USSB1}} = \frac{\pi^2 E_{T3E}}{\left(\frac{L_{eff}}{\rho}\right)^2} \quad (91)$$

where $\sigma_{crEuler_{USSB1}}$ is the critical buckling stress allowable for the stringer.

Plugging in the values,



$$\sigma_{crEuler_{USSB1}} = \frac{\pi^2(1.08 \times 10^7 \text{ psi})}{\left(\frac{20.10 \text{ in}}{0.08 \text{ in}}\right)^2} \quad (92)$$

$$\sigma_{crEuler_{USSB1}} = 1484.81 \text{ psi}, \quad (93)$$

and converting to a load,

$$P_{crUSSB1} = \sigma_{crEuler_{USSB1}} \times A_{USS1}, \quad (94)$$

$$P_{crUSSB1} = 27.32 \text{ lb.} \quad (95)$$

Now, the margin of safety for upper stringer buckling can be completed using the critical buckling load allowable, $P_{crUSSB1}$, and the previously calculated load in the stringer due to the maximum compressive load, $P_{BSMNC1_{1311526}}$, in Equation 96 below

$$M.S._{USSB1} = \frac{P_{crUSSB1}}{1.5 \times FS \times P_{BSMNC1_{1311526}}} - 1. \quad (96)$$

Plugging values in,

$$M.S._{USSB1} = \frac{27.32 \text{ lb}}{1.5 \times 1.5 \times 613.72 \text{ lb}} - 1, \quad (97)$$

$$\underline{\underline{M.S._{USSB1} = -0.98.}} \quad (98)$$

This negative margin of safety value indicates that the stringer cannot take the maximum compressive load as described in the bar stresses, minimum combined .f06 file value. The stringer and other surrounding structural components will need to be resized to take on the required load.

6.1.6 Lower Skin Stringer

The stringers attached to the lower skin have two modes of failure, tensile and compressive. In this section, both these are analyzed in order to perform margin of safety checks and conclude whether or not this section of stringers will fail in either of the two modes. Figure 6.1.6.1 shows the geometry of the lower skin section and the three stringer locations.



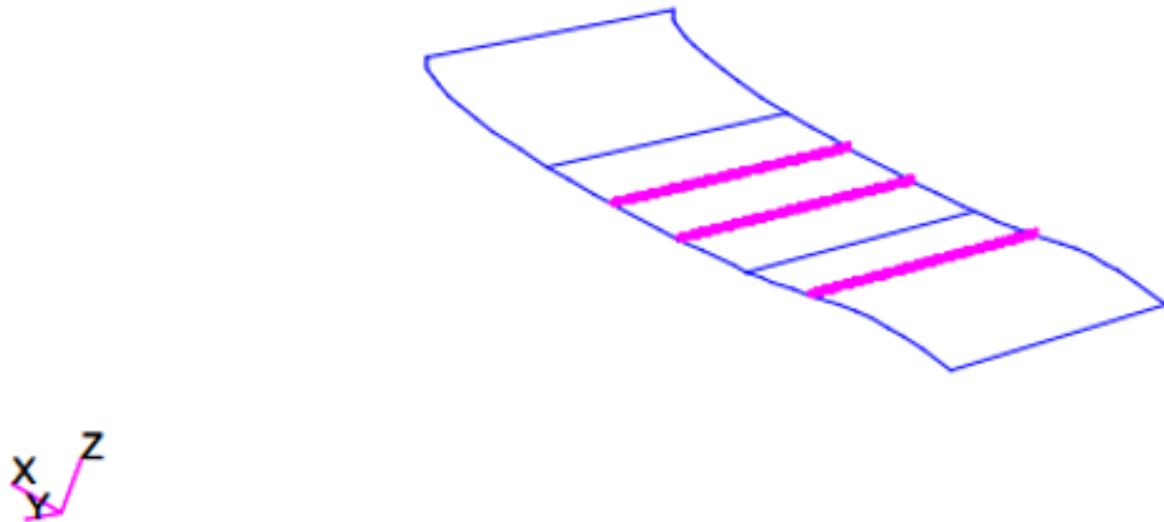


Fig. 6.1.6.1 Geometry of Lower Skin and Stringers

Tension The fringe plot of maximum bar stresses is used to locate the region of highest tensile stress. This is found to be the forward most stringer in the most inboard element location. Figure 6.1.6.2 shows the maximum combined bar stress fringe plot of the three stringers, with the region of interest circled.

Patran 2024.1 05-May-25 15:45:44

Fringe: SC1:DEFAULT, A1:Static subcase, Bar Stresses, Maximum Combined, , At Center

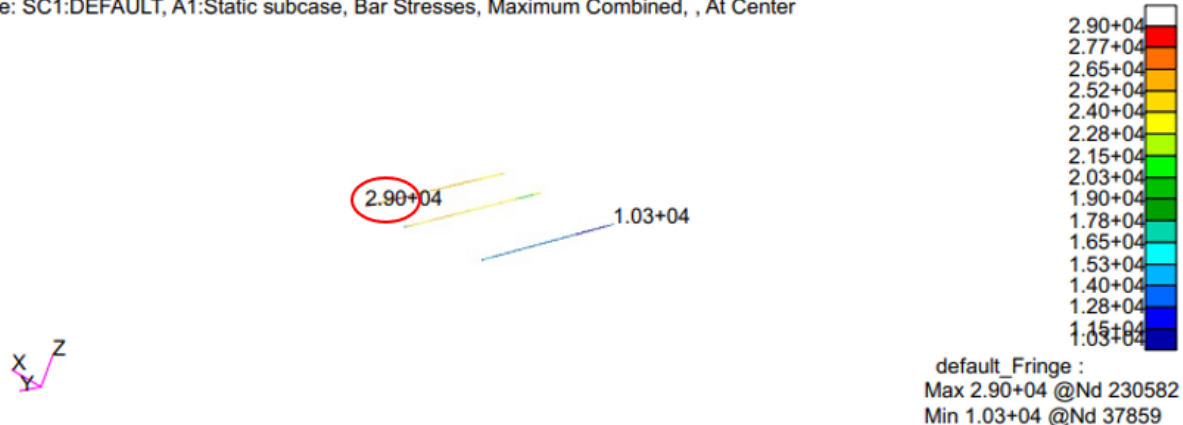


Fig. 6.1.6.2 Fringe: SC1:DEFAULT, A1: Static Subcase, Bar Stresses, Maximum Combined, At Center of Lower Stringers for WS 1

The specific element of interest is identified as Element 1302857. This element and the surrounding skin sections



are shown from a cross section view in Figure 6.1.6.3 .

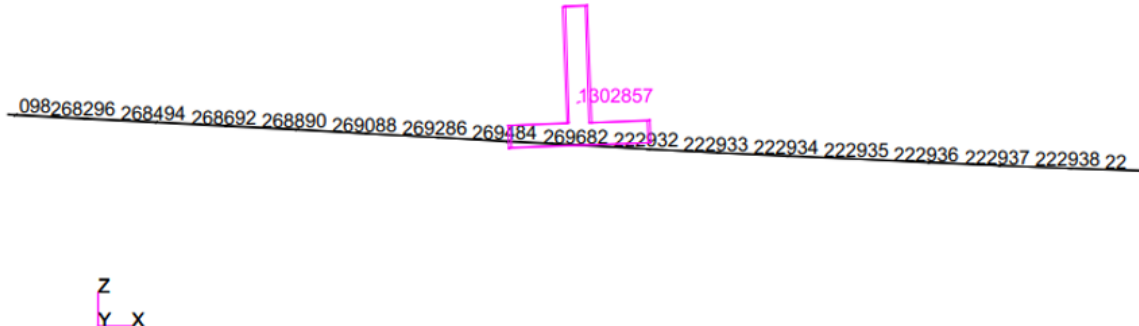


Fig. 6.1.6.3 Lower Stringer Max Stress Element of Interest and Surrounding Skin

Since the tensile stress is the stress of interest in this case, the .f06 file is searched for Element 1302857 and the maximum bar stress is found. The location of the maximum principal stress, $\sigma_{BSMXC}_{1302857}$, of 2.9×10^4 psi within the .f06 file is highlighted in Figure 6.1.6.4 .

ELEMENT ID.	S T R E S S E S I N B A R E L E M E N T S					(C B A R)		
	SA1 SB1	SA2 SB2	SA3 SB3	SA4 SB4	AXIAL STRESS	SA-MAX SB-MAX	SA-MIN SB-MIN	M.S.-T M.S.-C
0 1302857	-2.153928E+04 -2.322429E+04	9.182523E+03 1.020908E+04	9.959268E+03 1.047118E+04	-2.141500E+04 -2.318235E+04	1.883271E+04 2.879198E+04 2.930389E+04	-2.706576E+03 -4.391579E+03		

Fig. 6.1.6.4 .f06 NASTRAN Results for Lower Stringer Max Stress

This maximum tensile stress value is used along with the material allowable tensile stress in order to perform a margin of safety calculation using Equation 99.

$$M.S.LST1 = \frac{F_{ty\ T3E}}{FS \times \sigma_{BSMXC}_{1302857}} - 1, \quad (99)$$

The tensile yield stress of the 2024 T3 Extrusion from Table 3.2.2 and the maximum tensile stress in Element 1302857, $\sigma_{BSMXC}_{1302857}$, are plugged into Equation 99 to get the following:

$$M.S.LST1 = \frac{3.7 \times 10^4}{1.5 \times 2.93 \times 10^4} - 1, \quad (100)$$

$$\underline{\underline{M.S.LST1 = -0.158}} \quad (101)$$

The calculated margin of safety for the lower stringer in tension yields a negative value, therefore the stringer would fail under the given load.

Compression The section is subsequently analyzed for compressive failure. Similar to before, the fringe plot for minimum combined bar stresses is used to identify the region of interest, as shown in Figure 6.1.6.5 .



Patran 2024.1 05-May-25 16:26:54

Fringe: SC1:DEFAULT, A1:Static subcase, Bar Stresses, Minimum Combined, , At Center

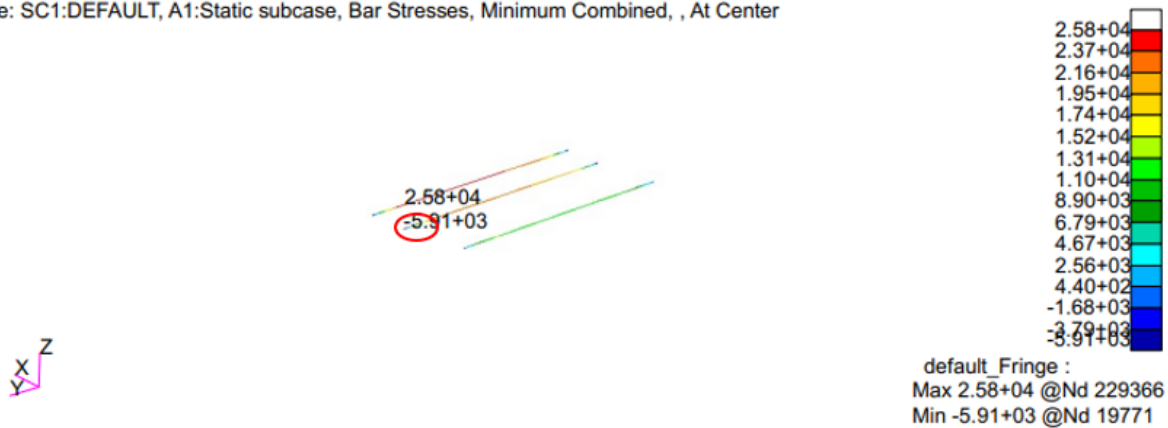


Fig. 6.1.6.5 Fringe: SC1:DEFAULT, A1: Static Subcase, Bar Stresses, Minimum Combined, At Center of Lower Stringers for WS 1

A closer inspection of the fringe results reveals that Element 1304434 is the element of minimum stress. This element and the surrounding skin are shown with a cross section view in Figure 6.1.6.6 .

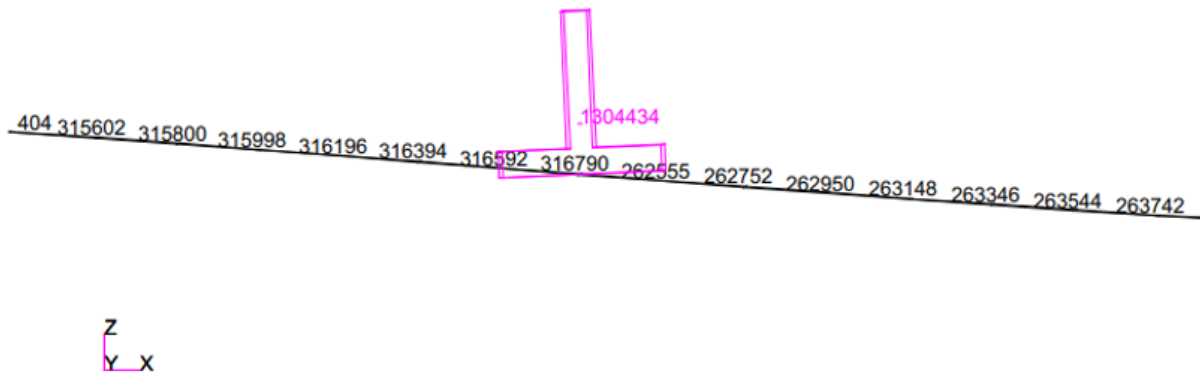


Fig. 6.1.6.6 Lower Stringer Min Stress Element of Interest and Surrounding Skin

Since the compressive stress is the stress of interest in this case, the .f06 file is searched for Element 1304434 and the minimum bar stress is found. The location of the minimum principal stress, $\sigma_{BSMNC}_{1304434}$, of -5.03×10^3 psi within the .f06 file is highlighted in Figure 6.1.6.7 .



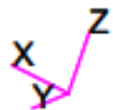
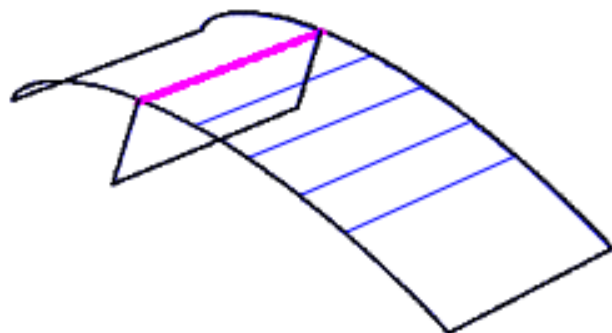


Fig. 6.1.7.1 WS1 Geometry of Upper Skin and Upper Spar Cap

The region of interest was found by creating a fringe plot of the minimum combined bar stress. The plot below in Figure 6.1.7.2 highlights the region of high absolute stress on the inboard edge. This region contains the element of interest, which will be used to investigate compressive failure further.

Patran 2024.1 06-May-25 19:08:36

Fringe: SC1:DEFAULT, A1:Static subcase, Bar Stresses, Minimum Combined, , At Center



Fig. 6.1.7.2 Fringe: SC1:DEFAULT, A1: Static Subcase, Bar Stresses, Minimum Combined, At Center of Upper Spar Cap for WS 1

From the fringe plot, the individual element of interest can be identified as Element 1288673. This element and the surrounding skin and spar web elements can be seen in the cross section view showcased in Figure 6.1.7.3 .

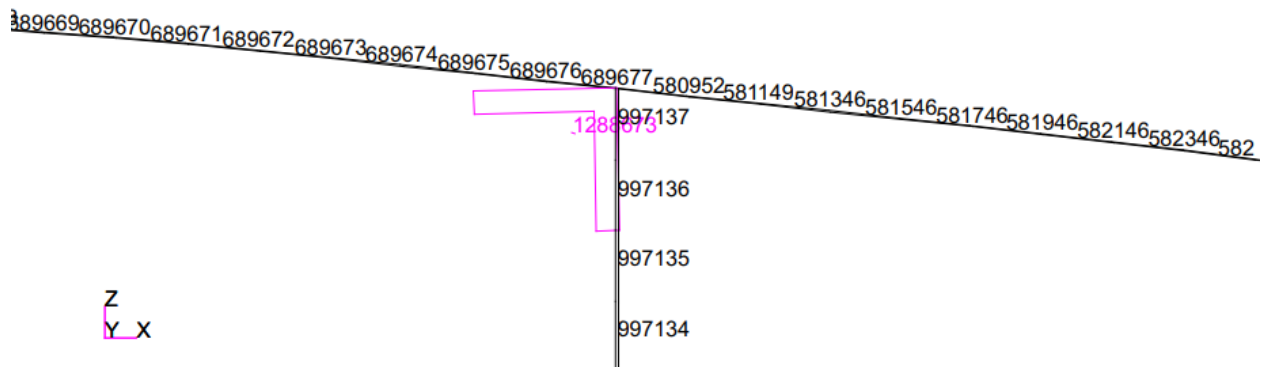


Fig. 6.1.7.3 WS1 Upper Spar Cap Element of Interest and Surrounding Skin

A search of the NASTRAN output .f06 file reveals the minimum stress corresponding to the bar element. The location of the stress, $\sigma_{BSMNC}_{1288673}$, within the file is shown in Figure 6.1.7.4 .



where $F_{cc_{totUSPC1}}$ is the total crippling stress of the upper spar caps, F_{cc_i} is the individual crippling stress of the flange elements, b_i and t_i are the individual width and thickness of the flange elements, respectively. For the upper spar cap, this becomes Equation 110,

$$F_{cc_{totUSPC1}} = \frac{F_{cc_{1USPC1}} b_{1USPC1} t_{1USPC1} + F_{cc_{2USPC1}} b_{2USPC1} t_{2USPC1}}{b_{1USPC1} t_{1USPC1} + b_{2USPC1} t_{2USPC1}}, \quad (110)$$

$$F_{cc_{totUSPC1}} = \frac{((4.40 \times 10^2 \text{ psi}) \times 0.25\text{in} \times 0.04\text{in}) + ((5.00 \times 10^4 \text{ psi}) \times 0.21\text{in} \times 0.04\text{in})}{0.25\text{in} \times 0.04\text{in} + 0.21\text{in} \times 0.04\text{in}}, \quad (111)$$

$$F_{cc_{totUSPC1}} = 46739.1304 \text{ psi}. \quad (112)$$

Now using page C4 of the Crippling Methods Handout, the non-dimensional unbuckled skin width can be determined with the stringer's crippling stiffness. This graphical method is demonstrated in Figure 6.1.5.9

After the non-dimensional effective skin width is determined, the dimension of the effective skin width can be found by multiplying this value with the sheet's thickness. For skins, this is shown in Equation 113.

$$w_{e_{skin}} = \left(\frac{2w_e}{t} \right)_{spar \ cap} \times \left(\frac{t_{USPC1}}{2} \right), \quad (113)$$

where $\left(\frac{2w_e}{t} \right)_{spar \ cap}$ is the spar cap's non-dimensional effective sheet value and t_{USPC1} is the sheet thickness of the wing skin.

$$w_{e_{skin}} = 37 \times \left(\frac{0.035 \text{ in}}{2} \right), \quad (114)$$

$$w_{e_{skin}} = 0.6475 \text{ in}. \quad (115)$$

Following a similar process to determine the non-dimensional spar web width, using Equation 116,

$$w_{e_{sparweb}} = \left(\frac{2w_e}{t} \right)_{spar \ cap} \times \left(\frac{t_{USPC1}}{2} \right), \quad (116)$$

where $\left(\frac{2w_e}{t} \right)_{sparcap}$ is the spar cap's non-dimensional effective sheet value and t_{USPC1} is the sheet thickness of the wing skin.

$$w_{e_{spar \ web}} = 37 \times \left(\frac{0.06 \text{ in}}{2} \right), \quad (117)$$

$$w_{e_{spar \ web}} = 1.11 \text{ in}. \quad (118)$$

The skin thickness and effective skin width can be multiplied together to get the area of the cross section. Then, the critical crippling load can be found for each element with Equation 119 below,

$$P_{cc_{USPCi}} = \frac{F_{cc_{USPC}}}{A_{USPCi}}, \quad (119)$$

where $P_{cc_{USPCi}}$ is the upper spar cap element critical load and A_{USPCi} is the upper spar cap element area. The following table, Table 6.1.1, is a summary of this spar cap crippling process. The final spar cap-unbuckled skin critical



load is highlighted in yellow. The elements critical load is found in the same way, by dividing the max compressive stress by the spar cap area to get the critical load.

Table 6.1.1 Spar Cap Unbuckled Crippling Table

Spar Cap Element	b (in)	t (in)	b/t (-)	$F_{cc_{tot}}$	$\frac{2w_e}{t}$	w_e (in)	Area (in^2)	P_{cc}
1	0.25	0.04	6.25	46739.13043	-	-	0.01	4.67E+02
2	0.25	0.04	6.25	46739.13043	-	-	0.01	4.67E+02
3	-	0.035	-	46739.13043	37	0.6475	0.0227	1.06E+03
4	-	0.035	-	46739.13043	37	0.6475	0.0227	1.06E+03
5	-	0.06	-	46739.13043	37	1.11	0.0667	3.11E+03
Sum							0.1219	6166.0598

Now, the MS of the upper spar cap can be calculated using the value displayed in Table 6.1.1 . The stress displayed in Figure 6.1.7.4 can be converted to a load using the same area used in converting the critical crippling stress to a critical load. Using Equation 108 from above, the process is as follows,

$$M.S.USPC1 = \frac{2978.4511 \text{ lb}}{1.5 \times 1.5 \times 613.99 \text{ lb}} - 1, \quad (120)$$

$$\underline{\underline{M.S.USPC1 = 3.46.}} \quad (121)$$

The positive margin of safety indicates the structure is adequately sized according to the structural analysis applied to this structure. For future analysis, it would be more appropriate to take the margin of safety of the unbuckled spar cap allowable against the summation of spar cap and unbuckled skin loads. This would result in a lower margin of safety for this structural component.

Finding the critical buckling allowable for the upper spar cap is identical to the upper skin stringer due to the upper skin stringer and upper spar cap sharing the same material and related geometric properties. Therefore,

$$P_{crUSCB1} = P_{crUSSB1} = 27.32 \text{ lb}, \quad (122)$$

where $P_{crUSCB1}$ is the upper spar cap critical buckling allowable in wing section one. The following equation, Equation 123 displays the margin of safety calculation for the upper spar cap,

$$M.S.USCB1 = \frac{P_{crUSCB1}}{1.5 \times FS \times P_{BSMNC1}_{1288673}} - 1. \quad (123)$$

where $P_{BSMNC1}_{1288673}$ is the critical buckling load in Element 1288673 which is derived from bar stresses minimum combined value in the .f06 file for the spar cap. Plugging in these values,

$$M.S.USCB1 = \frac{27.32 \text{ lb}}{1.5 \times 1.5 \times (613.40 \text{ lb})} - 1, \quad (124)$$

$$\underline{\underline{M.S.USCB1 = -0.98.}} \quad (125)$$

This negative margin of safety value indicates that the upper spar cap cannot take the maximum compressive load



as described in the bar stresses, minimum combined .f06 file value. The spar cap and other surrounding structural components will need to be resized to take on the required load.

6.1.8 Lower Spar Cap

Tension The lower spar caps are subjected to tensile forces, as shown in Figure 6.1.8.1 , which illustrates the placement and orientation of the spar caps in Section 1 of the wing. The spar cap is a critical structural element designed to carry significant bending moments.

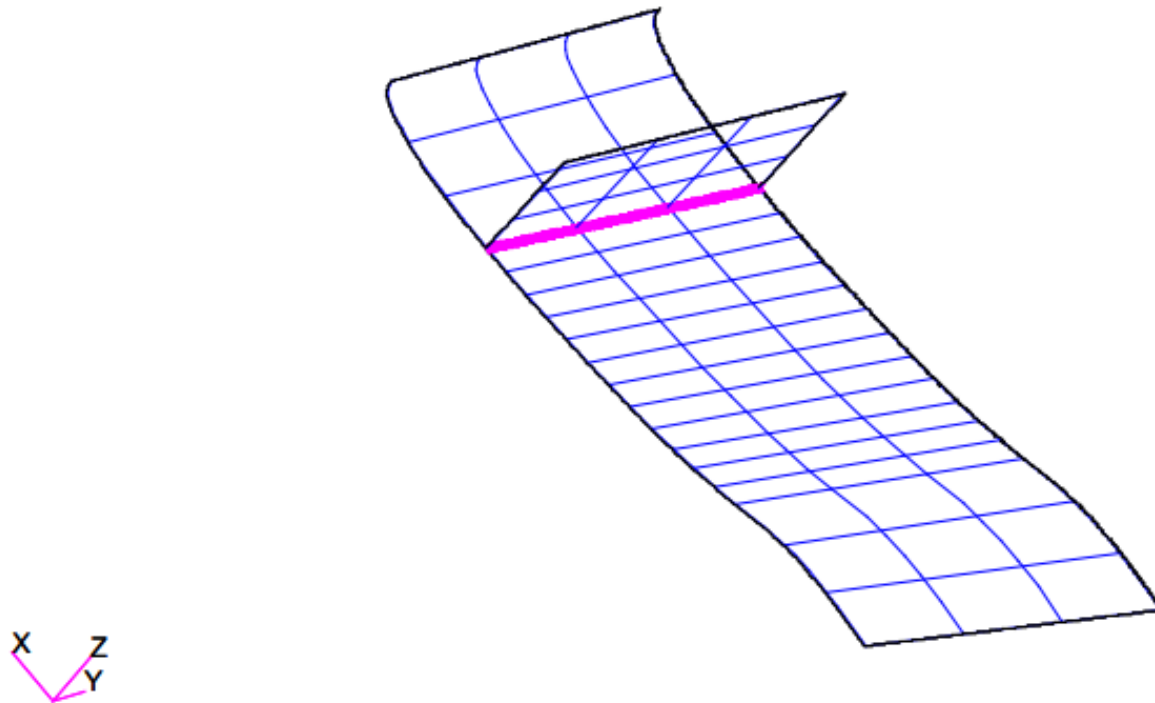


Fig. 6.1.8.1 WS1 Geometry of Lower Skin and Lower Spar Cap

The maximum combined stress due to tension occurs at the most inboard element of Section 1, as seen in Figure 6.1.8.2 , where the stress distribution is shown across the spar cap. This stress distribution provides insight into where the largest stresses occur under the applied load, with the highest stress located at the center of the lower spar cap.

Patran 2024.1 06-May-25 18:17:09

Fringe: SC1:DEFAULT, A1:Static subcase, Bar Stresses, Maximum Combined, , At Center

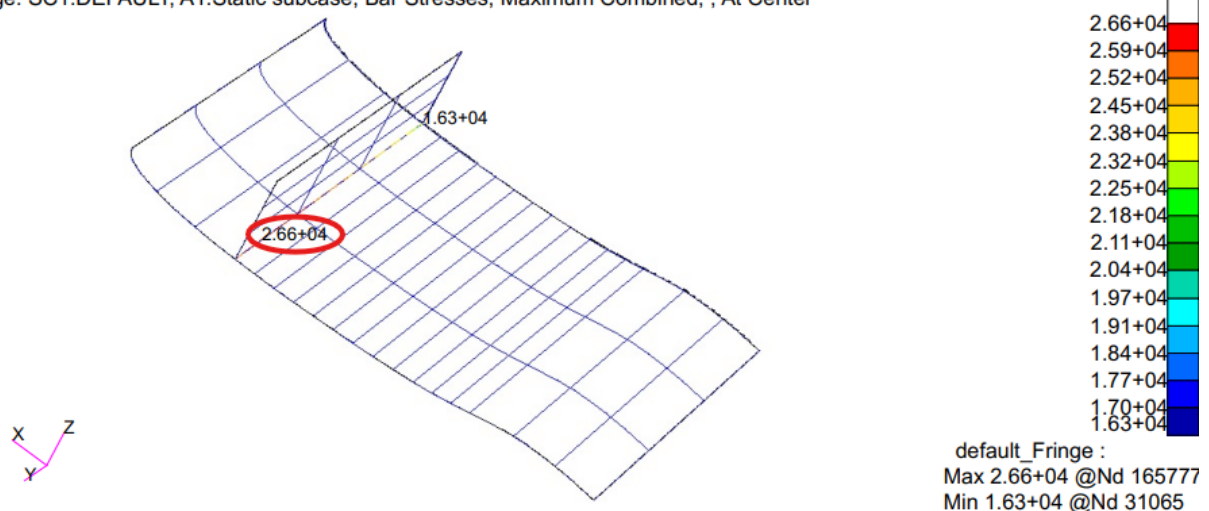


Fig. 6.1.8.2 Fringe: SC1:DEFAULT, A1: Static Subcase, Bar Stresses, Maximum Combined, At Center of Lower Spar Cap for WS 1

The region of interest was found by creating a fringe plot of the minimum combined bar stress. The plot above in Figure 6.1.8.2 highlights the region of high absolute stress on the inboard edge. This region contains the element of interest, Figure 6.1.8.3 which will be used to investigate compressive failure further.

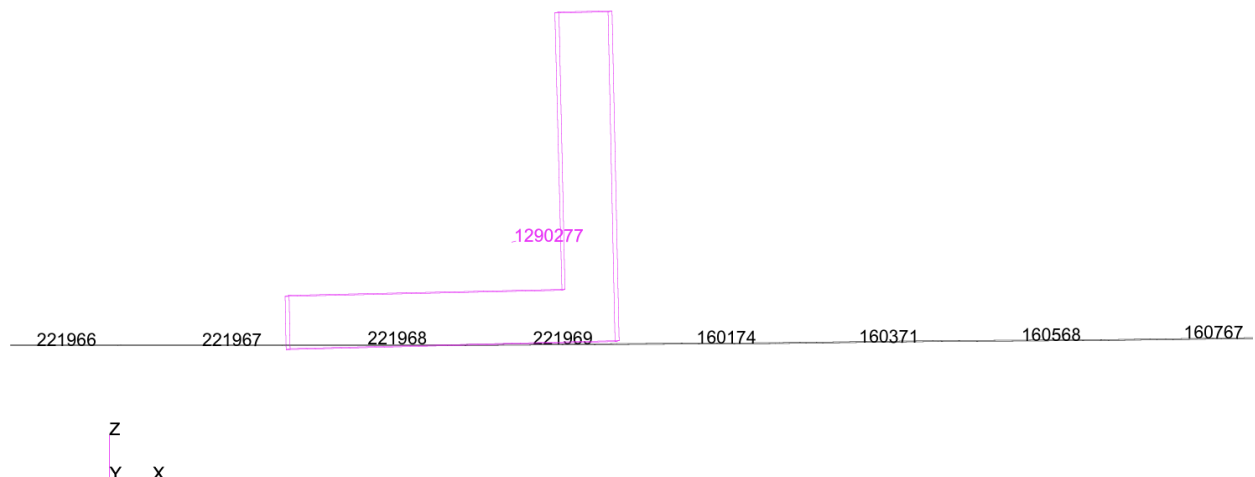


Fig. 6.1.8.3 WS1 Lower Spar Cap Element of Interest and Surrounding Skin



Compression The member experiences no compression forces, as shown in Figure 6.1.8.5 , so failure modes caused by compression were ignored. This figure shows the stress distribution under compressive loading conditions, where the lower spar cap is unaffected by compressive forces. Since the stresses in the cap are dominated by tension, the potential failure modes were ignored due to compression in this analysis.

Patran 2024.1 08-May-25 00:43:56

Fringe: SC1:DEFAULT, A1:Static subcase, Bar Stresses, Minimum Combined, , At Center

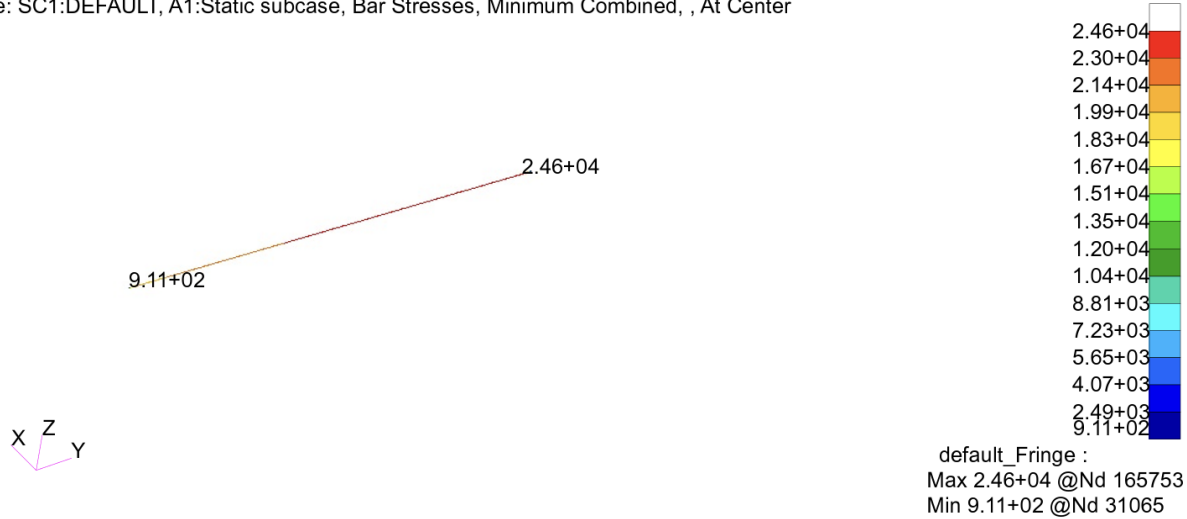


Fig. 6.1.8.5 Fringe: SC1:DEFAULT, A2: Static Subcase, Bar Stresses, Minimum Combined, At Center of Lower Spar Cap for WS 1

6.2 Wing Section 2

6.2.1 Upper Skin

Compression Figure 6.2.1.1 displays the distribution of the minimum principal stress over the upper skin of Section 2. This stress distribution indicates that the highest compressive stress occurs on the most inboard side of the section, near the root of the wing. This is an important area of focus as it often corresponds to regions that experience the greatest loading during flight, especially under bending moments.

Patran 2024.1 06-May-25 11:49:39

Fringe: SC1:DEFAULT, A2:Static subcase, Stress Tensor, Min Principal, 2 of 2 layers (Minimum)

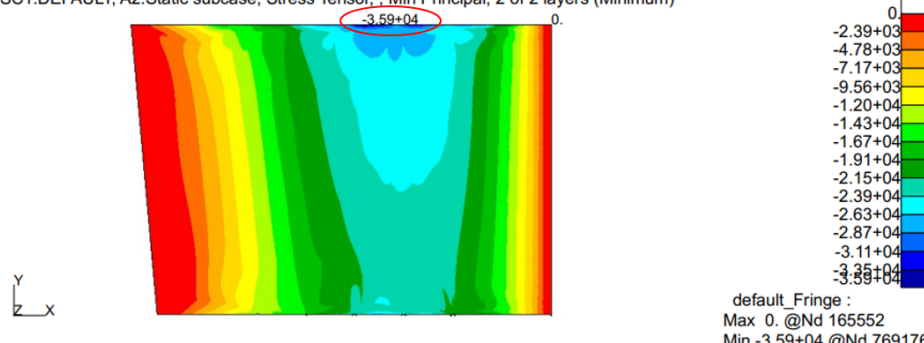


Fig. 6.2.1.1 Fringe: SC1:DEFAULT, A2: Static Subcase, Stress Tensor, Min Principal, 2 of 2 layers (Minimum) of Upper Skin for WS 2



Upon zooming in on the affected region, it is evident that the largest compressive stress occurs at Element 746842, which is located at a value of -3.37×10^4 psi, as seen in Figure 6.2.1.2 a. This is a critical element that warrants closer examination to ensure the structure can withstand these stresses. The detailed excerpt from the .f06 file in Figure 6.2.1.3 further supports this finding, confirming the stress levels at this specific location.

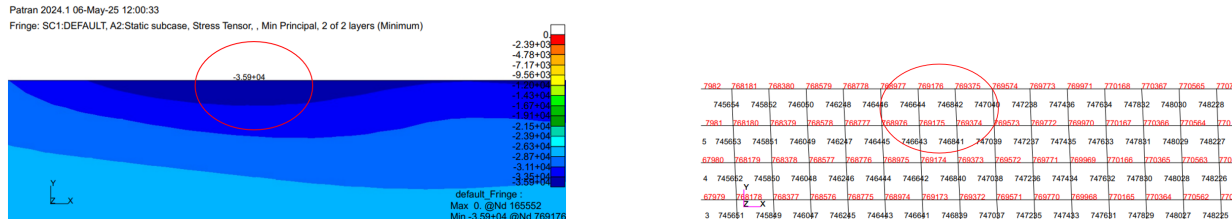


Fig. 6.2.1.2 Zoomed Fringe and Elements of Interest for Upper Skin on WS2

(a) Fringe: SC1:DEFAULT, A2: Static Subcase, Stress Tensor, Min Principal, 2 of 2 layers (Minimum) of Zoomed Upper Skin for WS2

(b) Zoomed Region of Upper Skin of WS2

Fig. 6.2.1.3 .f06 NASTRAN Results for Upper Skin in WS2

To assess the structural integrity of the wing component, the margin of safety (M.S.) for this section can be calculated using the following Equation 129,

$$M.S.USC2 = \frac{F_{cy} 2024-T3S}{FS \times |F_{MNMNP}_{746842}|} - 1, \quad (129)$$

where $F_{cy} 2024-T3S$ is the compressive yield stress as previously outlined in Table 3.2.1 and F_{MNMNP}_{746842} is the major principle stress value circled in Figure 6.1.1.8 for Element 746645. Plugging in the values,

$$M.S.USC2 = \frac{3.7 \times 10^4 \text{ psi}}{1.5 \times |-3.37 \times 10^4 \text{ psi}|} - 1, \quad (130)$$

$$\underline{\underline{M.S.USC2 = -0.27}} \quad (131)$$

Tension In contrast to the compressive stresses, Figure 6.2.1.4 also highlights the distribution of the maximum principal stress over the upper skin of Section 2 under tensile loading conditions. This region is critical because tensile



stresses are often associated with the potential for material stretching and failure, particularly when the structure is subjected to aerodynamic forces during flight.

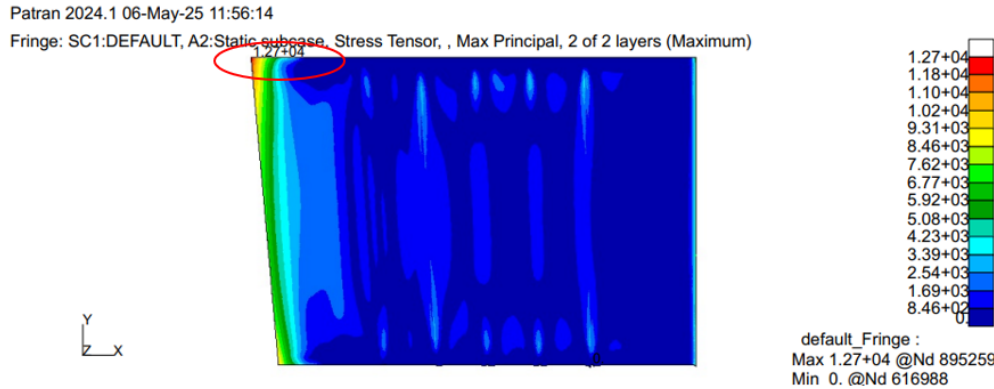
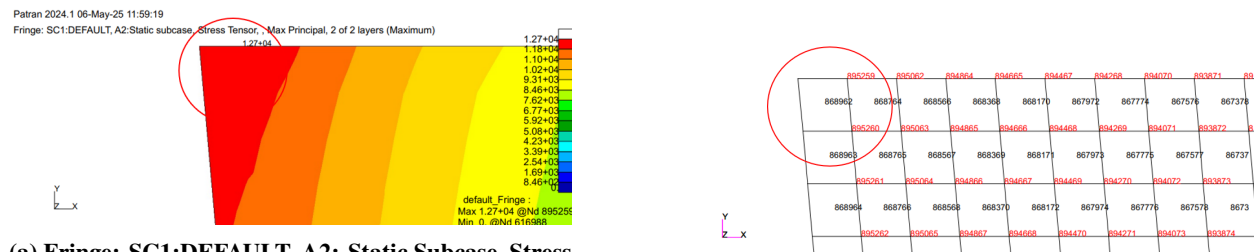


Fig. 6.2.1.4 Fringe: SC1:DEFAULT, A2: Static Subcase, Stress Tensor, Max Principal, 2 of 2 layers (Maximum) of Upper Skin for WS 2

As seen in Figure 6.2.1.4 , the maximum tensile stress occurs at different locations, with the highest values appearing more outboard on the section. The zoomed-in views in Figures 6.2.1.5 a and 6.2.1.5 b provide further detail on these regions of interest, allowing for a more accurate assessment of stress concentrations.



(a) Fringe: SC1:DEFAULT, A2: Static Subcase, Stress Tensor, Max Principal, 2 of 2 layers (Maximum) of Zoomed Upper Skin for WS 2

(b) Zoomed Region of Upper Skin of WS2

Fig. 6.2.1.5 Zoomed Fringe and Elements of Interest for Upper Skin on WS2

Figure 6.2.1.6 shows the .f06 file results for the tension stress. With Element 868962 highlighted as the critical element.



$$M.S._{USB2} = \frac{\sigma_{cr\ 769176}}{FS \times |F_{MN MNP\ 769176}|} - 1, \quad (135)$$

where $\sigma_{cr\ 769176}$ is the critical buckling stress for Element 746842, which is determined by the material properties of the skin and the geometry of the wing section. This stress represents the maximum compressive stress the skin can withstand before buckling occurs. FS is the safety factor, typically set to 1.5, which accounts for uncertainties and ensures the structure has an adequate strength margin. $F_{MN MNP\ 769176}$ is the minor principal stress at element 746842, obtained from the finite element analysis (FEA) results. The absolute value is used to ensure a positive input for the equation, as it represents the compressive stress (which is negative).

Next, the critical buckling stress $\sigma_{cr\ 769176}$ is calculated using the following formula, which depends on the material properties of 2024-T3S and the geometry of the wing section:

$$\sigma_{cr\ 769176} = C_{SS2} \frac{\pi^2 E_{2024-T3S}}{12(1 - \nu_{2024-T3S}^2)} \left(\frac{t_{skin}}{b_{SS2}} \right)^2 \quad (136)$$

By substituting the values for the material properties and geometric factors into Equation 136, the critical buckling stress $\sigma_{cr\ 769176}$ for the wing component can be computed. Finally, substituting this value into the margin of safety Equation 135 allows us to assess the safety of the wing section under buckling conditions.

An average of the clamped, $C_{clamped}$, and simply supported, C_{ss} , curves is taken at the aspect ratio of 5.55 to get a compression buckling coefficient, as shown in Equation 137.

$$C_{SS2} = \frac{C_{ss} + C_{clamped}}{2} \quad (137)$$

$$C_{SS2} = \frac{6.98 + 4.00}{2} \quad (138)$$

$$C_{SS2} = 5.49 \quad (139)$$

Substituting into Equation 136 to solve for $\sigma_{cr\ 769176}$ gives the following:

$$\sigma_{cr\ 769176} = 5.49 \frac{\pi^2 \times 1.05 \times 10^7 \text{ psi}}{12(1 - 0.33^2)} \left(\frac{0.035 \text{ in}}{4.43 \text{ in}} \right)^2 \quad (140)$$

$$\sigma_{cr\ 769176} = 3.32 \times 10^3 \text{ psi} \quad (141)$$

Finally, plugging this value into Equation 135 along with $F_{MN MNP\ 769176}$ from Figure 6.1.1.8 the margin of safety for the skin section can be calculated.

$$M.S._{USB2} = \frac{3.32 \times 10^3 \text{ psi}}{1.5 \times |-3.37 \times 10^4 \text{ psi}|} - 1, \quad (142)$$

$$\underline{M.S._{USB2} = -0.934} \quad (143)$$

The analysis shows that the material will fail in buckling and compression. The large negative value of the margin of safety indicates that the member will fail in buckling before it fails in compression.



6.2.2 Lower Skin

Tension Figure 6.2.2.1 illustrates the distribution of the maximum principle stress present on the lower skin of Section 2. This region exhibits the highest stress values, which are primarily located on the most inboard elements, closest to the rib. The location of the peak stress and its magnitude are shown in Figure 6.2.2.1. For a more detailed view, Figure 6.2.2.2 a highlights the critical elements where the maximum stress occurs, providing a clearer picture of the stress concentration in this area.

Patran 2024.1 05-May-25 12:35:12

Fringe: SC1:DEFAULT, A1:Static subcase, Stress Tensor, , Max Principal, Maximum,2 of 2 layers

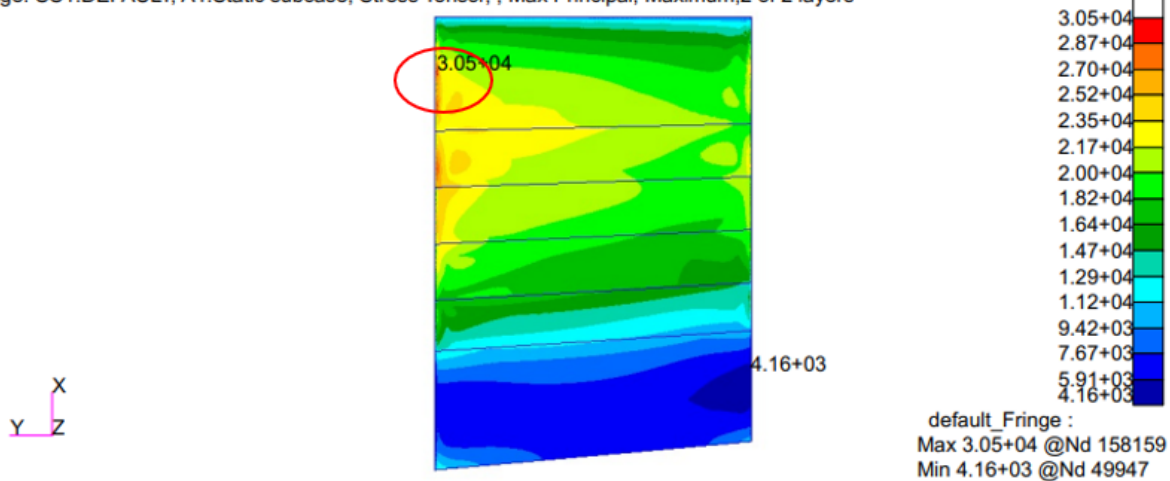
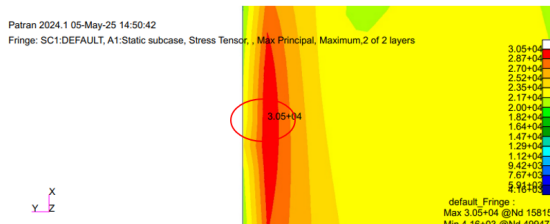
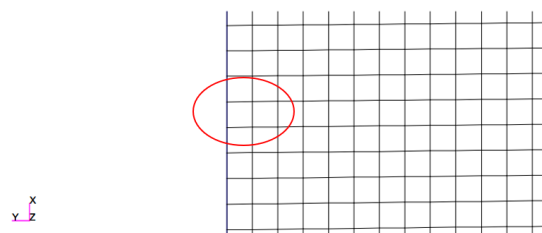


Fig. 6.2.2.1 Fringe: SC1:DEFAULT, A1: Static Subcase, Stress Tensor, Max Principal, Maximum, 2 of 2 layers of Lower Skin for WS 2



(a) Fringe: SC1:DEFAULT, A1: Static Subcase, Stress Tensor, Max Principal, Maximum, 2 of 2 layers, of Zoomed Lower Skin for WS 2



(b) Zoomed Lower Skin Region of WS2

Fig. 6.2.2.2 Zoomed Fringe and Elements of Interest for Lower Skin on WS2

Further zooming into the region of interest, a specific Element of interest can be identified. In this case, the element of interest is Element 152788 which is surrounded by Nodes 31103, 158159, 158359, 31104. Element 152788 and the surrounding Nodes are identified in Figure 6.2.2.3 below.



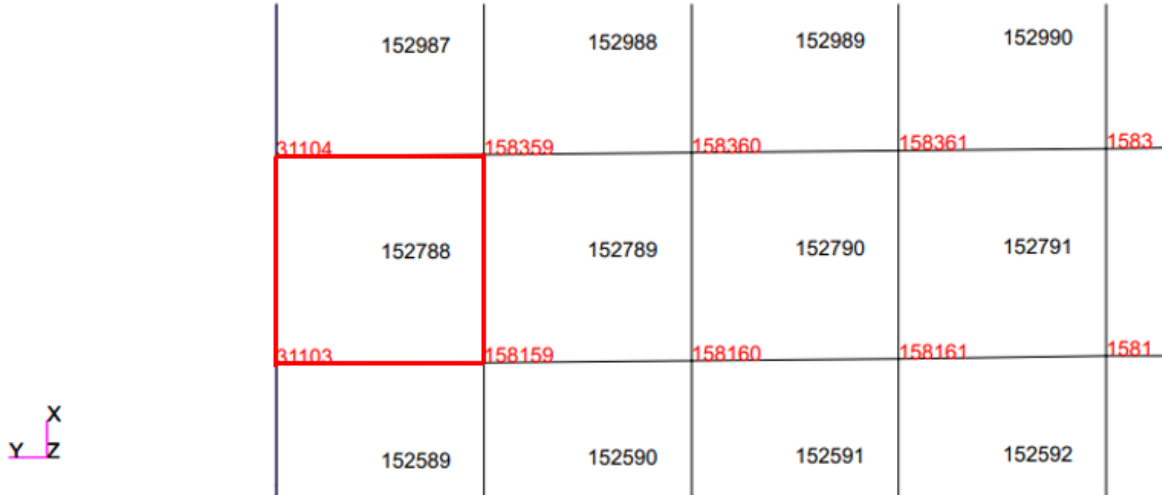


Fig. 6.2.2.3 WS2 Lower Skin Max Stress Element of Interest

From the NASTRAN .f06 results, shown in Figure 6.2.2.4 , the maximum principle stress in the critical element is seen to be 3.27×10^4 ‘ psi. This value represents the highest level of stress observed in this region, indicating a potential area for further evaluation in terms of structural integrity and possible failure.

STRESSES IN QUADRILATERAL ELEMENTS (QUAD 4)									OPTION = BILIN
ELEMENT ID	GRID-ID	FIBER DISTANCE	STRESSES IN ELEMENT COORD SYSTEM			PRINCIPAL STRESSES (ZERO SHEAR)			VON MISES
			NORMAL-X	NORMAL-Y	SHEAR-XY	ANGLE	MAJOR	MINOR	
0 152788	CEN/4	-1.75000E-02 1.75000E-02	3.267498E+04 1.241636E+04	8.196226E+03 2.060733E+03	-3.448851E+02 -1.337697E+02	-0.8070 -0.7400	3.267984E+04 1.241809E+04	8.191368E+03 2.059006E+03	2.945128E+04 1.152734E+04
	31103	-1.75000E-02 1.75000E-02	3.271455E+04 1.245633E+04	8.324150E+03 2.011436E+03	-3.440160E+02 -1.338145E+02	-0.8079 -0.7339	3.271940E+04 1.245805E+04	8.319298E+03 2.009722E+03	2.945450E+04 1.158468E+04
	158159	-1.75000E-02 1.75000E-02	3.271456E+04 1.245635E+04	8.068291E+03 2.110038E+03	-3.453385E+02 -1.333048E+02	-0.8026 -0.7381	3.271939E+04 1.245807E+04	8.063453E+03 2.108321E+03	2.952536E+04 1.154915E+04
	158359	-1.75000E-02 1.75000E-02	3.263540E+04 1.237638E+04	8.068289E+03 2.110036E+03	-3.457543E+02 -1.337249E+02	-0.8062 -0.7461	3.264027E+04 1.237812E+04	8.063423E+03 2.108294E+03	2.944849E+04 1.147023E+04
	31104	-1.75000E-02 1.75000E-02	3.263542E+04 1.237639E+04	8.324147E+03 2.011434E+03	-3.444317E+02 -1.342345E+02	-0.8115 -0.7419	3.264030E+04 1.237813E+04	8.319269E+03 2.009696E+03	2.937782E+04 1.150568E+04

Fig. 6.2.2.4 .f06 NASTRAN Results for WS2 Lower Skin Max Stress

To quantify the margin of safety (M.S.) for the wing component, Equation 144 is used to assess the structural integrity under applied stresses

$$M.S._{LST2} = \frac{F_{ty}_{2024-T3S}}{FS \times F_{MXMXP}_{152788}} - 1, \quad (144)$$

where $F_{ty}_{2024-T3S}$ represents the yield strength of the material used for the wing component (in psi), denoted as 2024-T3S. FS is the safety factor, a dimensionless number that accounts for uncertainties in the design, material properties, manufacturing processes, and operating conditions. F_{MXMXP}_{152788} is the maximum principle stress at Element152488, located in the critical region of the wing. This stress value is obtained from the finite element analysis



(FEA) results, and in this case, it is 3.27×10^4 psi.

The margin of safety equation essentially compares the applied stress with the material strength, scaled by the safety factor, and then subtracts 1 to express the difference relative to the allowable strength. The result indicates whether the material can withstand the applied loads without failure.

Next, the known values are substituted into the equation:

$$M.S._{LST2} = \frac{4.00 \times 10^4 \text{ psi}}{1.5 \times 3.27 \times 10^4 \text{ psi}} - 1, \quad (145)$$

After performing the calculation:

$$\underline{\underline{M.S._{LST2} = -0.185}} \quad (146)$$

This result indicates that the margin of safety for the wing component is -0.185. A negative margin of safety suggests that the applied stresses exceed the material's allowable strength, even with the safety factor applied. In other words, the component is likely to fail under the given loading conditions.

Compression In contrast to the tension analysis, Figure 6.2.2.6 a presents the distribution of the minimum principle stress over the lower skin of Section 2. This stress distribution differs from the maximum principle stress distribution and is located more outboard within the section. The region of interest shifts slightly compared to the tension zone, highlighting areas where compressive stresses dominate.

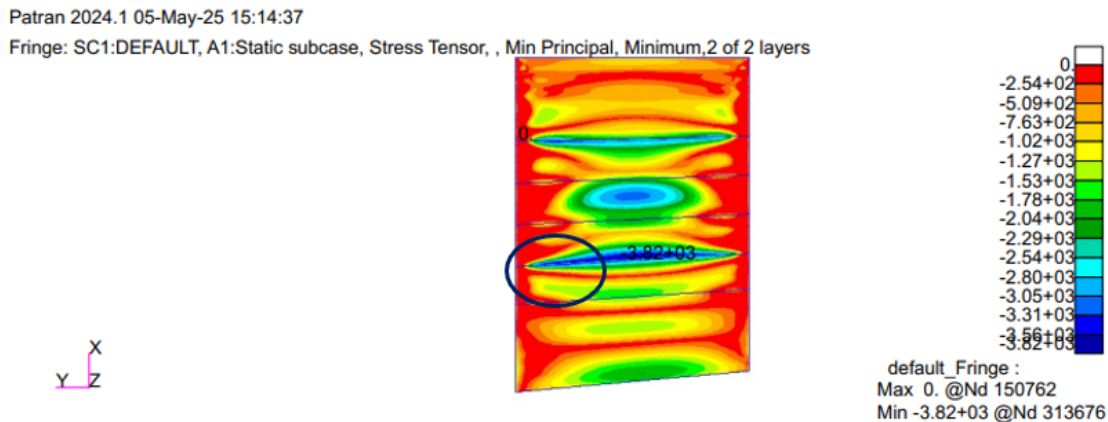
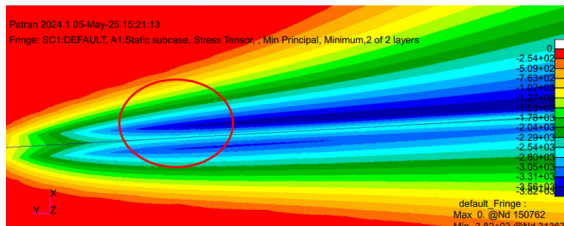
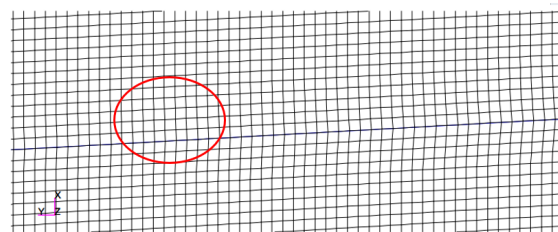


Fig. 6.2.2.5 Fringe: SC1:DEFAULT, A1: Static Subcase, Stress Tensor, Min Principal, Minimum, 2 of 2 layers of Lower Skin for WS 2





(a) Fringe: SC1:DEFAULT, A1: Static Subcase, Stress Tensor, Min Principal, Minimum, 2 of 2 layers of Lower Skin for WS 2



(b) Zoomed Lower Skin Region of WS2

Fig. 6.2.2.6 Zoomed Fringe and Elements of Interest for Lower Skin on WS2

Further zooming into the region of interest, a specific Element of interest can be identified. In this case, the element of interest is Element 302569 which is surrounded by Nodes 313416, 313417, 313619, and 313620. Element 302569 and the surrounding Nodes are identified in Figure 6.2.2.7 below.



Fig. 6.2.2.7 WS2 Lower Skin Min Stress Element of Interest

In addition, Figure 6.2.2.8 presents the .f06 NASTRAN results for the lower skin in Section 2 under compressive loading conditions. The data reveals critical compressive stresses in elements located more outboard compared to the tension case.



After performing the calculation:

$$\underline{\underline{M.S.}_{LSC2} = 5.01} \quad (149)$$

This result indicates that the margin of safety for the component under compressive loading is 5.01. A positive margin of safety suggests that the material can withstand the compressive stress with a comfortable margin, indicating that the design is structurally sound under the given loading conditions.

6.2.3 Spar Web

The two stresses analyzed for the forward spar web are shear in the xy direction and shear buckling, respectively. Figure 6.2.3.1 indicates the shear stress gradients in the xy direction for the forward spar web.

Patran 2024.1 05-May-25 13:34:04

Fringe: SC1:DEFAULT, A1:Static subcase, Stress Tensor, XY Component, Maximum,2 of 2 layers

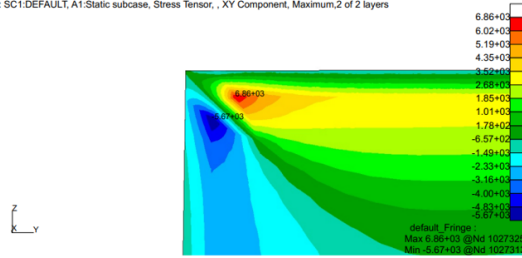


Fig. 6.2.3.1 Fringe: SC1:DEFAULT, A1: Static Subcase, Stress Tensor, XY Component, Maximum, 2 of 2 layers of Forward Spar Web for WS 2

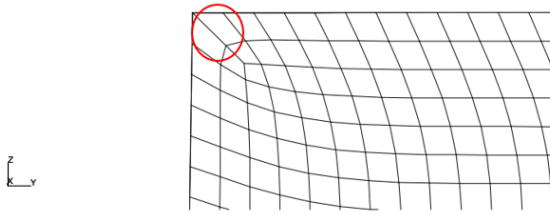
Figure 6.2.3.1 shows the fringe plot of shear stress in the xy direction for the forward spar web. Typically it is best practice to use a seventy percent shear gradient to capture the shear stress throughout the panel. For the purposes of this preliminary analysis, the most conservative approach to capturing shear stress will be taken from the maximum xy shear stress values. The area of interest in the web is outlined by the red circle as seen in the upper left region of the plot. For clarity, a closer look at the region of interest will be shown in Figures 6.2.3.2 a and 6.2.3.2 b below.



Patran 2024.1 05-May-25 13:37:15
Fringe: SC1:DEFAULT, A1:Static subcase, Stress Tensor, XY Component, Maximum, 2 of 2 layers



(a) Fringe: SC1:DEFAULT, A1: Static Subcase, Stress Tensor, XY Component, Maximum, 2 of 2 layers of Zoomed Forward Spar Web for WS 2



(b) Zoomed Region of Interest for Forward Spar Web for WS 2

Fig. 6.2.3.2 Zoomed Fringe and Elements of Interest for Forward Spar Web for WS 2

Figure 6.2.3.2 a shows opposing shear stresses in close proximity to each other. Figure 6.2.3.2 b shows unequal angle Elements near the upper left corner of the spar web. These unequal angle Elements yield inaccurate shear stress results. An ideal discretization of the spar web would consist of perfectly rectangular Elements with no skewed interior angles. A closer view of the element of interest is shown in Figure 6.2.3.3 .

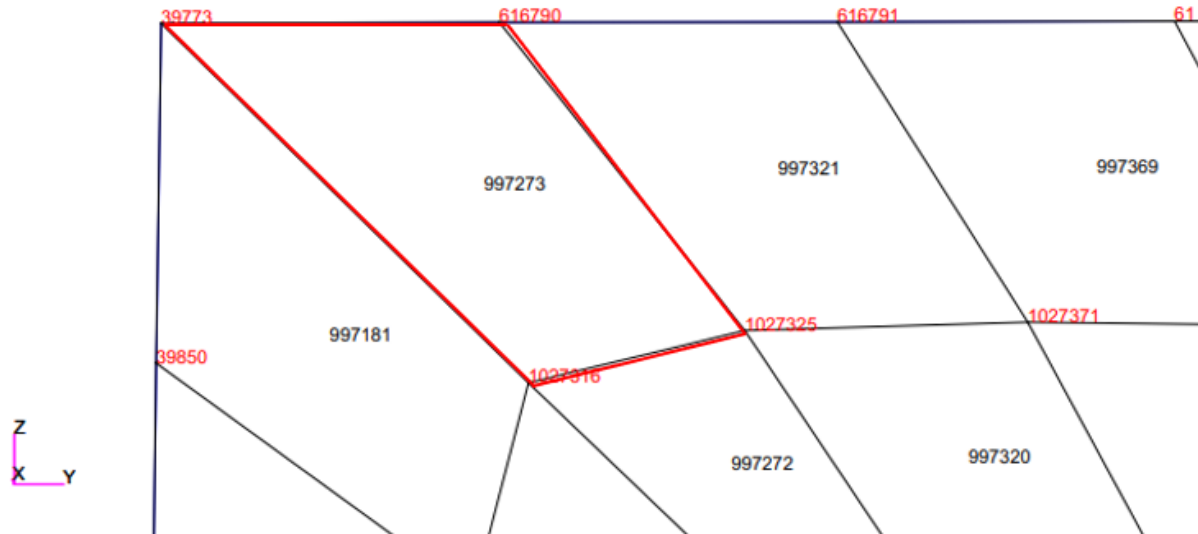


Fig. 6.2.3.3 Element of Interest for Forward Spar Web for WS 2

As seen in Figure 6.2.3.3 Element 997273 outlined in red is the element of interest that contains the absolute maximum shear value in the xy direction. Figure 6.2.3.4 is an excerpt of the .f06 file results from NASTRAN concerning maximum shear in the xy direction for the forward spar web.



$E_{2024-T3}$ is the elastic modulus for a 2024 – T3 aluminum sheet, $\nu_{2024-T3}$ is Poisson ratio, t_{SW} is the thickness of the spar web and b_{SW2} is the height of the spar web.

To obtain $K_{s_{SW}}$ the graph seen in Figure 6.1.3.5 is used. Since the spar web is clamped between the upper and lower spar caps, the clamped curve will be used. Obtaining the aspect ratio for the spar web from Table 3.1.1 , the value for $K_{s_{SW}}$ is thus:

$$K_{s_{SW}} = 9.5. \quad (154)$$

Using values from Table 3.1.1 and Table 3.2.4 , the buckling allowable from Equation 153 is thus:

$$\tau_{cr_{SW2}} = 9.5 \times \frac{\pi^2 \times (1.05 \times 10^7 \text{ psi})}{12(1 - 0.33^2)} \left(\frac{0.06 \text{ in}}{5.00 \text{ in}} \right)^2, \quad (155)$$

$$\tau_{cr_{SW2}} = 13251.57 \text{ psi} \quad (156)$$

To determine the shear buckling margin of safety, Equation 157 is used below.

$$M.S._{SWSB2} = \frac{\tau_{cr_{SW2}}}{1.5 \times FS \times F_{SXY}_{997273}} - 1, \quad (157)$$

where $M.S._{SWSB2}$ is the margin of safety in the forward spar web that accounts for shear buckling, and $F_{su_{2024-T3S}}$ is the material allowable obtained from Table 3.2.1 , and F_{SXY}_{997273} is xy direction shear stress in Element 997273 at Node 39773. Substituting and solving:

$$M.S._{SWSB2} = \frac{13251.57 \text{ psi}}{1.5 \times 1.5 \times 10499.48 \text{ psi}} - 1, \quad (158)$$

$$\underline{\underline{M.S._{SWSB2} = -0.44}} \quad (159)$$

The negative results indicates that the structure will fail at ultimate shear despite having a factor of safety. Essentially, the spar web should be redesigned/resized to account for shear buckling at ultimate shear stress.

6.2.4 Rib Web

The two methods of analysis used for the inboard rib web are shear stress in the xy direction and shear buckling, respectively. Figure 6.2.4.1 indicates the shear stress gradients in the xy direction for the inboard rib web.



Patran 2024.1 05-May-25 13:51:39

Fringe: SC1:DEFAULT, A1:Static subcase, Stress Tensor, XY Component, Maximum,2 of 2 layers

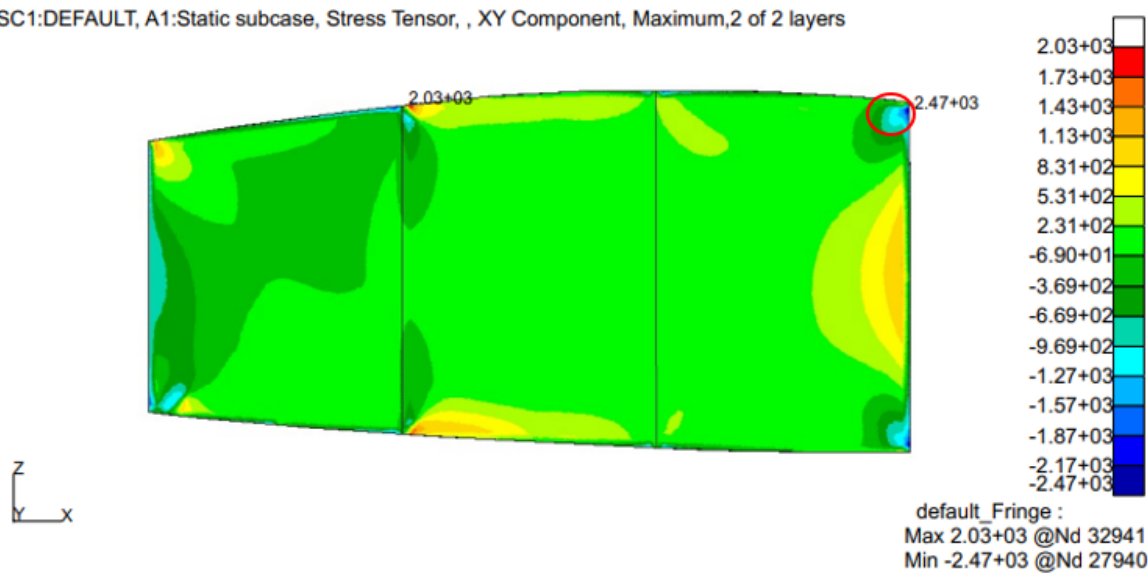
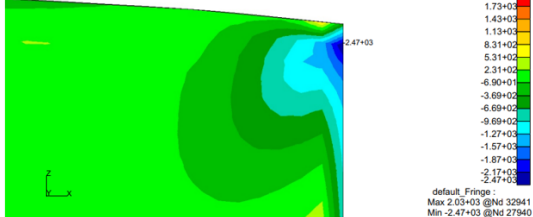


Fig. 6.2.4.1 Fringe: SC1:DEFAULT, A1: Static Subcase, Stress Tensor, XY Component, Maximum, 2 of 2 layers of Inboard Rib Web for WS 2

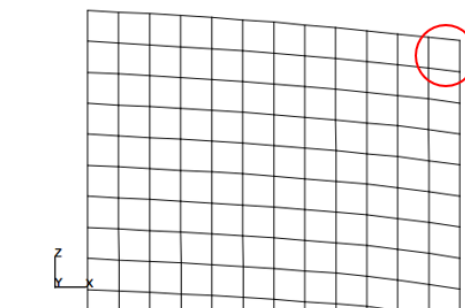
6.2.4.1 shows the fringe plot of shear stress in the xy direction for the inboard rib web. Typically it is best practice to use a seventy percent shear gradient to capture the shear stress throughout the panel. For the purposes of this preliminary analysis, the most conservative approach to capturing shear stress will be taken from the maximum xy shear stress values. The area of interest in the web is indicated by the red circle in the upper right region of the plot. An rectangular approximation of the rib sheet was made due to the complex curvature present in the wing's airfoil shape. This rectangular approximation is a conservative approximation because the resulting rectangular panel has a larger aspect ratio than compared to the exact shape of the wing's airfoil. For clarity, a closer look at the region of interest will be visible in Figures 6.2.4.2 a and 6.2.4.2 b below.

Patran 2024.1 05-May-25 13:52:29

Fringe: SC1:DEFAULT, A1:Static subcase, Stress Tensor, XY Component, Maximum,2 of 2 layers



(a) Fringe: SC1:DEFAULT, A1: Static Subcase, Stress Tensor, XY Component, Maximum, 2 of 2 layers of Zoomed Inboard Rib Web for WS 2



(b) Zoomed Region of Interest for Inboard Rib Web for WS 2

Fig. 6.2.4.2 Zoomed Fringe and Elements of Interest for Inboard Rib Web for WS 2

Figure 6.2.4.2 a shows a shear stress gradient that concentrates near the corner of the rib web. Figure 6.2.4.2 b shows the quad elements the rib web is composed of and the region of interest indicated by the red circle. A closer view



of Figure 6.2.4.2 b to identify the specific element will be shown in Figure 6.2.4.3 .

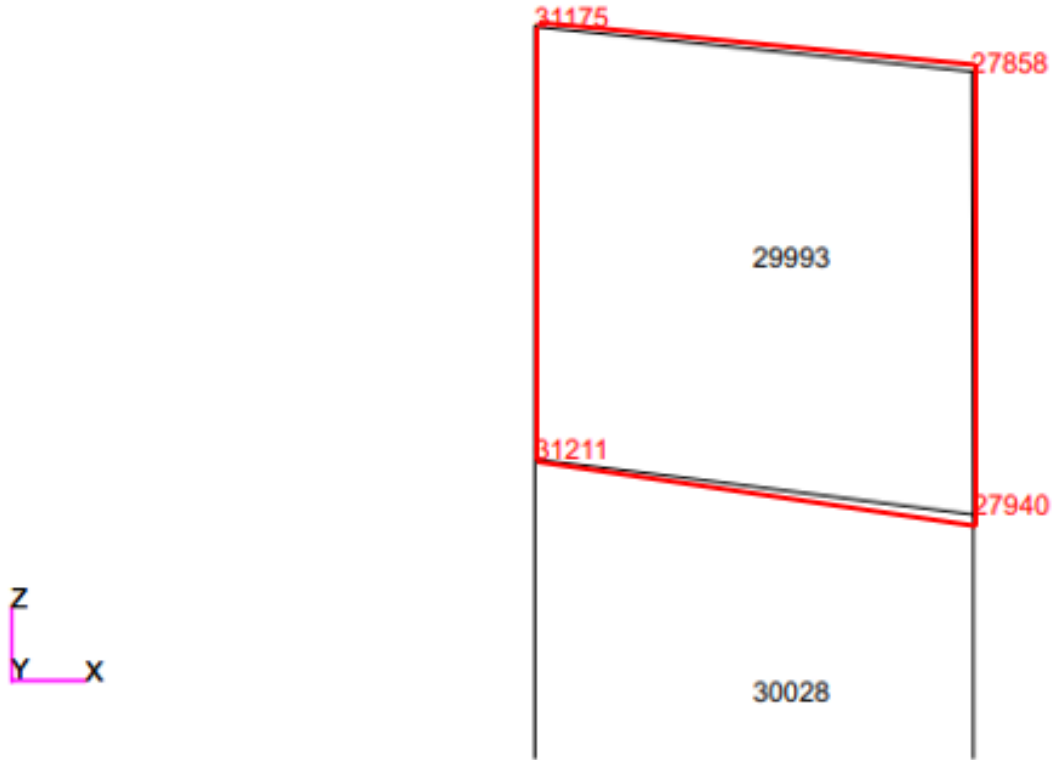


Fig. 6.2.4.3 Element of Interest for Inboard Rib Web for WS 2

As outlined in red in Figure 6.2.4.3 the element of interest is Element 29993. Figure 6.2.4.4 is an excerpt of the .f06 file results from NASTRAN concerning the maximum shear in the xy direction for the inboard rib web.

STRESSES IN QUADRILATERAL ELEMENTS (QUAD 4)									OPTION = BILIN
ELEMENT ID	FIBER GRID-ID	DISTANCE	STRESSES IN ELEMENT COORD SYSTEM			PRINCIPAL STRESSES (ZERO SHEAR)			VON MISES
			NORMAL-X	NORMAL-Y	SHEAR-XY	ANGLE	MAJOR	MINOR	
29993	CEN/4	-3.000000E-02	6.468331E+03	4.289662E+03	-2.427359E+03	-32.9154	8.039583E+03	2.718410E+03	7.083061E+03
		3.000000E-02	6.294002E+03	4.023891E+03	-1.571925E+03	-27.0839	7.097838E+03	3.220056E+03	6.155699E+03
31175		-3.000000E-02	9.338949E+03	1.811693E+03	-2.406743E+03	-16.2989	1.004268E+04	1.107960E+03	9.537093E+03
		3.000000E-02	8.707551E+03	3.481112E+03	-1.465038E+03	-14.6381	9.090204E+03	3.098459E+03	8.004163E+03
27858		-3.000000E-02	9.287805E+03	6.766739E+03	-2.121650E+03	-29.6421	1.049513E+04	5.559410E+03	9.094401E+03
		3.000000E-02	8.654234E+03	4.578111E+03	-1.404330E+03	-17.2844	9.091215E+03	4.141130E+03	7.883606E+03
27940		-3.000000E-02	3.665646E+03	6.748116E+03	-2.445212E+03	-61.1118	8.097291E+03	2.316471E+03	7.223227E+03
		3.000000E-02	3.937488E+03	4.562488E+03	-1.675784E+03	-50.2816	5.954660E+03	2.545316E+03	5.174951E+03
31211		-3.000000E-02	3.580790E+03	1.792622E+03	2.738132E+03	-35.9583	5.567114E+03	-1.937023E+02	5.666449E+03
		3.000000E-02	3.876707E+03	3.465112E+03	-1.743058E+03	-41.6332	5.426075E+03	1.915745E+03	4.766276E+03

Fig. 6.2.4.4 .f06 NASTRAN Results for Inboard Rib Web Shear Stress for WS 2



Figure 6.2.4.4 identifies the node of interest within Element 29993 and provides the respective xy shear stress value. First, the rib web's shear stress margin of safety equation is used to check if the panel fails at ultimate shear stress. This is done using the following equation as seen in Equation 160,

$$M.S.RWS2 = \frac{F_{SU\ 5052-H32S}}{1.5 \times FS \times F_{SXY\ 29993}} - 1, \quad (160)$$

$$M.S.RWS2 = \frac{1.90 \times 10^4 \text{ psi}}{1.5 \times 1.5 \times (2738.13 \text{ psi})} - 1, \quad (161)$$

$$\underline{\underline{M.S.RWS2 = 2.08.}} \quad (162)$$

The result yields a positive margin of safety which indicates that the inboard rib web does not fail at shear ultimate. Due to the value being over one, there could be additional material reduction or redesign to better optimize the structure for weight savings.

Next, focusing on the shear buckling analysis of the rib web, Equation 163 is used to calculate the shear buckling allowable.

$$\tau_{cr\ RW2} = K_{s\ 5052-H32S} \frac{\pi^2 E_{5052-H32}}{12(1 - \nu_{2024-T3}^2)} \left(\frac{t_{RW}}{b_{RW2}} \right)^2, \quad (163)$$

where $\tau_{cr\ RW2}$ is the shear stress in the rib web, $K_{s\ RW}$ is the rib shear-buckling-stress coefficient, $E_{5052-H32}$ and $\nu_{5052-H32}$ are the elastic modulus and Poisson's ratio for a 5052-H32 aluminum sheet used in the rib web, respectively, t_{RW} is the panel thickness of the rib web, and b_{RW2} is the height of the rib web. $K_{s\ RW}$ is obtained in the same way as in the spar web by using Figure 6.1.3.5. Since the rib web is clamped between the wings spar and the lower and upper skin, the clamped curve will be used. This is also a conservative estimate due to clamped Elements having higher resulting stresses than a comparatively loaded hinged edge Element. Using the $(\frac{a}{b})$ ratio as described in Table 3.1.1, the resulting value for $K_{s\ RW}$ is:

$$K_{s\ RW} = 10. \quad (164)$$

Now, using the remaining values from Table 3.1.1 and Table 3.2.3, Equation 163 becomes,

$$\tau_{cr\ RW2} = 10 \times \frac{\pi^2 \times (1.01 \times 10^7 \text{ psi})}{12(1 - 0.33^2)} \left(\frac{0.06 \text{ in}}{2.24 \text{ in}} \right)^2, \quad (165)$$

$$\tau_{cr\ RW2} = 10494.49 \text{ psi.} \quad (166)$$

The margin of safety for rib web shear buckling can be calculated using Equation 167,

$$M.S.RWSB2 = \frac{\tau_{cr\ RW2}}{1.5 \times FS \times F_{SXY\ 29993}} - 1, \quad (167)$$

and plugging in the values becomes,

$$M.S.RWSB2 = \frac{10494.49 \text{ psi}}{1.5 \times 1.5 \times (2738.13 \text{ psi})} - 1, \quad (168)$$

$$\underline{\underline{M.S.RWSB2 = 0.70.}} \quad (169)$$



The positive MS indicates that the rib web is sized appropriately to resist buckling in shear. While MS values less than one are considered adequate, the rib web can be made more efficient by reducing the panel thickness.

Finding the critical buckling allowable for the upper spar cap in wing Section two is identical to the upper skin stringer in wing Section two due to the upper skin stringer and upper spar cap sharing the same material and related geometric properties. Therefore,

$$P_{crUSC1} = P_{crUSS1} = 27.32 \text{ lb}, \quad (170)$$

where P_{crUSC1} is the upper spar cap critical buckling allowable in wing Section one. The following equation, Equation 171 displays the margin of safety calculation for the upper spar cap,

$$M.S.USCB1 = \frac{P_{crUSCB1}}{1.5 \times FS \times P_{BSMNC1}_{1288673}} - 1. \quad (171)$$

where $P_{BSMNC1}_{1288673}$ is the critical buckling load in Element 1288673 which is derived from bar stresses minimum combined value in the .f06 file for the spar cap. Plugging in these values,

$$M.S.USCB1 = \frac{27.32 \text{ lb}}{1.5 \times 1.5 \times (613.40 \text{ lb})} - 1, \quad (172)$$

$$\underline{\underline{M.S.USCB1 = -0.98}}. \quad (173)$$

This negative margin of safety value indicates that the upper spar cap cannot take the maximum compressive load as described in the bar stresses, minimum combined .f06 file value. The spar cap and other surrounding structural components will need to be resized to take on the required load.

6.2.5 Upper Skin Stringer

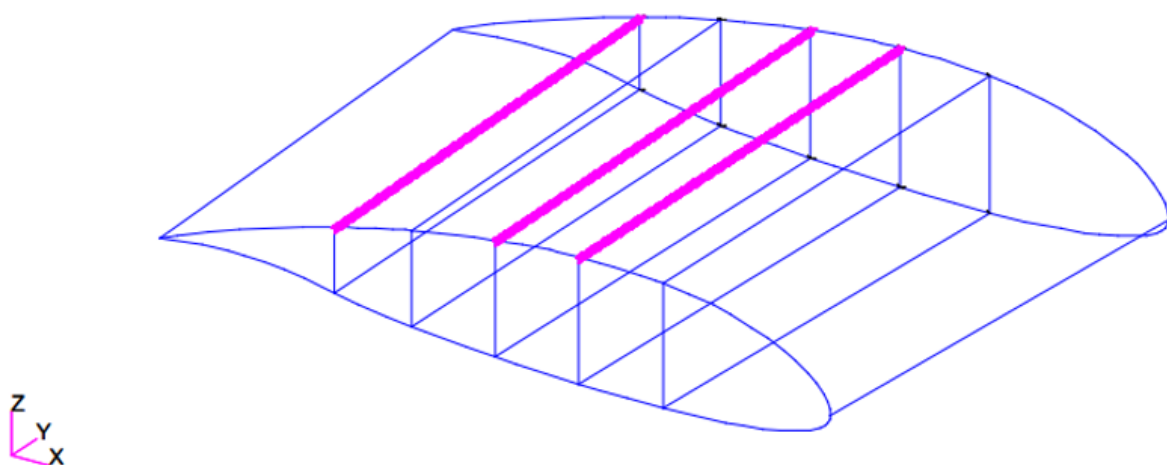


Fig. 6.2.5.1 Upper Skin Stringer Placement for WS 2

Compression Figure 6.2.5.2 shows the minimum combined stress on the aftmost upper stringer.



Patran 2024.1 07-May-25 17:47:35

Fringe: SC1:DEFAULT, A2:Static subcase, Bar Stresses, Minimum Combined, , At Center

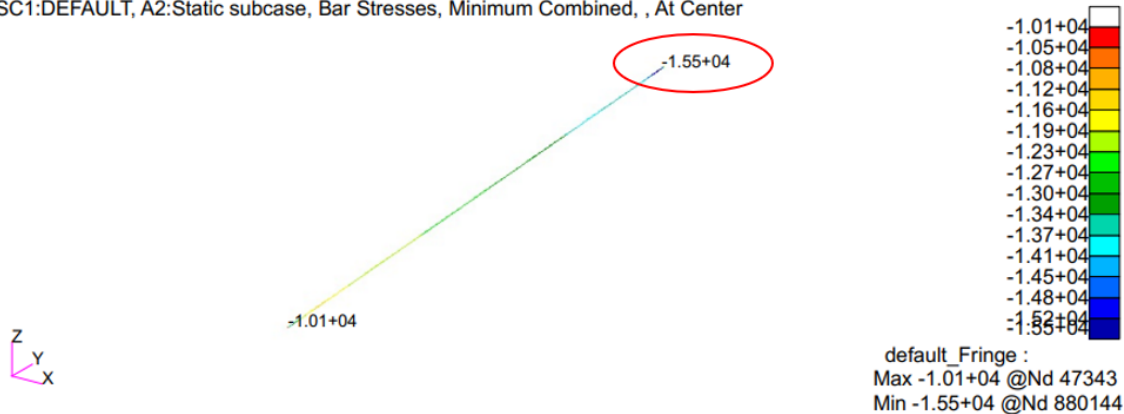


Fig. 6.2.5.2 Fringe: SC1:DEFAULT, A1: Static Subcase, Bar Stresses, Minimum Combined, Aft Upper Stringer for WS 2

The compressive stresses were taken from the resulting .f06, shown in Figure 6.2.5.3 .

ELEMENT ID.	S T R E S S E S I N B A R E L E M E N T S				(C B A R)			
	SA1 SB1	SA2 SB2	SA3 SB3	SA4 SB4	AXIAL STRESS	SA-MAX SB-MAX	SA-MIN SB-MIN	M.S.-T M.S.-C
0 1311721	1.031435E+04	-2.698051E+03	-6.242061E+03	9.747310E+03	-9.717823E+03	5.965289E+02	-1.595988E+04	
	1.136954E+04	-2.758171E+03	-7.067799E+03	1.068000E+04		1.651714E+03	-1.678562E+04	
0 1311722	1.133078E+04	-2.661130E+03	-7.119676E+03	1.061741E+04	-9.616016E+03	1.714760E+03	-1.673569E+04	
	1.229204E+04	-2.321878E+03	-8.213485E+03	1.134938E+04		2.676021E+03	-1.782950E+04	
0 1311723	1.196510E+04	-4.024023E+03	-6.465918E+03	1.157439E+04	-9.475847E+03	2.489248E+03	-1.594176E+04	
	1.116956E+04	-3.805858E+03	-5.993199E+03	1.081958E+04		1.693710E+03	1.546905E+04	
0 1311724	1.134794E+04	-3.937460E+03	-6.027521E+03	1.101353E+04	-9.601038E+03	1.746904E+03	-1.562856E+04	
	1.038316E+04	-3.450062E+03	-5.647398E+03	1.003159E+04		7.821258E+02	-1.524844E+04	

Fig. 6.2.5.3 .f06 NASTRAN Results for Aft Upper Stringer in WS 2

Using the compressive stresses found in Element 1311724, the stringer's margin of safety equation can check if the panel will fail at ultimate compressive stress; this is calculated using Equation 174.

$$M.S.USSC2 = \frac{F_{cy} \text{ 2024-T3S}}{FS \times F_{MNMMNP} \text{ 1311724}} - 1, \quad (174)$$

where $F_{cy} \text{ 2024-T3S}$ is the tensile yield stress as previously outlined in Table 3.2.1 , FS is the factor of safety, and $F_{MNMMNP} \text{ 1311724}$ is the minor principle stress value circled in Figure 6.2.5.3 for Element 1311724. Plugging in the values,

$$M.S.USSC2 = \frac{3.40 \times 10^4 \text{ psi}}{1.5 \times |-1.56 \times 10^4 \text{ psi}|} - 1, \quad (175)$$

$$\underline{\underline{M.S.USSC2 = 0.45.}} \quad (176)$$

The margin of safety is positive, indicating that the element would survive an ultimate load.



Crippling and Buckling The method for crippling analysis is solely dependent upon the geometry of the upper stringers. Since the geometry of the stringers are uniform throughout both wing sections, the results and processes outlined in wing Section one are valid for wing Section two. Therefore, Table 6.1.1 is valid for wing Section two. The MS for upper stringer crippling is as follows in Equation 180,

$$M.S.USSC_2 = \frac{P_{ccUSSC_2}}{1.5 \times FS \times P_{BSMNC2_{1311919}}} - 1, \quad (180)$$

Now, the MS of the upper skin stringer can be calculated using the value displayed in Table 6.1.1. The stress displayed in Figure 6.2.5.5 can be converted to a load using the same area used in converting the critical crippling stress to a critical load. Using Equation 180 from above, the process is as follows,

$$M.S.USSC_2 = \frac{2978.4511 \text{ lb}}{1.5 \times 1.5 \times (531.74 \text{ lb})} - 1, \quad (181)$$

$$\underline{\underline{M.S.USSC_2 = 1.49}} \quad (182)$$

The positive margin of safety indicates the structure is adequately sized according to the structural analysis applied to this structure. For future analysis, it would be more appropriate to take the margin of safety of the unbuckled skin stringer allowable against the summation of stringer and unbuckled skin loads. This would result in a lower margin of safety for this structural component.

Finding the critical buckling allowable for the upper skin stringer in wing Section two is identical to the upper skin stringer in wing Section one as the same stringer was used between the two wing sections. Therefore,

$$P_{crUSSB_2} = P_{crUSSB_1} = 27.32 \text{ lb}, \quad (183)$$

where P_{crUSSB_1} is the upper skin stringer critical buckling allowable in wing Section two. The following equation, Equation 184 displays the margin of safety calculation for the upper skin stringer,

$$M.S.USSB_2 = \frac{P_{crUSSB_1}}{1.5 \times FS \times P_{BSMNC1_{1308177}}} - 1. \quad (184)$$

where $P_{BSMNC1_{1308177}}$ is the critical buckling load in Element 1308177 which is derived from bar stresses minimum combined value in the .f06 file for the upper skin stringer. Plugging in these values,

$$M.S.USCB_2 = \frac{27.32 \text{ lb}}{1.5 \times 1.5 \times (531.74 \text{ lb})} - 1, \quad (185)$$

$$\underline{\underline{M.S.USCB_2 = -0.98.}} \quad (186)$$

This negative margin of safety value indicates that the upper skin stringer cannot take the maximum compressive load as described in the bar stresses, minimum combined .f06 file value. The stringer and other surrounding structural components will need to be resized to take on the required load.

6.2.6 Lower Skin Stringer

The stringers attached to the lower skin have two modes of failure, tensile and compressive. In this section, both these are analyzed in order to perform margin of safety checks and conclude whether or not this section of stringers will fail in either of the two modes. Figure 6.2.6.1 shows the geometry of the lower skin section and the three stringer



locations.

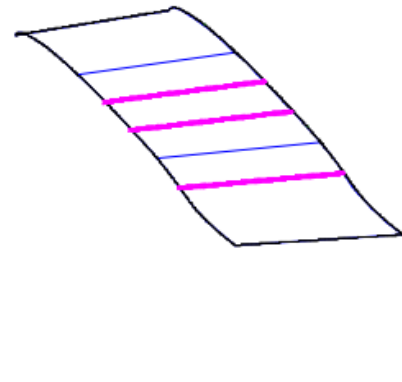


Fig. 6.2.6.1 Geometry of Lower Skin and Stringer

Tension The fringe plot of maximum bar stresses is used to locate the region of highest tensile stress. This is found to be the forward most stringer in the most inboard element location. Figure 6.2.6.2 shows the maximum combined bar stress fringe plot of the three stringers, with the region of interest circled.

Patran 2024.1 07-May-25 01:29:37

Fringe: SC1:DEFAULT, A1:Static subcase, Bar Stresses, Maximum Combined, , At Center

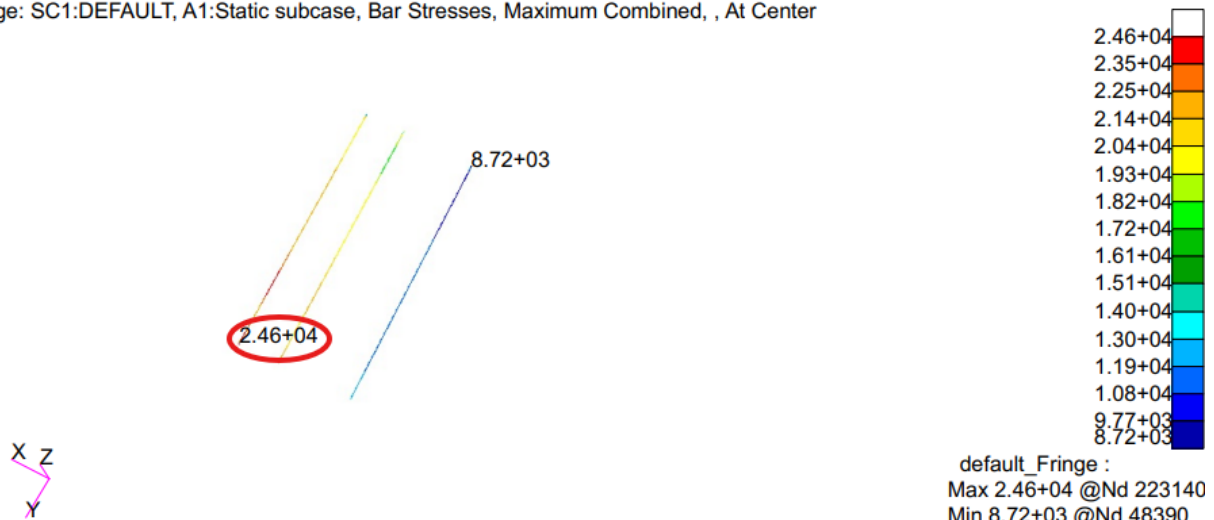


Fig. 6.2.6.2 Fringe: SC1:DEFAULT, A1: Static Subcase, Bar Stresses, Maximum Combined, At Center of Lower Stringers for WS 2

The specific element of interest is identified as Element 1303054. This element and the surrounding skin sections are shown from a cross section view in Figure 6.2.6.3 .



$$M.S._{LST2} = \frac{3.7 \times 10^4}{1.5 \times 2.46 \times 10^4} - 1, \quad (188)$$

$$\underline{\underline{M.S._{LST2} = 0.0028}} \quad (189)$$

The calculated margin of safety for the lower stringer in tension yields a slightly positive value.

Compression The section is subsequently analyzed for compressive failure. Similar to before, the fringe plot for minimum combined bar stresses is used to identify the region of interest, as shown in Figure 6.2.6.5 .

Patran 2024.1 07-May-25 02:05:04

Fringe: SC1:DEFAULT, A1:Static subcase, Bar Stresses, Minimum Combined, , At Center



Fig. 6.2.6.5 Fringe: SC1:DEFAULT, A1: Static Subcase, Bar Stresses, Minimum Combined, At Center of Lower Stringers for WS 2

A closer inspection of the fringe results reveals that Element 1304631 is the element of minimum stress. This element and the surrounding skin are shown with a cross section view in Figure 6.2.6.6 .



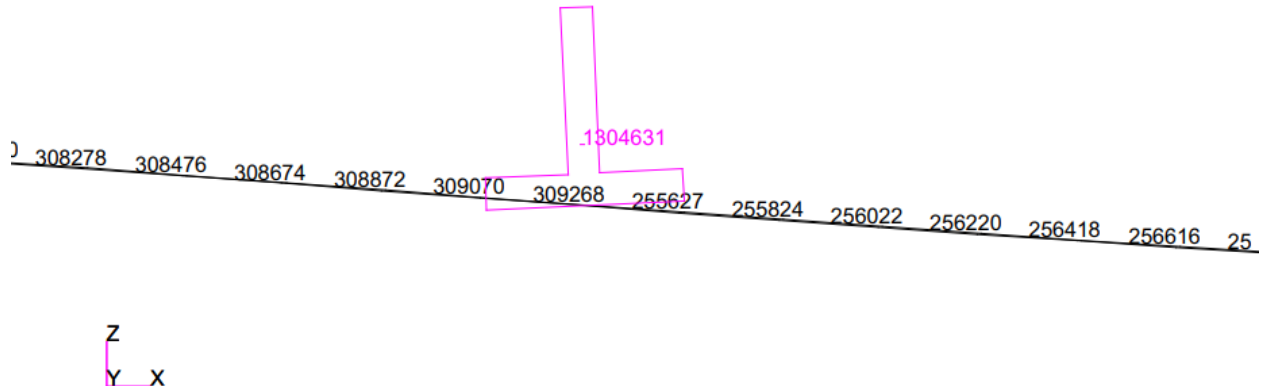


Fig. 6.2.6.6 Lower Stringer Min Stress Element of Interest and Surrounding Skin

Since the compressive stress is the stress of interest in this case, the .f06 file is searched for Element 1304631 and the minimum bar stress is found. The location of the minimum principal stress, $\sigma_c_{1304631}$, of -4.14×10^3 psi within the .f06 file is highlighted in Figure 6.2.6.7 .

is compression. Figure 6.2.7.1 below shows the geometry of the upper spar cap in context of the second section top skin and front spar web.

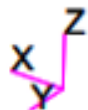
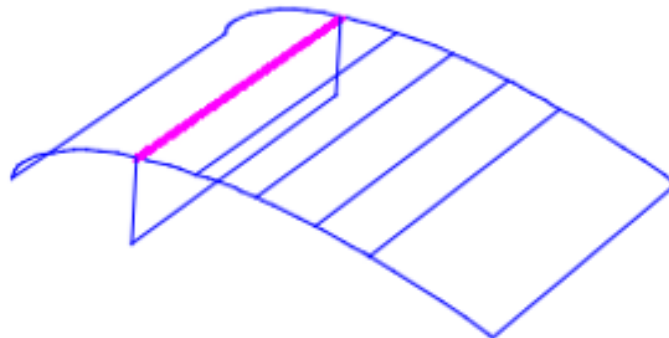


Fig. 6.2.7.1 WS2 Geometry of Upper Skin and Upper Spar Cap

In order to identify a region of interest, a fringe plot of minimum combined bar stress is created. Using this plot, as shown in Figure 6.2.7.2 , the region of high absolute stress at the inboard edge can be seen. This section contains the element of interest that will be used in further analysis of compressive failure.

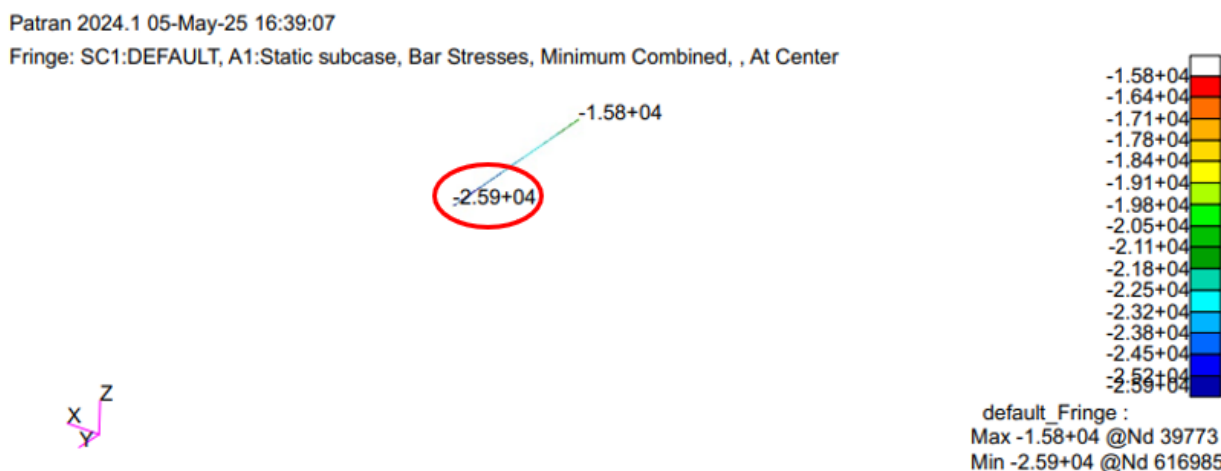


Fig. 6.2.7.2 Fringe: SC1:DEFAULT, A1: Static Subcase, Bar Stresses, Minimum Combined, At Center of Upper Spar Cap for WS 2



The compressive yield stress of the 2024 T3 Extrusion from Table 3.2.2 and the maximum tensile stress in Element 1288870, $\sigma_{BSMNC}_{1288870}$, are plugged into Equation 193 to get the following:

$$M.S.USCC2 = \frac{3.4 \times 10^4}{1.5 \times | -3.02 \times 10^4 |} - 1, \quad (194)$$

$$\underline{\underline{M.S.USCC2 = -0.249}} \quad (195)$$

The negative margin of safety value that has been calculated means the section is predicted to fail under the given load. More specifically, the upper spar cap in wing Section 2 is expected to fail in pure compression under the previously defined load conditions.

Crippling & Buckling The method for crippling analysis is solely dependent upon the geometry of the upper spar caps. Since the geometry of the spar caps are uniform throughout both wing sections, the results and processes outlined in wing Section one are valid for wing Section two. Therefore, Table 6.1.1 is valid for wing Section two. The MS for upper spar cap crippling is as follows in Equation 196,

$$M.S.USPC2 = \frac{P_{ccUSPC2}}{1.5 \times FS \times P_{BSMNC2}_{1288870}} - 1, \quad (196)$$

Now, the MS of the upper spar cap can be calculated using the value displayed in Table 6.1.1. The stress displayed in Figure 6.2.7.4 can be converted to a load using the same area used in converting the critical crippling stress to a critical load. Using Equation 196 from above, the process is as follows,

$$M.S.USPC2 = \frac{2978.4511 \text{ lb}}{1.5 \times 1.5 \times 555.66 \text{ lb}} - 1, \quad (197)$$

$$\underline{\underline{M.S.USPC2 = 3.93.}} \quad (198)$$

The positive margin of safety indicates the structure is adequately sized according to the structural analysis applied to this structure. For future analysis, it would be more appropriate to take the margin of safety of the unbuckled spar cap allowable against the summation of spar cap and unbuckled skin loads. This would result in a lower margin of safety for this structural component.

Finding the critical buckling allowable for the upper spar cap is identical to the upper skin stringer due to the upper skin stringer and upper spar cap sharing the same material and related geometric properties. Therefore,

$$P_{crUSCB2} = P_{crUSSB1} = 27.32 \text{ lb}, \quad (199)$$

where $P_{crUSCB2}$ is the upper spar cap critical buckling allowable in wing Section two. The following equation, Equation 200 displays the margin of safety calculation for the upper spar cap,

$$M.S.USCB2 = \frac{P_{crUSCB2}}{1.5 \times FS \times P_{BSMNC1}_{1288870}} - 1. \quad (200)$$

where $P_{BSMNC1}_{1288870}$ is the critical buckling load in Element 1288870 which is derived from bar stresses minimum combined value in the .f06 file for the spar cap. Plugging in these values,

$$M.S.USCB2 = \frac{27.32 \text{ lb}}{1.5 \times 1.5 \times (555.66 \text{ lb})} - 1, \quad (201)$$



$$\underline{\underline{M.S.USCB2 = -0.98.}} \quad (202)$$

This negative margin of safety value indicates that the upper spar cap cannot take the maximum compressive load as described in the bar stresses, minimum combined .f06 file value. The spar cap and other surrounding structural components will need to be resized to take on the required load.

6.2.8 Lower Spar Cap

Tension The lower spar caps are subjected to tensile forces, as shown in Figure 6.2.8.1 , which illustrates the placement and orientation of the spar caps in Section 2 of the wing. The spar cap is a critical structural element designed to carry significant bending moments. The maximum combined stress due to tension occurs at the most inboard element of Section 2, as seen in Figure 6.2.8.2 , where the stress distribution is shown across the spar cap. This stress distribution provides insight into where the largest stresses occur under the applied load, with the highest stress located at the center of the lower spar cap.

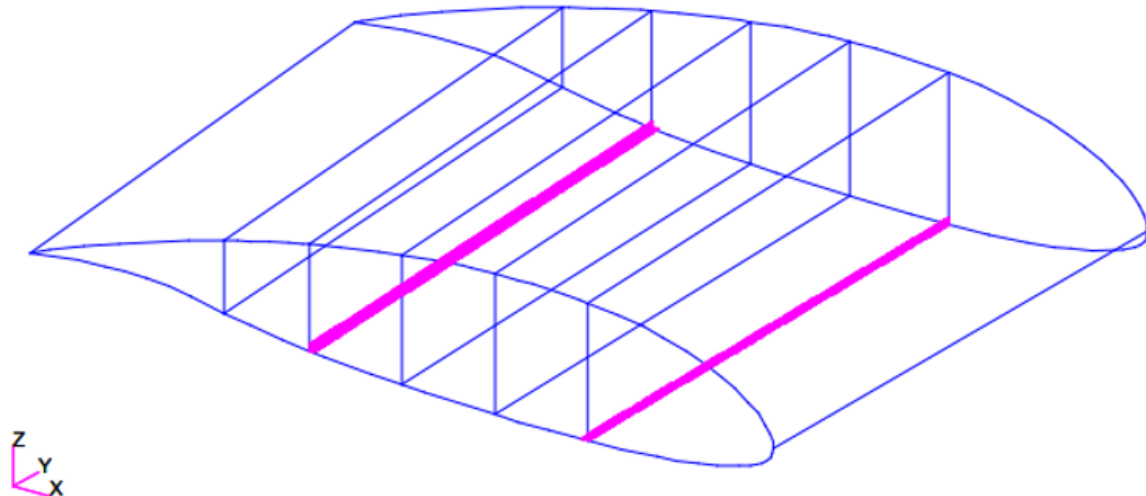


Fig. 6.2.8.1 Lower Spar Cap Placement WS2

Patran 2024.1 07-May-25 01:28:01

Fringe: SC1:DEFAULT, A2:Static subcase, Bar Stresses, Maximum Combined, , At Center

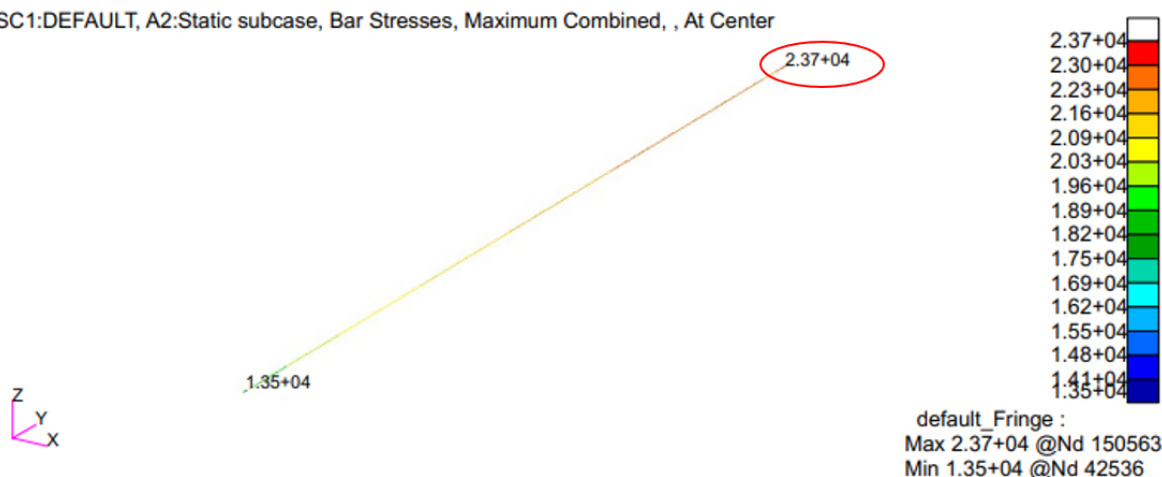


Fig. 6.2.8.2 Fringe: SC1:DEFAULT, A2: Static Subcase, Bar Stresses, Maximum Combined, At Center of Lower Spar Cap for WS 2

Figure 6.2.8.3 presents the NASTRAN .f06 file results, specifically showing the calculated stresses for the lower spar cap. These results are derived from finite element analysis (FEA), and the maximum principle stress found in the .f06 file corresponds to the critical element where the greatest stress concentration occurs. This critical stress is a result of both axial and bending forces acting on the spar cap. Given these results, material failure due to tensile stress was considered the primary failure mode for the lower spar cap, as it experiences the highest tensile loads.

ELEMENT ID.	S T R E S S E S I N B A R E L E M E N T S				(C B A R)		
	SA1	SA2	SA3	SA4	AXIAL STRESS	SA-MAX	SA-MIN
	SB1	SB2	SB3	SB4	SB-MAX	SB-MIN	
1290443	-3.642959E+02	7.702078E+02	-2.013372E+02	-5.197431E+02	2.207175E+04	2.284196E+04	2.155201E+04
	-6.645433E+02	1.130992E+03	-2.033394E+02	-8.780363E+02		2.320274E+04	2.119371E+04
1290444	-2.761097E+02	1.384260E+03	-6.315273E+02	-5.986356E+02	2.197943E+04	2.336369E+04	2.134790E+04
	-1.811159E+03	1.304697E+03	5.094094E+02	-1.938405E+03		2.328413E+04	2.004103E+04
1290445	-5.598569E+02	2.251843E+03	-9.484936E+02	-1.071911E+03	2.168342E+04	2.393527E+04	2.061151E+04
	-4.992277E+03	6.654212E+02	3.157623E+03	-4.593524E+03		2.484105E+04	1.669115E+04
1290446	-2.626209E+03	2.676688E+03	2.690807E+02	-3.011427E+03	2.110917E+04	2.378586E+04	1.809775E+04
	-1.166611E+04	-1.536507E+03	9.228432E+03	-9.943721E+03		3.033760E+04	9.443060E+03
1290447	-8.481419E+03	-6.138113E+02	6.408105E+03	-7.357912E+03	2.116150E+04	2.756961E+04	1.268009E+04
	-1.593355E+03	2.421006E+03	-3.135951E+02	-2.030892E+03		2.358251E+04	1.913061E+04

Fig. 6.2.8.3 Lower Spar Cap NASTRAN .f06 Results

The margin of safety (M.S.) for the lower spar cap under tension is calculated using Equation 203

$$M.S._{LSC2} = \frac{F_{t,y_{2024-T3E}}}{1.5 \times F_{MXMXP_{1290447}}} - 1, \quad (203)$$

Where, $F_{t,y_{2024-T3E}}$ is the yield strength of 2024-T3E material due to tension (in psi), which represents the maximum stress the material can handle before permanent deformation and $F_{MXMXP_{1290447}}$ represents the maximum principle stress at Element 1290447 in the .f06 file, which is subjected to axial and bending forces.

Substituting known values into Equation 203 yields:



$$M.S.LSC2 = \frac{3.70 \times 10^4 \text{ psi}}{1.5 \times 2.76 \times 10^4 \text{ psi}} - 1, \quad (204)$$

After performing the calculation, the resulting margin of safety is:

$$\underline{\underline{M.S.LSC2 = -0.105}} \quad (205)$$

This negative margin of safety indicates that the spar cap is at risk of failure under the applied tensile loads. The value of $M.S.LSC2 = -0.105$ suggests that the stress in the critical element exceeds the yield strength of the material, even with a safety factor of 1.5. This means the spar cap is likely to fail at or near the ultimate load, which necessitates design improvements to increase the margin of safety, such as reinforcing the spar cap or using a material with a higher tensile strength.

Compression In contrast to the tension analysis, the lower spar cap experiences no significant compressive forces, as demonstrated in Figure 6.2.8.4 . This figure shows the stress distribution under compressive loading conditions, where the lower spar cap is unaffected by compressive forces. Since the stresses in the cap are dominated by tension, the potential failure modes were ignored due to compression in this analysis.

Patran 2024.1 08-May-25 00:11:42

Fringe: SC1:DEFAULT, A2:Static subcase, Bar Stresses, Minimum Combined, , At Center

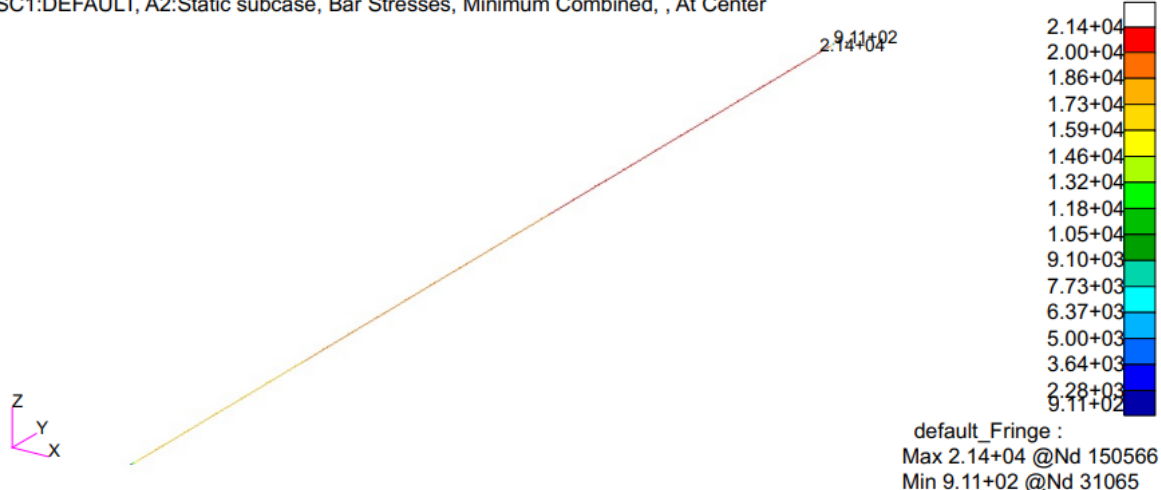


Fig. 6.2.8.4 Fringe: SC1:DEFAULT, A2: Static Subcase, Bar Stresses, Minimum Combined, At Center of Lower Spar Cap for WS 2

Since the compressive forces are negligible in this scenario, the failure modes associated with compression were not considered in the calculation. Instead, the focus remained on the tensile failure mode, which dictates the need for adjustments in the design to prevent failure under tensile loading conditions.

6.3 Wing Weight

To compute the weight of the outboard section of the wing, the specific weight of 2024-T3S, 2024-T3E, and 5052-H32S, as seen in Table 3.2.4 , is included within the material properties in the Patran [1] model. Using the mass properties tool within Patran [1], the following weight is generated as seen in Figure 6.3.0.1 below.



Mass Properties Display

Summary Display of Center of Gravity, Principal Inertias, Radii of Gyration, Mass, and Volume

	CG(CID 0)	CG(CID 0)	I-Principal	Radii of Gyr.	Mass	Volume
1	-1.449E+01	-1.449E+01	2.741E+05	6.312E+01	6.880E+01	6.900E+02
2	-2.681E+02	-2.681E+02	2.695E+05	6.258E+01		
3	9.038E-01	9.038E-01	5.133E+03	8.638E+00		

Fig. 6.3.0.1 Weight of Outboard Wing Section

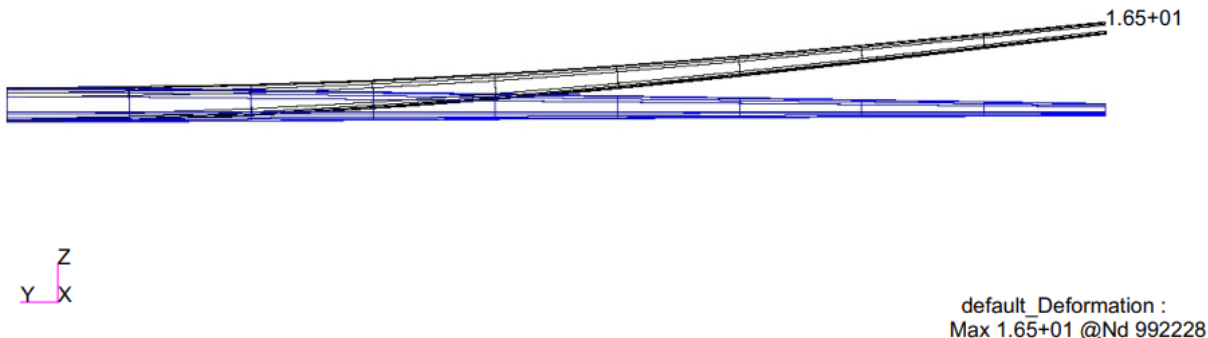
The red circle as seen in Figure 6.3.0.1 shows the weight of the wing section since the specific weights of each material were used rather than densities.

6.4 Wing Stress Distribution and Deflection

The stress distribution throughout the outboard wing and the maximum deflection at the wingtip are important factors to analyze during structural analysis. The maximum deflection at the wingtip directly affects the stress distribution in the two wing sections analyzed near the root. The deflection of the outboard portion of the wing can be seen in Figure 6.4.0.1 below.

Patran 2024.1 07-May-25 22:26:42

Deform: SC1:DEFAULT, A1:Static subcase, Displacements, Translational, , (NON-LAYERED)

**Fig. 6.4.0.1 Deform: SC1:DEFAULT, A1:Static subcase, Displacements, Translational, (NON-LAYERED) Deflection of Outboard Wing Section**

The deflection of the wingtip seen in Figure 6.4.0.1 results from the pressure loads documented in Figure 5.0.0.6 . The maximum deflection value can be obtained from Figure 6.4.0.2 below.

MAXIMUM DISPLACEMENTS							
SUBCASE/	DAREA ID	T1	T2	T3	R1	R2	R3
1	3.0577441E-02	2.1876853E-01	1.6498830E+01	1.1930405E-01	4.3944602E-02	7.0434900E-03	
MSC.NASTRAN JOB CREATED ON 30-APR-25 AT 09:58:55							
MAY 3, 2025 MSC Nastran 5/13/24							

Fig. 6.4.0.2 NASTRAN .f06 Results for Maximum Displacements

The maximum displacement seen in Figure 6.4.0.2 effects the stress distribution in the wing particularly near the root. Figure 6.4.0.3 below shows the distribution of minimum principal stress from a top down view of the outboard wing section.



Patran 2024.1 07-May-25 23:20:52

Fringe: SC1:DEFAULT, A1:Static subcase, Stress Tensor, , Min Principal, At Z1

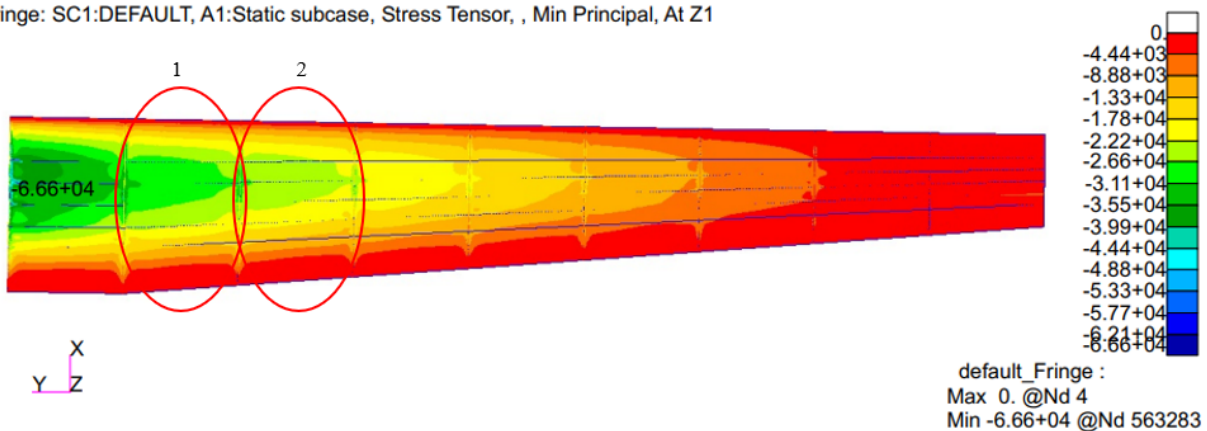


Fig. 6.4.0.3 Fringe: SC1:DEFAULT, A1:Static subcase, Stress Tensor, Min Principal, At Z1 Stress Distribution for Outboard Wing Section

As indicated by the stress gradient in Figure 6.4.0.3, the area of interest is near the root of the wing. Disregarding the boundary condition at the root, the analysis of the two sections labeled in Figure 6.4.0.3 prove to be critical due to wing flexure during pressure loading.

7. Summary

Conclusion As demonstrated in the analysis section, about half of the margins of safety for both wing sections are calculated to be negative values. This means that a large quantity of the substructure will fail under the given load conditions, and the design is highly incompetent for the desired flight conditions. The highest priority for future design should be resize the wing substructure to make all margins of safety positive, so the wing section is not at risk of failure. Some structures with particularly highly negative margins of safety are the upper skin, stinger, and spar cap for both wing sections. On the contrary, the rib webs for both sections have a positive margin of safety.

Recommendations for Further Analysis One of the assumptions that may have led to unrealistic results is the use of the principal values in buckling analysis. Although this is a conservative estimate because it uses the maximum compressive value experienced in the element and/or panel, it may not necessarily be the stress value in the direction the section will buckle in. This will lead to an overestimation of loads, and subsequently a lower margin of safety than reality.

Some possible remedies for the design in order to move towards positive margins in all structures would be to increase the number of stringers and decrease the rib spacing. In doing so, the aspect ratios of both the skin panels and the spar web will be lowered, making them less susceptible to buckling. The other effect this would have is causing the length of the stringers between ribs to be shortened, which would have a very similar effect in making the stringers less susceptible to buckling. If this course of action were to be taken, it would most likely be advisable to add lightening cuts into the ribs in order to save weight and lower the rib margins of safety due to the ribs having a safe margin of safety.



References

- [1] “MSC Patran,” , 2024.
- [2] Curtis, H. D., *Fundamentals of Aircraft Structures Analysis*, McGraw-Hill Science, Engineering Mathematics, 1999.
- [3] Ewing, M., *Aerospace Structures I*, University of Kansas, 2001.
- [4] *Military Handbook 5H*, 1998.
- [5] Hale, R., “AE 508 – Aerospace Structures II Design Project,” , 2025.
- [6] Hale, R., “Crippling Methods Handout,” , 2025.



Appendix A.**Table 1.0.1 Analysis Team Contributions**

	Wing Station 1	Wing Station 2	Checked By
Skin			
Upper Skin Stress	Zane	Tiger	Mayah
Upper Skin Buckling	Zane	Tiger	
Lower Skin Stress	Tiger	Zane	
Spar Web			
Spar Web Shear Stress	Kyron	Hunter	Tiger
Spar Web Shear Buckling	Hunter	Kyron	
Rib Web			
Rib Web Shear Stress	Hunter	Kyron	Zane
Rib Web Shear Buckling	Kyron	Hunter	
Stringer			
Upper Stringer Stress	Mayah	Tiger	Hunter
Upper Stringer Crippling/Buckling	Mayah	Tiger	
Lower Stringer Stress	Zane	Mayah	
Spar Cap			
Upper Spar Cap Stress	Mayah	Zane	Kyron
Upper Spar Cap Crippling/Buckling	Mayah	Zane	
Lower Spar Cap Stress	Mayah	Tiger	

